JPRS L/10379

11 March 1982

USSR Report

PHYSICS AND MATHEMATICS

(FOUO 2/82)

FBIS FOREIGN BROADCAST INFORMATION SERVICE

FOR OFFICIAL USE ONLY

APPROVED FOR RELEASE: 2007/02/09: CIA-RDP82-00850R000500040025-5

NOTE

JPRS publications contain information primarily from foreign newspapers, periodicals and books, but also from news agency transmissions and broadcasts. Materials from foreign-language sources are translated; those from English-language sources are transcribed or reprinted, with the original phrasing and other characteristics retained.

Headlines, editorial reports, and material enclosed in brackets [] are supplied by JPRS. Processing indicators such as [Text] or [Excerpt] in the first line of each item, or following the last line of a brief, indicate how the original information was processed. Where no processing indicator is given, the information was summarized or extracted.

Unfamiliar names rendered phonetically or transliterated are enclosed in parentheses. Words or names preceded by a question mark and enclosed in parentheses were not clear in the original but have been supplied as appropriate in context. Other unattributed parenthetical notes within the body of an item originate with the source. Times within items are as given by source.

The contents of this publication in no way represent the policies, views or attitudes of the U.S. Government.

APPROVED FOR RELEASE: 2007/02/09: CIA-RDP82-00850R000500040025-5

JPRS L/10379

11 March 1982

USSR REPORT

PHYSICS AND MATHEMATICS

(FOUO 2/82)

CONTENTS

APPROVED FOR RELEASE: 2007/02/09: CIA-RDP82-00850R000500040025-5

ASTROPHYSICS AND COSMOLOGY

COMBUSTION AND EXPLOSION IN OUTER SPACE AND ON THE EARTH

Moscow GORENIYE I VZRYV V KOSMOSE I NA ZEMLE in Russian 1980 (signed to press 15 Jan 80) pp 2, 152-155

[Annotation, table of contents and abstracts from collection of articles "Combustion and Explosion in Outer Space and on the Earth", edited by E. I. Andriankin, doctor of physical and mathematical sciences, Vsesoyuznoye astronomo-geodezicheskoye obshchestvo pri Akademii nauk SSSR, 1000 copies, 156 pages]

[Text] The collection contains articles that outline the results of theoretical and experimental research in the field of mechanics of a continuous medium as applied to problems of combustion physics. An examination is made of problems of the singular state of the universe, expansion of the metagalaxy, questions of radiation in a shock wave in inert gases, of the mechanism and limiting conditions of ignition of mixtures, shock waves in the presence of magnetic fields, and also analytical methods of studying equations that describe the corresponding processes.

The collection is intended for specialists in the field of astrophysics, cosmology, physics of explosion, shock wave physics, plasma physics and so on.

Contents page

UDC 530.12:531.51

SOME COROLLARIES OF THE THEORY OF INTERACTING FIELDS IN COSMOLOGY AND ASTROPHYSICS

[Abstract of article by Krechet, V. G., Nikolayenko, V. M. and Shikin, G. N.]

[Text] An examination is made of the influence that terms of interaction of classical fields have on the singular initial state and isotropization of the process of evolution of the universe. The problem of the cosmological background of quantum field theory and the mass of the Higgs boson is discussed. References 27.

UDC 530.12:531.51

ENERGETICS AND MASS SPECTRUM OF PLANCKEON AND GRAVITATIONAL VACUUM

[Abstract of article by Stanyukovich, K. P. and Mel'nikov, V. N.]

[Text] Two fundamental relations, the Mach relation and Dirac's equation, are derived from a model of a vacuum based on two hypotheses: a) dense packing of planckeons; b) density of de-excited energy coincides with the energy density of the field of the metagalaxy. References 12.

UDC 535.89+535.21

TOTAL OUTPUT OF RADIATION FROM SHOCK WAVE FRONT IN INERT GASES

[Abstract of article by Kiselev, Yu. N.]

[Text] The article describes a method of measuring spectrally integrated radiation fluxes from a shock wave front using quick-response pyroelectric radiation receivers, and gives the results of measurement of radiation fluxes from a shock wave front in xenon and argon, and also brightness temperatures of the front in the red and violet regions of the spectrum.

It is shown that in xenon at velocities of 5.5-11 km/s, despite considerable screening in the red region of the spectrum, the total radiation output is close to the calculation from the shock adiabat. With further increase in shock wave

velocity, radiation fluxes do not exceed $1.8 \cdot 10^7$ W/cm^2. In argon at velocities of 6.8-15 km/s, the shock wave radiation is close to that of an ideal black body. The total radiation output is close to calculation up to 20 km/s. At velocities of 20-37 km/s, considerable excess of radiation temperatures over brightness temperatures is observed. The radiation fluxes registered from the wave front in argon are up to $1.2 \cdot 10^8$ W/cm^2. The experimental results are used to estimate the spectral average absorption coefficients of shock-heated xenon and argon, which are much lower than the absorption coefficients in the visible region of the spectrum. References 8.

UDC 534.222.2:539.63

ELECTROTHERMAL ANALOG OF DETONATION

[Abstract of article by Kononenko, M. M.]

[Text] Supply of energy from outside sources to a shock wave front with some conductivity leads to an effect similar to detonation. Joule heat release on the front gives rise to the detonation mode. It is shown that the "shock adiabat" in such a mode coincides with that of a substance absorbing intense luminous flux. References 5.

UDC 536.46

INVESTIGATION OF MECHANISM AND LIMITING CONDITIONS OF IGNITION OF FUEL MIXTURES WITH IODIC ACID ANHYDRIDE

[Abstract of article by Ivanov, V. G., Ivanov, G. V. and Kuznetsov, V. P.]

[Text] The mechanism and processes that limit spontaneous combustion of mixtures of inorganic fuels (metals and non-metals) with I_2O_5 are studied by thermal differential analysis. It is shown that in contrast to conventional mixtures, the mechanism of spontaneous combustion of the investigated mixtures is determined by the formation and properties of iodides of the fuels. The authors establish the lower limits of ignition of the mixtures as a function of their relative density and fuel content. References 12.

UDC 532.5-1/-9:532:011.11

ANALYTICAL STUDIES OF EQUATIONS OF UNSTEADY NON-ADIABATIC ONE-DIMENSIONAL FLOWS OF CONTINUOUS MEDIUM MODELED BY VISCOUS THERMALLY CONDUCTIVE PERFECT GAS

[Abstract of article by Sarukhanov, G. I.]

[Text] An investigation is made of equations of unsteady non-adiabatic flows of a continuous medium modeled by a viscous thermally conductive perfect gas. Solutions of the equation of motion are obtained in the class of solutions of a continued system of equations by reducing the differential corollary of the initial equation to a Darboux equation. The resultant solutions enable evaluation of the way that temperature, heat flux and static pressure depend on time and mass coordinate, and can be used in studying some patterns of explosive processes: combustion, explosion, detonation. References 12.

UDC 539.1

DOUBLE EXPLOSION IN WATER AT LOW ENERGY DENSITIES

[Abstract of article by Ageyev, A. N. and Andriankin, E. I.]

[Text] At low energy densities, a spherical explosion in water is described by an approximation that differs from the solution of the corresponding problem for an incompressible liquid only in the accounting for delay time. The problem of double explosion in water is solved in such an approximation. An analysis is made of the dynamics of the cavity formed as a result of double explosion. It is shown that the principal characteristics of pulsations of the cavity as well as the magnitude and shape of the pressure pulse propagating in water can be varied over a wide range by controlling the parameters of the double explosion. References 7.

UDC 532.11+534.222.2

SOME CLASSES OF SOLUTIONS OF THE MONGE-AMPERE EQUATION FOR AN INHOMOGENEOUS MEDIUM

[Abstract of article by Dolgov, A. A.]

[Text] An examination is made of one-dimensional plane movements of an ideal fluid with variable initial density and speed of sound. Exact solutions of the Monge-Ampere equation are found for some distributions of these parameters. References 3.

UDC 533.1:533.2

RAREFACTION WAVE IN MEDIUM WITH EQUATION OF STATE INCLUDING SECTION WITH NEGATIVE PRESSURE

[Abstract of article by Ivanov, M. Yu.]

[Text] An investigation is made of qualitative peculiarities of rarefaction waves in a medium with an equation of state that includes a section with negative pressure. Assuming that the results of rarefaction processes may lead to breakup of the medium into individual particles, the author evaluates the mass of such a particle. References 5.

UDC 537.84:539.63

MOTION OF FLUID IN MAGNETIC FIELD WITH CLAPPING OF TWO PLATES

[Abstract of article by Andriankin, E. I. and Kononenko, M. M.]

[Text] The flow of a conductive fluid in a magnetic field resulting from convergence of channel walls may be of interest for getting strong currents in MHD operation. This paper gives an exact solution of such an unsteady two-dimensional problem for a slit channel at low magnetic Reynolds number when plates clap together in accordance with a special law. The solution depends on three constants that can be used for approximations. References 2.

UDC 539.9

THEORY OF NONLINEAR WAVE PROPAGATION

[Abstract of article by Andriankin, E. I. and Malkin, A. I.]

[Text] A method is proposed for studying nonlinear waves in weakly dispersing media. The evolution of initial perturbation reduces to propagation of a certain number of modes. In the first order of the method, modes interact with near phase velocities. References 4.

6610
CSO: 1862/79

CRYSTALS AND SEMICONDUCTORS

UDC 539.216,535.33,537.533

ELECTRONIC PROCESSES IN ISLAND METAL FILMS

Kiev ELEKTRONNYYE PROTSESSY V OSTROVKOVYKH METALLICHESKIKH PLENKAKH in Russian 1980 (signed to press 17 Nov 80) pp 4-8

[Annotation, preface and table of contents from book "Electronic Processes in Island Metal Films", by Petr Grigor'yevich Borzyak and Yuriy Aleksandrovich Kulyupin, Institute of Physics, UkSSR Academy of Sciences, Izdatel'stvo "Naukova dumka", 1200 copies, 240 pages]

[Text] The book examines new problems in the physics of island metal films: "cold" electron emission and "cold" luminescence, the relation between these effects and conduction current, and between luminescence resulting from conduction current and a new kind of luminescence when metals are bombarded by electrons. An investigation is made of the nature of conductivity of island films, the relation between their characteristics and structure determined by the conditions of growth. Also examined are problems of the physics of small metal island particles that are new with respect to their solution.

The book is intended for scientific workers, specialists in the field of electronic technology and electron microscopy, and also for graduate students and upperclassmen majoring in physics and physical engineering.

Figures 127, tables 2, references 355.

Preface

Our attention was first drawn to island metal films and small particles during research on the nature of silver-oxygen-cesium photocathodes. A study of the very interesting optical and photoelectric properties of silver island films, especially when coated with cesium and its oxide, enabled us to explain the appreciable influence of small silver particles on the properties of these photocathodes. Later we were to observe completely new effects occurring in gold films. In studying the emission of hot electrons from silicon p-n junctions, we had to apply a gold film on the end face of the junction. At a certain voltage across the junctions, electron emission was observed that seemed to emanate from the gold film. Numerous control experiments with films of different thicknesses on different dielectric backings confirmed the effect of electron emission from gold films upon application of sufficient voltage and with passage of current. The emission was only from island films, and only cold, i. e. not associated with

heating of the film by the transmitted current. Moreover, we learned that cold electron emission is accompanied by cold luminescence of the films, i. e. by luminescence of film islands that are not incandescent. It is not surprising that these striking and completely unexpected effects have long riveted our attention on island metal films and small particles.

The desire to explain the nature of observed new effects, and the mutual relation between these effects and conduction current has led to many experiments and theoretical studies. The very effect of conductivity of films consisting of individual metal island particles on dielectric substrates is of independent interest, and it has been necessary to give attention to the mechanism of this conductivity as well. Some interesting properties of island films have also been observed in the study of conductivity. Some of these properties have been associated with peculiarities of film structure, which has necessitated a study of the problem of growth of islands and the structure of the films. In studying the properties of island films, we cannot avoid dealing with the properties of the separate islands themselves, which are microparticles of the metallic substance. And since physical arguments tell us that the properties of such particles with sufficiently small dimensions must differ from those of massive metals, their investigation is of considerable physical interest.

In studying the nature of luminescence, island metal films were subjected to electron bombardment. In doing this, unknown luminescence was observed. It was found that bombarding continuous films and massive metal with the same kind of electrons produces the same kind of luminescence. It was necessary to study the nature of this effect, the moreso as it promises important applications.

Generalization of these studies has been the content of this book. But if the work delineates research in the given area, it does so on an initial stage. The physics of fine solid particles and island films is still far from complete study, and our main goal has been to call attention to this interesting field. The wider the class of people who are involved in the area, the greater the depth and the faster the pace of investigation will be in studying these interesting objects, and the more intense will be the generation of new physical and practical ideas and the acceleration of their realization. If the publication of this book is in any way conducive to the attainment of this goal, the authors will feel that their labor has been rewarded.

Contents

6610
CSO: 1862/73

FLUID DYNAMICS

UDC 350.145.6

NONLINEAR DEFORMATION WAVES

Moscow NELINEYNYYE VOLNY DEFORMATSII in Russian 1981 (signed to press 4 Mar 81) pp 2-4, 256

[Annotation, preface and table of contents from book "Nonlinear Deformation Waves", by Yuriy Kustavich Engel'brekht and Uno Karlovich Nigul, USSR Academy of Sciences, ESSR Academy of Sciences, Institute of Cybernetics, Izdatel'stvo "Nauka", 1700 copies, 256 pages]

[Text] On the basis of general equations of the mechanics of continuous media, by introducing appropriate supplementary postulates, nonlinear mathematical models are constructed for describing wave processes of deformation of thermoviscoelastic, thermoelastic, viscoelastic and elastic solids and ideal compressible liquid. An examination is made of the construction of solutions of wave problems by sequential integration of simplified quasilinear equations (systems) derived by the ray method. Some specific examples are given.

In contrast to the conventional approach of nonlinear acoustics, where sine-wave pulses are considered as a rule, this book examines finite pulses of arbitrary shape.

The publication is intended for scientific workers, graduate students and upperclassmen interested in the theory of nonlinear waves.

Tables 11, figures 44, references 161.

Preface

Mathematical modeling of nonlinear wave processes has lately become more and more topical in mechanics, acoustics, plasma physics, electrodynamics, oceanology, seismology, astronomy and other areas of science and engineering. This can be attributed to the fact that an in-depth understanding of physical phenomena that take place in wave propagation, as well as their use in various technical applications in many cases are beyond the capacity of the linear theory of wave propagation. Although nonlinear wave processes have their own specific features in the different areas of science, it should be noted that systems of equations used to model the wave process, as well as efficient methods of constructing solutions, are in many cases analogous or even identical from the mathematical standpoint.

Therefore the nonlinear theory of wave propagation has now begun to take shape as a discipline developing at the confluence of several sciences.

This book is an attempt to treat a certain class of problems in the nonlinear theory of deformation wave propagation from a unified standpoint. Its content is divided into two parts.

The first part (chapters 1 and 2) deals with problems of construction of mathematical models (systems of equations) to describe the mechanics of nonlinear wave processes of deformation of thermoviscoelastic, thermoelastic, viscoelastic and elastic solids and ideal compressible liquid within the framework of classical (newtonian, nonrelativistic) mechanics.

The second part (chapters 3-5) examines methods of reducing the initial problems to sequential integration of simplified equations, as well as methods and results of construction of solutions of these simplified equations in the case of actions by finite pulses of arbitrary shape. In choosing material for the second part of the monograph, the authors took into consideration that U. K. Nigul's monograph "Echo Signals From Elastic Objects" (Tallin: Valgus, 1976, Vol 1) contains a detailed description of a method of sequential integration of linear equations of hyperbolic type, which has been used to solve many direct and inverse problems of propagation of one-dimensional pulses in laminar media. Therefore, to avoid repetition, this book has focused its main attention (chapters 3-5) on a different asymptotic approach known as the ray method, reducing the initial problem to sequential integration of simplified nonlinear equations. Of the two asymptotic approaches mentioned here, the former is more simply realized, but is suitable only in the region of minor nonlinear distortions of the pulse, while the latter, which is more complicated, enables description of the principal part of a nonlinear solution on any stage of pulse propagation.

Let us note that other important aspects of nonlinear wave theory have been examined recently in monographs by O. V. Rudenko and S. I. Soluyan "Theoretical Principles of Nonlinear Acoustics" (Moscow, Nauka, 1975), and [Dzh. Uizem] "Linear and Nonlinear Waves", Moscow, Mir, 1977.

Chapter 1 was written by U. K. Nigul, chapters 2-5--by Yu. K. Engel'brekht.

Contents page

6610
CSO: 1862/61

NUMERICAL MODELING OF GASDYNAMIC PROCESSES OCCURRING WHEN LASER EMISSION WITH MODERATE FLUX DENSITY ACTS ON METALLIC OBSTACLE IN AIR

Novosibirsk FIZIKA GORENIYA I VZRYVA in Russian Vol 17, No 6, Nov-Dec 81 (manuscript received 3 Oct 80) pp 77-82

[Article by G. S. Romanov and Yu. A. Stankevich, Minsk]

[Text] The mechanisms of formation and development of a plasma layer at the surface of a metal target that is located in air and absorbs intense laser emission have been both experimentally and theoretically investigated in a number of papers. Ref. 1-8 are most thorough and definite from the standpoint of tying in measurement data to laser pulse parameters (smooth neodymium laser pulse with duration of ~1 μs). These papers cover experimental and (in the case of the phase of one-dimensional planar expansion of the plasma layer) theoretical investigation of mechanisms that successively replace one another as radiation flux density increases: subsonic radiation wave, light detonation wave and supersonic radiation wave.

In view of the fact that time-profiled radiation pulses are generally realized in experiments, while calculations are done for constant density of the radiation flux, experiment and theory are compared in these works for certain selected parameters of the process such as maximum pressure on the target, maximum rate of dispersal of the plasma layer and certain others in time intervals $t_* \sim r_a/c_*$ limited by the condition of one-dimensional dispersal (r_a is the radius of the irradiated area on the target, c_* is the characteristic speed of sound in the plasma layer, $c_* \sim 10^5$-10^6 cm/s). This comparison showed satisfactory qualitative agreement, and with respect to the series of parameters named above, quantitative agreement as well between theoretical concepts and observed phenomena.

At the same time, available experimental information that is much more detailed than that used in theoretical analysis of phenomena in Ref. 1-8 enables us to consider the problem of direct numerical modeling of the aggregate of observed phenomena based on a gasdynamic computational model [Ref. 9-13] that accounts for one-dimensional and two-dimensional movement of plasma and of the ambient medium under the action of radiation pulses with the intensity distributions over the beam cross section and in time that are realized in an experiment. Such a computational model and comparison of the data that it yields on the dynamic characteristics of phenomena with the quite complete results of measurements given in Ref. 7 are considered in this article. In accordance with the data of Ref. 7

we study below the gasdynamic processes that take place at the surface of a bismuth target irradiated by bell-shaped monopulse laser radiation (with duration at half power level of $\tau_{1/2} \approx 0.4$-0.5 μs) with wavelength $\lambda = 1.06$ μm in the range of maximum radiation flux densities $q_{max} \sim 5$-200 W/cm^2 (so-called "moderate" flux densities) in which the subsonic radiation wave and light detonation wave conditions are realized.

1. The computational technique that is used here was described in Ref. 9-13 where it was used to model processes of formation and dynamics of the light detonation wave and supersonic radiation wave at the surface of an aluminum target in air. The method includes solution of the unsteady axisymmetric problem of heat conduction on heating and vaporization of an obstacle under the action of absorbed laser radiation on a circular spot of radius r_a, and solution of the unsteady axisymmetric gasdynamic problem of movement of vapor and the displaced ambient gas (air). We will briefly describe the procedure as applied to the given problem.

It was assumed in accordance with Ref. 7 that radiation traveling toward the surface of the target has intensity $q_0 = q_0(t)$ that is constant within the limits of the cross section of a cylinder with radius of 0.4 and 0.2 cm, and has a time dependence that is tabulated (Fig. 1). The quantity q_{max} and the total energy density E on the target are related by the expression $E = 0.53 q_{max}$, and the total energy E_0 for a target with $r_a = 0.4$ cm is defined by the relation $E_0 = 0.27 \times q_{max}$. Here q_{max} is expressed in MW/cm^2, E--in J/cm^2, and E_0--in J. Surface reflectivity R was determined by surface temperature T_0 in accordance with data of Ref. 14, i. e. the vapor and the air heated by the vapor-generated shock wave partly or totally absorbed both the incident radiation and that reflected from the surface. The obstacle was heated and vaporized in region $r \leqslant r_a$ under the action of incident radiation with flux density $q_a(r, t) = q_0(t)[1 - R(T_0)] \times \exp\left[-\int_0^\infty \varkappa_\nu(r, z)\, dz\right]$ (here $\varkappa_\nu$ is the coefficient of absorption of radiation by vapor and air, z is read out along the normal to the surface). Heat transfer was disregarded in the target in the radial direction, heating into the target ($z < 0$) was determined by the magnitude of the energy flux $q_a(r, t)$ delivered to the surface. The boundary parameters for vapor at the surface were assigned in accordance with Ref. 15 with consideration of ambient counterpressure; in accordance with this, vapor motion started upon heating of the surface above the boiling point, equal to $T_b = 1830$ K for bismuth [Ref. 16].

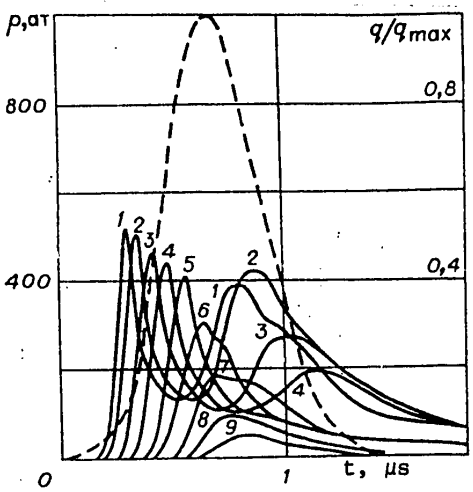

Fig. 1. Time dependence of laser emission intensity and pressure in the center of exposure spot on target surface: q_{max} [MW/cm^2] 1--200; 2--140; 3--70; 4--45; 5--25; 6-16; 7--10; 8--7; 9--5

To describe the movement of vapor and air in an eulerian coordinate system, the finite difference method of "coarse particles" was used [Ref. 17], generalized to the case of accounting for absorption of incident and reflected radiation by the vapor-air plasma. In contrast to Ref. 12, 13, re-radiation of energy by the plasma was disregarded due to a lack of data on the group coefficients of absorption of bismuth vapor. Motion of the contact boundary between vapor and air was followed by using markers--passive particles having a velocity equal to the localized velocity of motion of the medium. The equation of state and coefficients of absorption were tabulated in the form of dependences $p = p(\rho,\varepsilon)$ and $\kappa_\nu = \kappa_\nu(\rho,\varepsilon)$, where p is pressure, ρ is density, ε is the internal energy of a unit of mass of the medium, for air in accordance with the tables of Ref. 18, and for bismuth vapor in accordance with data of Ref. 19.

The computational grid for solving the problem [had] up to 34 cells along the r-coordinate (over the surface) and up to 60 cells along the z-coordinate (normal to the surface), providing satisfactory spatial resolution of flow parameters. As the gasdynamic perturbations approached one of the boundaries of the computational region, the dimensions of the computational cells in this direction were doubled, and as a result development of flow of the medium was traced over a fairly long time interval. In the given case motion was nearly one-dimensional over a considerable part of the emission pulse (up to $t \sim 1$ μs), appreciably improving the detail of motion description at the beginning of the process through introduction of cells $\Delta z \ll \Delta r$.

2. Calculations are done for versions with $q_{max} = 5$, 7, 10, 12, 16, 25, 46, 70, 140 and 200 MW/cm^2. We begin examination of the results with Fig 2, giving the distributions of parameters in a plasma jet formed by an emission pulse with $q_{max} = 200$ MW/cm^2 acting on a bismuth target with $r_a = 0.2$ cm. Time $t = 1.3$ μs corresponds to nearly total cessation of energy release. The given example is of interest in particular in the respect that here in the process of energy release there is a change in the conditions of propagation of the plasma front contrary to the radiation: the mode of the subsonic radiation wave is replaced by that of the light detonation wave when the radiation flux density on the target reaches $q_a \sim 130$ MW/cm^3 on the leading edge of the pulse (at $t \approx 0.5$ μs). The distribution of density in the jet shows a pronounced minimum of $\sim 5 \cdot 10^{-4}$ g/cm^3 (air density outside of the jet $\rho = 1.29 \cdot 10^{-3}$ g/cm^3) in the middle part in a region at a distance of from 2 to 5 mm from the surface. Schlieren photographs for the same kind of conditions given in Ref. 6, 7 for an aluminum target (as calculations

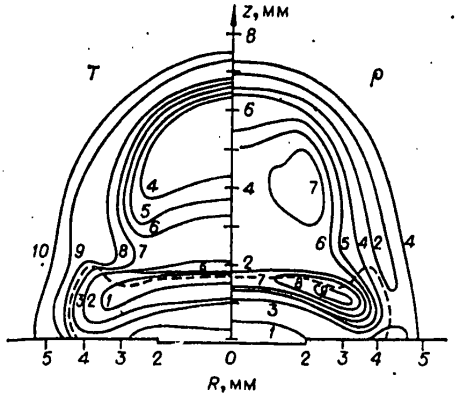

Fig. 2. Distribution of temperature T and density ρ in plasma jet at time $t = 1.3$ μs. T, eV: 1--5.6; 2--3.2; 3--2.5; 4--1.8; 5--1.6; 6--1.4; 7--1.3; 8--1; 9--0.4; 10-0.022. $\rho \cdot 10^3$, g/cm^3: 1--10; 2--3.2; 3--1.6; 4--1.3; 5--0.6; 6--0.5; 7--0; 8--0.3; 9--0.25

show, the latter circumstance does not alter matters since the vapor is situated much nearer the surface than the indicated region when aluminum and bismuth targets are used) clearly show a more transparent disk-shaped region at distances of ~3-5 mm that can be identified with the above-mentioned density minimum. The general shape, as well as the dimensions of the jet in the axial and transverse directions as measured from the schlieren pattern from Ref. 6, 7 and also with respect to Fig. 2 are likewise similar to one another. Even this implies that the given calculation satisfactorily transmits the dynamics of the phenomenon over the entire duration of the emission pulse.

Let us examine in more detail the space-time dependences of parameters for two typical versions of calculations. The distributions of parameters in the z direction at r = 0 for different instants within the duration of the emission pulse are shown in Fig. 3 and 4 for $q_{max} = 45$ and 140 MW/cm^2 respectively. Under these

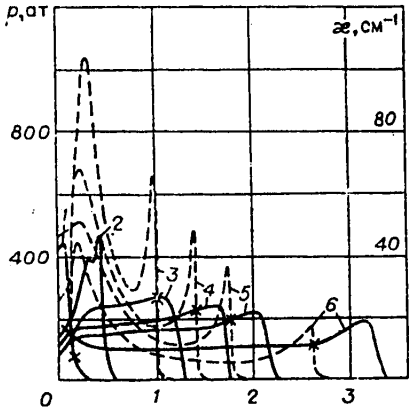

Fig. 2. Distribution along the z-axis for pressure p (—) and absorption coefficient κ_ν (---) at $q_{max} = 45$ MW/cm^2 at times t, μs: 1--0.5; 2--0.63; 3--0.795; 4--0.9; 5--1.0; 6--1.26

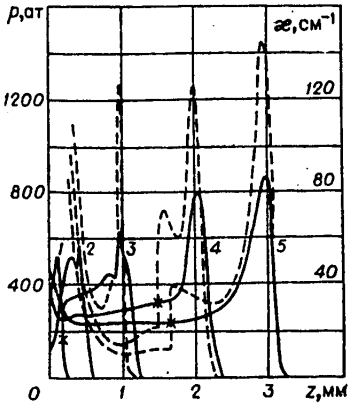

Fig. 4. Distribution along the z-axis for pressure p (—) and absorption coefficient κ_ν (---) at $q_{max} = 140$ MW/cm^2 at times t, μs: 1--0.4; 2--0.5; 3--0.63; 4--0.795; 5--0.9

conditions the pattern of motion in the paraxial region of the jet is still close to one-dimensional although its lateral distribution along the surface of the target may influence the integral characteristics (recoil momentum, etc.). It can be seen that the optical thickness of the vapor is great for both versions at $t \gtrsim 0.6$-0.8 μs, but formation of light detonation wave is possible only at sufficient magnitude of q: for the second version at $t \sim 0.6$ μs, when $q \cong 130$ MW/cm^2. The intensity of the shock wave generated by the vapor in air is here sufficient for the shock-compressed layer to begin to completely absorb radiation in the vicinity of the wave front, and to form a light-detonation complex.

Both versions of calculation are characterized by considerable vapor temperature --up to 5-7 Ev. These temperatures, calculated without consideration of processes

of radiative cooling of vapor, are apparently overstated by about 30%, which as noted in Ref. 5 is implied by the estimate of equality of the radiative and outwardly incident emission fluxes. The air temperature between the contact boundary and the shock wave front is considerably lower: in the first version it is less than 1 eV; in the second version by time ~0.6 μs and later it begins to exceed 1 eV, which is sufficient to change absorption from vapor to air [Ref. 20].

Transition from the subsonic radiation wave to the light detonation wave in the given case takes place under the action of gasdynamic forces: the piston action of vapor on air is decisive in the process of increasing its temperature to the point of initiation of absorption $T_* \sim 1.2\text{-}1.5$ eV [Ref. 20]. However, estimates of the rate of propagation of a subsonic radiation wave according to Ref. 20 show that under the given conditions the difference between the propagation velocity and the mass velocity of the medium in the vicinity of the contact boundary is still small, i. e. actually the motion of the plasma front is determined by gasdynamic processes. Supplementary to this, let us mention the nearly complete coincidence of measurements in Ref. 7 and the calculated maximum velocities of dispersal u_{max} of the plasma front from the surface both in the region of existence of subsonic radiation wave conditions and in the region of values $q_{max} > 130$ MW/cm^2 that ensure transition to the light detonation wave conditions in the process of action: at $q_{max} = 50$, 140, 200 MW/cm^2 these velocities were $u_{max} = 4$, 8, 11 km/s respectively. The measured and calculated hodographs of the jet front also coincide.

Let us consider the time dependences of pressure in the center of the target for versions of calculations with different values of q_{max} (see Fig. 1). Here, just as in the experiments of Ref. 1, 7, two pronounced pressure maxima can be observed: the first corresponding to vaporization of the target, and the second corresponding to arrival of perturbations from the absorption spike on the vapor-air interface at the surface. In the calculations the time of onset of the second maximum is somewhat less than in the experiment of Ref. 7, and its value p_{max} at $q_{max} > 100$ MW/cm^2 is somewhat greater. It must be borne in mind here that pressure averaged over the surface of the sensor (and target) was recorded in the experiment. If the calculated pressure were averaged over the target, the value of p_{max} would be reduced (due to two-dimensional vapor movement); these differences continue to decrease with increasing averaging surface, although some discrepancy remains. This can be attributed to the peculiarities of the registration system in Ref. 7 (some time lag of the pressure sensor, some arbitrariness in combining the emission pulse and pressure oscillograms and so on), as well as to incomplete reproduction of the emission pulse parameters in the calculation (for example the nonuniformity of distribution of radiation intensity over the spot that was unaccounted for in the calculations was estimated in Ref. 7 by a value of ±20%). At the same time, just as in Ref. 7, p_{max} falls off somewhat beginning at $q_{max} \sim 130$ MW/cm^2.

A quantity of definite interest is the specific recoil momentum η: the ratio of the recoil momentum I acting on the target to the energy E_0 delivered to the target ($\eta = I/E_0$). The quantity η by time $t = 20$ μs from the start of the emission pulse is plotted as a function of q_{max} on Fig. 5, from which we see that the discrepancy between calculation and experiment does not exceed the spread of measurement results. The nature of the dependence of η on q_{max} is also reproduced--the

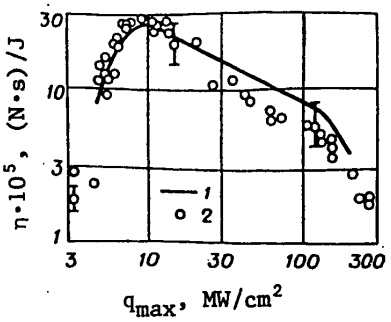

Fig. 5. Specific recoil momentum as a function of maximum flux density of laser emission: 1--calculation; 2--Ref. 7

rise in η up to $q_{max} \cong 10$ MW/cm^2 due to increase in vapor mass and reduction in losses to thermal conduction in the target, the relatively smooth fall-off in the region $q_{max} \leqslant 100$ MW/cm^2 due to absorption of emission in the vapor and reduction of energy losses on vapor heating, and finally the steeper drop at $q_{max} >$ 100 MW/cm^2 due to formation of the light detonation wave and more rapid departure of the absorption front from the surface as well as to the considerable influence of two-dimensionality.

Thus, the aggregate of the cited computational data and their comparison with the experiment of Ref. 6, 7 show that the described computational model properly imparts the behavior of gasdynamic processes at the surface of a target in the one-dimensional and two-dimensional phases of development.

REFERENCES

1. Kozlova, N. N., Petrukhin, A. I., et al., FIZIKA GORENIYA I VZRYVA, Vol 11, No 4, 1975, p 650.

2. Kozlova, N. N., Markovich, I. E., et al., KVANTOVAYA ELEKTRONIKA, Vol 2, No 9, 1975, p 1930.

3. Petrukhin, A. I., Nemchinov, V. A., Rybakov, V. A., PIS'MA V ZHURNAL TEKHNICHESKOY FIZIKI, Vol 3, No 4, 1977, p 158.

4. Nemchinov, V. A., Orlova, T. I., FIZIKA PLAZMY, Vol 4, No 4, 1978, p 949.

5. Nemchinov, V. A., Polozova, I. A., KVANTOVAYA ELEKTRONIKA, Vol 6, No 6, 1979, p 1223.

6. Nemchinov, V. A., Petrukhin, A. I., et al., DOKLADY AKADEMII NAUK SSSR, Vol 244, No 4, 1979, p 877.

7. Markovich, I. E., Petrukhin, A. I., et al., FIZIKA GORENIYA I VZRYVA, Vol 15, No 4, 1979, p 30.

8. Markovich, I. E., Nemchinov, V. A., et al., FIZIKA GORENIYA I VZRYVA, Vol 15, No 4, 1979, p 37.

9. Romanov, G. S., Stankevich, Yu. A., DOKLADY AKADEMII NAUK BELORUSSKOY SSR, Vol 21, No 6, 1977, p 503.

10. Romanov, G. S., Stankevich, Yu. A., in: "Dinamika sploshnoy sredy" [Dynamics of Continuous Medium], No 9, Novosibirsk, 1979.

11. Romanov, G. S., Stankevich, Yu. A., "Tezisy dokladov Tret'yey Vsesoyuznoy konferentsii po dinamike izluchayushchego gaza" [Abstracts of Reports to the Third All-Union Conference on Dynamics of a Radiating Gas], Moscow, 1977.

12. Bonch-Bruyevich, A. M., Zinchenko, V. I. et al., "Tezisy dokladov Chetvertogo Vsesoyuznogo soveshchaniya po nerezonansnomu vzaimodeystviyu opticheskogo izlucheniya s veshchestvom" [Abstracts of Reports to the Fourth All-Union Convention on Nonresonant Interaction of Optical Radiation With Matter], Leningrad, 1978.

13. Yel'yashevich, M. A., Romanov, G. S., Stankevich, Yu. A., "Tezisy dokladov Chetvertogo Vsesoyuznoy konferentsii po dinamike izluchayushchego gaza" [Abstracts of Reports to the Fourth All-Union Conference on Dynamics of a Radiating Gas], Moscow, 1980.

14. Golub', A. P., Markovich, I. E., et al., Article deposited in the All-Union Institute of Scientific and Technical Information, No 3300-79, 1979.

15. Anisimov, S. I., Imas, Ya. A. et al., "Deystviye izlucheniya bol'shoy moshchnosti na metally" [Action of High-Power Radiation on Metals], Moscow, Nauks, 1970.

16. Slavinskiy, M. P., "Fiziko-khimicheskiye svoystva elementov" [Physicochemical Properties of Elements], Moscow, Metallurgizdat, 1952.

17. Belotserkovskiy, O. M., Davydov, Yu. M., ZHURNAL VYCHISLITEL'NOY MATEMATIKI I MATEMATICHSKOY FIZIKI, Vol 11, No 1, 1971, p 182.

18. Kuznetsov, N. M., "Termodinamicheskiye funktsii i udarnyye adiabaty vozdukha pri vysokikh temperaturakh" [Thermodynamic Functions and Shock Adiabats of Air at High Temperatures], Moscow, Mashinostroyeniye, 1965.

19. Yel'yashevich, M. A., Borovik, F. N. et al., "Tezisy dokladov Chetvertogo Vsesoyuznoy konferentsii po dinamike izluchayushchego gaza" [Abstracts of Reports to the Fourth All-Union Conference on Dynamics of a Radiating Gas], Moscow, 1980.

20. Rayzer, Yu. P., "Lazernaya iskra i rasprostraneniye razryadov" [Laser Spark and Propagation of Discharges], Moscow, Nauka, 1974.

21. Bergel'ston, V. I., Loseva, G. V., Nemchinov, V. A., ZHURNAL PRIKLADNOY MEKHANIKI I TEKHNICHESKOY FIZIKI, No 4, 1974, p 12.

6610
CSO: 1862/85

LASERS AND MASERS

UDC 621.373

MECHANISM OF PULSED LASING IN HIGH-PRESSURE ELECTRIC DISCHARGE Ar-Xe-LASER

Moscow KVANTOVAYA ELEKTRONIKA in Russian Vol 8, No 11(113), Nov 81 (manuscript received 13 Feb 81) pp 2425-2432

[Article by V. N. Lisitsyn and A. R. Sorokin, Thermophysics Institute of the Siberian Department, USSR Academy of Sciences, Novosibirsk]

[Text] On the basis of studying the characteristic behavior of spontaneous and induced emission during pulsed electric discharge in a mixture of Ar and Xe, an analysis was made of the population processes of the atomic laser levels of xenon, and the efficiency of excitation transfer from argon to xenon atoms was estimated. A conclusion was drawn regarding the excitation of laser levels by direct electron impact from the ground state. Improvement of the energy characteristics of the laser and variation of the spectral composition of the emission with an increase in xenon pressure and the addition of argon are connected with significant variation of the electron distribution function with respect to energies. It is possible to neglect the excitation transfer from argon to xenon atoms in the electric discharge. The latter is important for creating electron beam preionized and electric discharge XUV lasers utilizing Xe_2 dimers.

This paper is devoted to the study of the processes of exciting xenon levels in the working mixture of a high-pressure Ar-Xe laser.

It is known [1] that in low-pressure lasers utilizing IR transitions of inert atoms, the output power of the emission does not exceed a few tens of watts with an efficiency of $\sim 10^{-5}$. Increasing the heavy inert gas content in mixtures with helium made it possible significantly to increase the radiation power ($\sim 10^5$ watts) and efficiency ($\sim 10^{-3}$) [2, 3]. The replacement of helium by argon in an electron beam preionized Ar-Xe-laser led to further increase in efficiency (10^{-2}) [4]. The use of discharge through a dielectric having increased stability expanded the operating range of the Ar-Xe-laser to 7 atm [5]. The transition to high pressures was accompanied by variation of the spectral composition of the emission.

The level population processes in an Ar-Xe mixture were investigated in an electric discharge with small ($\leq 0.1\%$) [6] xenon content and in an electron beam preionized laser with large (0.7%) [4] xenon content. The excitation transfer from

argon molecules to xenon atoms on excitation by an electron beam and with a xenon content $p_{Xe} \geq 0.3 p_{Ar}$ was investigated in [7]. In an electric discharge laser with optimal xenon content (~1.5%) such studies were not performed.

The discovery of population channels of atomic levels in an Ar-Xe mixture is important not only for the Ar-Xe-laser, but on the whole for high-pressure lasers in which, as a rule, inert gases are used, in particular, to create electron beam preionized [8] and electric discharge [5] lasers utilizing Ar_2, Xe_2 dimers.

The purpose of this experiment was to determine the basic mechanisms participating in the excitation of laser levels of the electric discharge Ar-Xe-laser and estimation of the efficiency of the excitation transfer from argon to xenon atoms based on studying the characteristic behavior of spontaneous and induced emissions of a gas discharge plasma under various conditions.

Experimental Results and Discussion

1. Experimental Setup. Two discharge cell designs were used in the experiments: for investigation of lasing, a cell with double transverse discharge [2] 60×1.5×0.6 cm (electrode spacing 1.5 cm); to study spontaneous emission, a cell with exposure through a cathode grid 4×0.9×0.5 cm. The exposure discharge was realized between an auxiliary electrode coated with glass and the grid. For attenuation of the radiation reabsorption, the observations were made across the cell so that the thickness of the plasma column focused on the MDR-2 monochromator was 0.5 cm.

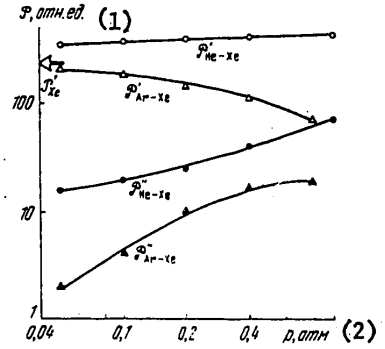

Figure 1. Spontaneous emission power on the 0.47 micron line for the first ($\mathcal{P}'$) and second ($\mathcal{P}''$) glow components as a function of the pressures of Ar-Xe and He-Xe mixtures (the subscripts on $\mathcal{P}$); p_{Xe}=0.01 atm; the current was kept constant.

Key:
1. relative units
2. atmospheres

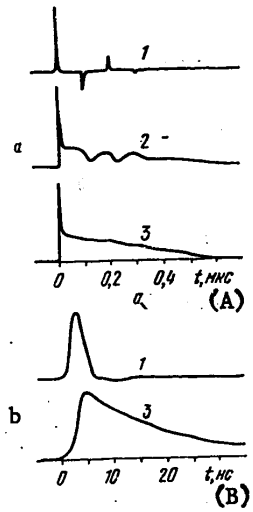

Figure 2. Oscillograms of the current (1) and spontaneous emission at λ=0.47 (a) and 0.98 microns (b) in mixtures of He-Xe (2) and Ar-Xe (3) for p=0.5 atm, p_{Xe}=0.01 atm.

Key:

A. microseconds
B. nanoseconds

A cable energy storage element commuted by a gas-filled discharger through a transmitting cable line to the cell was used to excite the discharge. The ratio of the maximum voltage on the cell to the closest secondary peak was 60, the discharge current duration was $\lesssim$7 nanoseconds with respect to the base. The electromagnetic pumping wave reflected from the cell was again incident on the cell after 100 nanoseconds.

A high-speed recording system including the "Dnepr" and ELU-FK14 photodetectors and also the S1-75 oscillograph made it possible to take the measurements with time resolution of 10 nanoseconds.

2. Spontaneous Emission. In reference [6] it was demonstrated that with a small xenon content (<0.1%) in the Ar-Xe mixture, the glow of the Xe lines on the transitions 6p', 7p-6s belonging to the spectral region of 0.45-0.5 micron is appreciably more intense than with pure Xe. The growth of the intensity is caused by radiation cascades from 9d level which, in turn, are populated as a result of resonance excitation transfer from the $4s'[1/2]_1$ level of argon. The corresponding resonance defect ~100 cm^{-1}. It was of interest to discover that this emission behaves in accordance with the optimal conditions for lasing with time with large xenon concentration.

The emission in the spectral range of 0.45 to 0.5 micron is observed in the form of two components. The first component lasting 7 nanoseconds coincided in time with the pumping pulse, the second component was observed in the discharge afterglow. The λ=0.47 micron line ($7p[5/2]_2$-$6s[3/2]^0_2$) which is most intense in the afterglow was selected for the investigations.

Figure 1 shows the spontaneous emission power for both components $\mathcal{P}'$ and $\mathcal{P}''$ as a function of the pressure of the Ar-Xe and the He-Xe mixtures, and the arrow indicates the intensity of the $\mathcal{P}'_{Xe}$-line in pure Xe.

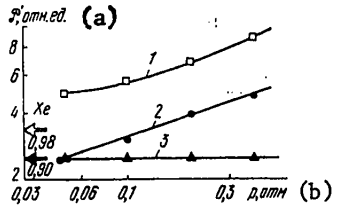

Figure 3. Spontaneous emission power $\mathcal{P}'$ at λ=0.98 (1) and 0.9 micron (2, 3) as a function of the pressure of Ar-Xe (1,3) and He-Xe (2) mixtures. The arrows indicate the radiation intensities in pure xenon; p_{Xe}=0.01 atmosphere, the current was kept constant

Key:
a. Relative units
b. atmospheres

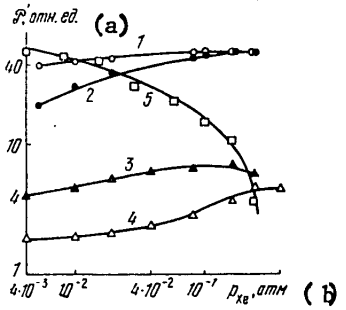

Figure 4. Spontaneous emission power $\mathcal{P}'$ on λ=0.47 (1, 2) and 0.98 micron (3,4) in xenon (1,4) and in an Ar-Xe mixture (2,3) as a function of the xenon pressure; 5 -- also in an Ar-Xe mixture are the 0.91 micron line of argon $(4p[1/2]_1-4s[3/2]^0_2$. In the mixture p_{Ar}=0.4 atm, the current was kept constant.

Key:
a. Relative units
b. atmospheres

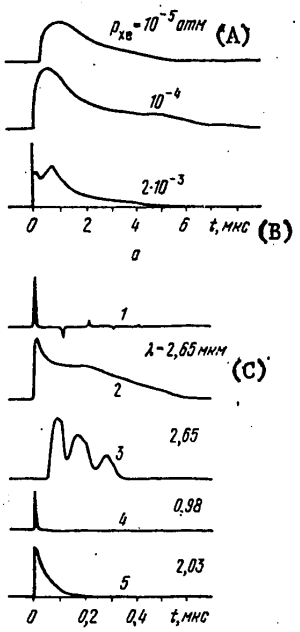

Figure 5. Lasing oscillograms at λ=2.65 microns in an Ar-Xe mixture for p=0.1 atm and different xenon contents (a) and also current (1) and lasing oscillograms for p=0.5 atm, $p_{Xe}=5\cdot10^{-3}$ atm in Ar-Xe mixtures (2,4,5) and He-Xe mixtures (3) (b)

Key:
A. atmospheres
B. microseconds
C. microns

Figure 2, a shows spontaneous glow oscillograms on the 0.47 micron line. It is obvious that the origin of the components $\mathcal{P}_{He-Xe}$ and $\mathcal{P}_{Ar-Xe}$ is different. In the former case the troughs in the glow from the damping pumping oscillations indicate the recombination nature of the population [9], as should occur for the He-Xe-laser [10]. In the second case the afterglow pulse is naturally related to the excitation transfer from argon.

Let us note that the absence or small magnitude of the recombination flux on the 7p level indicates either "capture" of it at higher levels by argon or the presence of other recombination channels; we did not study this question.

The first glow component theoretically can also be connected with transfer from argon. The transfer constant $k\sim5\cdot10^{-9}$ cm^3/sec [6]. For $p_{Xe}=10^{-2}$ atm equalization of the 9d level populations of xenon and 4s of argon must take place in the time ~1 nanosecond. However, for $p_{Xe}\sim10^{-5}$ to 10^{-4} atm this time is sufficiently large to note a delay t_m of the maximum spontaneous glow of the first component after completion of the exciting pulse under the condition that the 7p level population of Xe predominates as a result of transfer from Ar*.

This delay was absent on all of the investigated lines 6p', 6p, 7p-6s, including the IR transition lines. In addition, the glow of the first component (λ=0.47 micron) decreases with an increase in the argon content, and the glow of the second component increases, that is, the mechanisms of their excitation are different.

Thus, the first component of the glow must be connected with electron excitation. Let us note that measurements in a mixture of Ar-Kr where resonance transfer from the argon is absent demonstrated [6] that the basic method of populating the Kr levels is also electron excitation.

The study of the IR transitions 6p-6s is of special interest. The most powerful laser lines end on the 6p levels, and lasing is observed from the 6p $[1/2]_1$ level. Spontaneous emission on the 6p-6s transition also consisted of two components, but the afterglow pulse was so small that it was hardly distinguishable against the detector background noise. In contrast to the emission $\mathcal{P}_{Ar-Xe}$ from the higher levels 7p and 6p', the spontaneous glow, for example, of the transition $6p[1/2]_1$-$6s[3/2]_2^0$ (λ=0.98 micron) increased on addition of argon and increasing the pressure of the Ar-Xe mixture (Figure 3).

Figure 2,b shows the radiation oscillogram on the 0.98 micron line. The maximum glow was reached during pumping. The upper level of this line is located above the resonance level $6s'[1/2]_1$ by a total of 84 cm^{-1}. In the case of Boltzmann distribution the populations of these levels at kT~300 cm^{-1} are related by the expression $[6p[1/2]_1]=0.75[6s'[1/2]_1]$. The reaction constant

$$Xe(6s'[1/2]_1) + Xe(^1S_0) \rightarrow Xe(6p[1/2]_1) + Xe(^1S_0) - \Delta E$$

$k=6.65\cdot10^{-11}$ cm^3/sec [11]. For pure xenon when p_{Xe}=0.01 atm the characteristic excitation transfer time ~60 nanoseconds. However, even in pure xenon at this pressure t_m=0. This indicates satisfaction of the inequality for the populations $[6p[1/2]_1]>0.75[6s'[1/2]_1]$ so that inversion possibly occurs on this transition.

For the XUV laser utilizing Xe_2 dimers, higher xenon concentrations in the argon are used than those investigated above. Excitation of the Ar-Xe mixture by an electron beam with xenon content $p_{Xe}\geq 0.3\ p_{Ar}$ demonstrated the high efficiency of population of the Xe levels as a result of excitation energy transfer from argon molecules [7]. During electron beam pumping where the electrons have an energy of hundreds of kiloelectron volts, the argon excitation efficiency is maintained for the xenon content.

In an electric discharge as a result of a relative decrease in efficiency of interaction of the electrons with the argon with an increase in the Xe content in the mixture, the influence of the argon on the Xe level population processes is reduced [see Figure 4). Thus, the intensity of the spontaneous emission on all of the investigated transitions Xe in a mixture Ar:Xe=2:1 (p_{Xe}=0.2 atm) becomes the same as in pure Xe.

Thus, from the nature of the behavior of spontaneous glow of xenon on the transition 7p, 6p'-6s and 6p-6s in an Ar-Xe mixture it is possible to conclude that the first component $\mathcal{P}'$ is related to the electron excitation, and the second component $\mathcal{P}''$ is related to the excitation transfer from the argon. With

a high xenon content in the mixture ($p_{Xe} \geq 0.5\ p_{Ar}$) it is possible to neglect the influence of the argon on the Xe population processes. With an increase in argon pressure, the number of fast electrons in the discharge decreases with a simultaneous increase in the number of electrons which belong energywise to the zone of effective excitation of the low xenon levels.

3. Laser Emission. Lasing of an Ar-Xe-laser was observed in the form of one or two components.

With a small xenon content ($p_{Xe} \sim 10^{-5}$ to 10^{-4} atm) when the population of the Xe levels by electrons is small [6] lasing was observed only on the 2.65 micron line in the afterglow (Figure 5,a). Its duration was reduced with an increase in both the Xe content and the total pressure of the mixture. In contrast to the He-Xe laser, the modulation of the radiation from pumping oscillations in the case of the Ar-Xe laser was absent (Figure 5, b). Under optimal conditions for the total output power, the contribution of the 2.65 micron line to the emission did not exceed 5% (see the table).

Increasing the xenon pressure led to the appearance of the first component both on the 2.65 micron line (see Figure 5) and on all remaining lines (see the table). The emission of the first component for the self-limited transition 6p-6s ended simultaneously with the current pulse, and for the 5d-6p transitions it continued also in the discharge afterglow (see Figure 5, b).

Thus, almost all of the emission of an Ar-Xe-laser is concentrated in the first component, the excitation of which is realized in the pumping process. The lasing duration is determined in this case by the ratio of the lifetime of the upper and lower laser levels. In the investigated case 6s levels are metastable, and the 5d lifetimes are greater than 6p.

Comparing the presented lasing characteristics with the behavior of spontaneous emission, it is possible to conclude that the first component is related to excitation by electrons, and the second, to energy transfer from argon.

The laser levels can be populated by electrons either from the ground state or in steps through the lower 6s-levels.

For explanation of the high efficiency of an electron beam preionized Ar-Xe laser utilizing 5d-6p transitions, in reference [4] the mechanism of stepped excitation was used. In this laser an electron beam and discharge in the initial phase when E/N is large creates high concentration of metastable xenon. Then when E/N decreases by an order, during the course of about 7 microseconds the laser operates as a result of excitation and ionization of the atoms in the 6s-states by relatively slow electrons.

In reference [4] it was demonstrated that the mechanism of step excitation of the upper laser levels is not basic in the initial discharge phase when E/N is large. In addition, in [4] approximately 75% of the emitted power fell to the 1.73 micron line, and lasing on the 2.03 micron line which was more powerful in our case was observed only during operation of the electron beam (see the table).

Laser Transitions in XeI

(1) Длина волны λ, мкм	(2) Переход, [jl]-связь	(3) Сила осциллятора, отн. ед. [14]	(4) Распределение излучения по линиям				
			(5) Электроразрядные лазеры				(6) Электронно-ионизационные лазеры
			Xe, 10^{-5} атм [1][a]	He—Xe, 1 атм [3,15]	Ar—Xe, 1 атм [5]	Ar—Xe, 7 атм [5]	Ar—Xe, 2 атм [4]
0,82	$6p\,[3/2]_2 - 6s\,[3/2]_2^0$	9	—	<0,05[d]	—	—	—
0,98	$6p\,[1/2]_1 - 6s\,[3/2]_2^0$	5	—	<0,05	<0,05	<0,05	—
1,73	$5d\,[3/2]_1^0 - 6p\,[5/2]_2$	9	0,097	<0,05	0,4	—	0,75
2,03	$5d\,[3/2]_1^0 - 6p\,[3/2]_1$	80	0,23	0,5	0,4	0,25	0,03[b]
2,48	$5d\,[5/2]_3^0 - 6p\,[5/2]_3$	120	—	—	<0,05	—	—
2,63	$5d\,[5/2]_2^0 - 6p\,[5/2]_2$	84	—	—	0,1	0,3	0,15
2,65	$5d\,[3/2]_1^0 - 6p\,[1/2]_0$	50	0,048	0,15	0,05	0,1	0,06[b]
3,11	$5d\,[5/2]_3^0 - 6p\,[3/2]_2$	294	0,045	—	<0,05	—	—
3,37	$5d\,[5/2]_2^0 - 6p\,[3/2]_1$	189	0,048	—	—	0,35	c
3,43	$7p\,[5/2]_2 - 7s\,[3/2]_1^0$	9	—	0,07	—	—	—
3,65	$7p\,[1/2]_1 - 7s\,[3/2]_2^0$	5	0,013	0,29	—	—	—
5,13	$7f\,[3/2]_{1,2} - 5d'\,[3/2]_1^0$	0	—	<0,05[d]	—	—	—
5,58	$5d\,[7/2]_4^0 - 6p\,[5/2]_3$	540	0,129	—	<0,05	—	—

Key:
1. Wavelength, λ, microns
2. Transition, [jl]-bond
3. Oscillator strength, relative units [14]
4. Radiation distribution by lines
5. Electric discharge laser
6. Electron beam preionized laser

a -- the only lines presented are those on which lasing is observed also at high pressures; b -- lasing is observed only from an electron beam at low Ar-Xe pressure; c -- weak lasing is observed only with a diffraction grating; d -- lasing is observed only at increased pressures

Thus, the first component of the lasing to which the major part of the emitted power fell is most probably connected with direct electron excitation from the ground state.

There are sufficient experimental data to explain a number of peculiarities in the variation of the spectral composition of the stimulated emission in different cases. In pure low-pressure xenon only 40 laser transitions are known [12], part of which are presented in the table. The addition of a buffer gas and transition to increased pressures greatly impoverishes the spectral composition of the laser emission which also depends on the grade of the buffer gas.

The absence of lasing from 7p and higher levels with the addition of argon is connected with a decrease in the population rate of the higher xenon levels under these conditions (see Figure 1). Decreasing the number of fast electrons with an increase in the argon pressure also leads to a decrease in the proportion of the laser emission from the $5d[3/2]^0_1$ level from 0.85 (p=1 atm) to 0.35 (p=7 atm, see the table). At the same time, growth of the number of electrons belonging to the zone of effective excitation of the lower level $5d[5/2]^0_2$ leads correspondingly to an increase in the proportion of the laser emission from 0.1 (p=1 atm) to 0.65 (p=7 atm). Let us pay attention to the fact that emission from this level leads to a population of the same levels as lasing from the $5d[3/2]^0_1$ level.

The probabilities of transitions for the 1.73 and 2.03 micron lines beginning with the $5d[3/2]^0_1$ level differ by an order, but in pure Xe the lasing intensities on them are distinguished by only two times, which indicates more efficient population of the lower laser level $6p(3/2)_1$ by comparison with $6p[5/2]_2$.

On addition of He the population of the $6p[5/2]_2$ level increases, and on addition of Ar it remains invariant (see Figure 2). As a result, lasing on λ=1.73 microns in an He-Xe mixture becomes weaker, and in an Ar-Xe mixture at atmospheric pressure, comparable with the lasing on 2.03 microns (see the table).

4. Analysis of the Xe Level Population Processes. The characteristic features of population of atomic levels by electrons under different conditions are determined by the nature of the dependence of the level excitation cross sections on the electron energy and the electron energy distribution function (EDF). In turn, the EDF is given by the value of E/N in the discharge.

Increasing the pressure leads to an increase in the frequency of the electron collisions with atoms. Consequently, the absolute number of acts of ionization and, consequently, n_e, increases. However, for this reason the electron drift rate decreases. The first process leads to reduction of the electric field E, and the latter process, to an increase in the electric field E. As a result, E increases with pressure, but the value of E/N decreases, in our cases approximately proportionately to $p^{-0.7}$, and for p=1 atm it is $2\text{-}3\cdot10^{-16}$ volt-cm^2.

Reduction of E/N with an increase in xenon pressure leads to a relative decrease in the number of fast electrons in the discharge. This, in turn, leads to the fact that the role of the lower levels having relatively large electron excitation cross sections near the excitation threshold increases in the absorbed energy balance. The growing efficiency of the excitation of these levels determines the spectral composition of the laser emission on addition of the buffer gas.

The energy distribution with respect to different levels of atoms is only sensitive to the value of E/N. For example, the maximum excitation cross section of the 2^3P level of helium is 5 times less than the resonance 2^1P (these levels are 0.27 ev from each other). However, there is a region of ~6 ev where the cross section 2^3P exceeds the cross section 2^1P. Therefore for E/N<$4\cdot10^{-16}$ V-cm^2 the 2^3P state must be excited more efficiently than 2^1P [13].

Addition of a buffer gas leads to an increase in the elastic scattering of the electrons and an additional increase in energy losses of the fast electrons to inelastic collisions with the buffer gas. A consequence of this is additional increase in the intensity E and an increase in the number of electrons belonging to the zone where the working levels are located. As a result, more favorable conditions are created for excitation of lower xenon levels.

The presented qualitative explanation of the xenon level population processes agrees with the experimental results described in items 2 and 3.

Conclusion

The basic conclusion of this work is that the determining mechanism of the excitation of the upper laser levels of xenon in an electric discharge Ar-Xe-laser is direct electron impact from the ground state. The improvement of the energy characteristics of the laser and variation of the spectral composition of the emission with an increase in xenon pressure and the addition of argon are connected with significant alteration of the EDF under these conditions.

For optimal xenon content for lasing of an IR laser utilizing Xe transitions and higher xenon content the excitation energy transfer from argon to the Xe atoms can be neglected. This conclusion is important for electron beam preionized and electric discharge XUV lasers utilizing Xe_2 dimers.

BIBLIOGRAPHY

1. Linford, G. J. IEEE J., QE-8, 1972, p 477.

2. Fahlen, T. S.; Targ., R. IEEE J., QE-9, 1973, p 609.

3. Sorokin, A. R. ZhTF [Journal of Technical Physics], No 49, 1979, p 1673.

4. Lawton, S. A.; Richards, J. B.; Newman, L. A.; Specht, L.; De Temple, T. A. J. APPL. PHYS., No 50, 1979, p 3888.

5. Lisitsyn, V. N.; Sorokin, A. R. PIS'MA V ZHTF [Letters of the Journal of Technical Physics], No 5, 1979, p 876.

6. Gedanken, A.; Jorther, J.; Raz, B.; Szoke, A. CHEM. PHYS., No 57, 1972, p 3456.

7. Danilychev, V. A.; Kerimov, O. M.; Kovsh, I. B. TRUDY FIAN [Works of the Physics Institute of the USSR Academy of Sciences], No 85, 1976, p 49.

8. Basov, N. G.; Danilychev, V. A.; Dolgikh, V. A.; Kerimov, O. M.; Lobanov, A. N.; Podsosonnyy, A. S.; Suchkov, A. F. KVANTOVAYA ELEKTRONIKA [Quantum Electronics], No 2, 1975, p 28.

9. Gudzenko, L. I.; Yakovlenko, S. I. PLAZMENNYYE LAZERY [Plasma Lasers], Moscow, Atomizdat, 1978.

10. Shuker, R.; Szöke, A.; Zamir, E.; Bimor, Y. PHYS. REV., No A11, 1975, p 1187.

11. Sadeghi, N.; Sabbagh, J. PHYS. REV., No A16, 1977, p 2336.

12. SPRAVOCHNIK PO LAZERAM [Laser Handbook], edited by A. M. Prokhorov, Moscow, Sov. radio, 1978.

13. Baranov, V. Yu.; Borisov, V. M.; Vysikaylo, F. I.; Kiryukhin, Yu. B.; Kochetov, I. V.; Mamontov, S. G.; Pavlov, V. G.; Pis'mennyy, V. D.; Stepanov, Yu. Yu.; Khristoforov, O. B. PREPRINT IAE [Preprint of the Nuclear Power Institute], Moscow, No 3080, 1979.

14. Faust, W. L.; McFarlane, R. A. J. APPL. PHYS., No 35, 1964, p 2010.

15. Chapovsky, P. L.; Lisitsyn, V. N.; Sorokin, A. R. OPTICS COMMS., No 16, 1976, p 33.

10845
CSO: 1862/75

UDC 621.375.826

CATALYTIC RECOVERY OF GAS MIXTURE OF CLOSED-CYCLE ELECTRON BEAM PREIONIZED CO_2 LASER

Moscow KVANTOVAYA ELEKTRONIKA in Russian Vol 8, No 11(113), Nov 81 (manuscript received 13 Feb 80) pp 2418-2424

[Article by Z. I. Ashurly, I. K. Babayev, A. P. Dzisyak, V. N. Komarov, S. Ye. Kupriyanov (deceased), A. I. Lazurchenkov, V. K. Orlov, A. A. Perov, V. V. Savel'yev and N. V. Cheburkin, Scientific-Research Physical Chemistry Institute imeni L. Ya. Karpov, Moscow]

[Text] We investigated the possibility of using a catalytic regenerator to recover the gas mixture in a continuous-wave CO_2-laser. The regenerator permits stabilization of the characteristics of a closed-cycle electron beam preionized CO_2-laser without replacing the gas mixture.

The electric discharge time characteristics of the laser are presented. A mass-spectrometric analysis was made of the variation of the gas mixture composition during operation of the laser. A procedure is described for calculating the parameters of the gas mixture regenerator.

1. At the present time the problem of creating electric discharge-pumped carbon dioxide gas lasers is an urgent problem. The high power and efficiency of such lasers will permit successful application of them in many branches of science and engineering. In particular, self-maintained discharged-pumped lasers are used to work materials [1, 2]. Lasers in which electron beam preionization is used to excite the gas mixture are prospective [3]. They have found application at the present time in engineering [4, 5].

Fast (to 100 m/sec) pumping of the gas mixture through the discharge gap is used in laser systems. The gas mixture is either discharged to the atmosphere (open cycle) or after cooling in a heat exchanger it is returned to the input of the discharge chamber (closed cycle). Operation of the laser in the open cycle permits higher power inputs to the gas mixture [6], but when solving problems requiring prolonged continuous operation, a closed-cycle laser is preferable.

2. During closed-cycle operation of a laser, products of decomposition of the gas mixture accumulate in its gas dynamic circuit (GDC). In references [8, 9] basic reactions that take place in an electric discharge and lead to variation of the initial composition of the gas mixture containing CO_2, N_2 and He are presented:

$$CO_2+\bar{e} \rightarrow CO+O+\bar{e}, \quad (1)$$

$$O+O+M \rightarrow O_2+M, \quad (2)$$

$$N_2^*+O \rightarrow NO+N, \quad (3)$$

$$NO+O \rightarrow NO_2. \quad (4)$$

Thus, oxygen, carbon monoxide and nitrogen oxides accumulate in the GDC. These materials even in small quantities can significantly alter the electrical and the lasing characteristics of the laser. For example, in the presence of electronegative molecules O_2, NO, NO_2 the following reactions take place intensely (with rates of 10^{-12} to 10^{-10} cm^3/sec):

$$O_2+\bar{e} \rightarrow O+O^-, \quad (5)$$

$$NO+\bar{e} \rightarrow N+O^-, \quad (6)$$

$$NO_2+\bar{e} \rightarrow NO+O^-, \quad (7)$$

$$NO_2+\bar{e}+M \rightarrow NO_2^-+M. \quad (8)$$

These processes lead to a decrease in conductivity of the plasma and development of discharge instability [7-10].

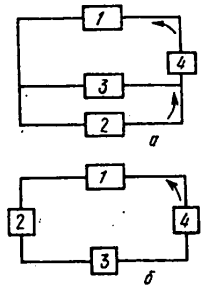

Figure 1. Diagrams of a closed-cycle laser with regenerator: 1 -- discharge chamber; 2 -- regenerator; 3 -- heat exchanger; 4 -- fan: the direction of circulation of the gas flow is illustrated by the arrows

The optimal gas composition can be maintained in two ways. The first method presupposes continuous renewal of some part of the gas mixture. Thus, in [2, 11] the gas mixture of initial composition was added in the amount of up to 1% of the mix pumped through the discharge gap and, correspondingly, the same amount

of gas mixture was pumped out of the laser. An industrial laser with self-maintained discharge requires renewal of up to 10% of the gas mixture for stable operation [12]. It is easy to see that this method is unacceptable for industrial lasers: in the case of mass flow of the gas mixture in the laser of about 1 kg/sec for 5 hours of continuous operation, about 100 kg of helium will be consumed. This leads to a significant increase in operating expenditures. The second procedure presupposes the presence in the laser of a recovery system in which the initial composition of the gas mixture is restored using the following reactions:

$$2CO+O_2 \to 2CO_2, \tag{9}$$

$$2NO \to O_2+N_2, \tag{10}$$

$$2NO+2CO \to N_2+2CO_2. \tag{11}$$

The catalytic method of maintaining the optimal composition of the working gas mixture is the most convenient. The application of a catalytic regenerator in a closed-cycle CO_2-laser is known [6]. The catalyst was copper oxide CuO and chromium oxide Cr_2O_3 applied to aluminum oxide granules. Catalytic reactions took place at a temperature of 600K.

3. Two versions of a closed-cycle laser with regenerator are possible (Fig 1). In the first, "by-pass" version (Figure 1, a) only part of the total flow reaches the regenerator at the same time as in the second, "direct-flow" version (Fig 1, b), the entire gas flow passes through the regenerator.

Let us consider continuous operation of lasers of these types. The equation describing the variation of the carbon dioxide concentration in the GDC c, moles/liter, has the form

$$V_к \frac{dc}{dt} = -ucV_{рк} + x\alpha\omega_к(c_0 - c), \tag{12}$$

where t is the operating time, sec; V_{pk}, V_k are the volumes of the discharge zone and the GDC, respectively, liters; u is the probability of decomposition of the carbon dioxide, sec^{-1}; c_0 is the initial concentration of CO_2 molecules, moles/liter; ω_k is the volumetric flow rate of the gas mixture in the GDC, liters/sec; $\alpha\omega_k$ is the volumetric flow rate of the gas mixture through the regenerator, ℓ/sec (in the second version of connection of the regenerator to the GDC α=1);

$$x=(c_к - c)/(c_0 - c) \tag{13}$$

is the degree of recovery of carbon dioxide in the regenerator; c_k is the carbon dioxide gas concentration after the regenerator, moles/liter.

Let us note that equation (12) is valid under the condition of smallness of decomposition of the carbon dioxide during passage of the gas flow through the discharge zone V_{pk}/ω_k. In addition, if oxidation of the carbon monoxide is described by a first-order equation with respect to the carbon monoxide concentration, then the degree of recovery does not depend on the magnitude of this concentration.

Thus, at the time t the carbon dioxide concentration with constant x

$$c=(c_0/uV_{pк}+x\,\alpha\omega_к)\{uV_{pк}\exp[-(uV_{pк}+x\,\alpha\omega_к)\,V_к^{-1}t]+x\,\alpha\omega_к\}. \quad (14)$$

In the time $t>>V_k/(uV_{pk}+x\alpha\omega_k)$ steady-state concentration of the carbon dioxide is established

$$c_{ст}=c_0x\alpha\omega_к/(uV_{pк}+x\alpha\omega_к). \quad (15)$$

Analogously, it is possible to determine the concentrations of the different products formed in the discharge.

Let us introduce the time t in which no noticeable change has yet taken place in the characteristics of a closed-cycle laser without a regenerator (the plasma conductivity, gain, lasing power). This time is characterized by the carbon dioxide concentration

$$c'=c_0\exp|-uV_{pк}V_к^{-1}\tau|. \quad (16)$$

Equating c_{ct} from (15) and c' from (16), it is possible to determine the necessary parameters of the regeneration system:

$$x\alpha=\tau_к\tau_p^{-1}[\exp(-\tau\tau_p^{-1})-1]^{-1}, \quad (17)$$

where $\tau_к=V_к\omega_к^{-1};\tau_p=V_к(uV_{pк})^{-1}$. For $\tau_p>>\tau$, which in practice is always present

$$x\alpha=\tau_к\tau^{-1}. \quad (18)$$

Thus, the value of xα characterizing the required degree of regeneration is determined by the laser system parameters τ_k and τ.

Under the condition of a first-order reaction with respect to carbon monoxide the mass of the catalyst can be determined by the formula

$$m=-[\alpha\omega_к\ln(1-x)]/K, \quad (19)$$

where K is the experimentally determined reaction rate constant of oxidation of carbon monoxide per unit mass of catalyst, which depends on the gas temperature and characterizes the activity of the catalyst. A specific calculation of the optimal diagram of a laser with regenerator must be performed considering the temperature dependence of the properties of the catalyst, the kinetic equations of the reaction and the gas dynamic resistance of the regenerator. The "by-pass" version (α<1) leads to smaller expenditures of energy on heating the gas mixture in the regenerator. The "direct-flow" version (α=1) is convenient in the case where catalytic reactions take place efficiently for a gas mixture temperature at the output from the discharge chamber (usually about 170°C), and additional heating is required.

4. A study was made of the continuous operation of an electron beam preionized closed-cycle CO_2-laser schematically depicted in Figure 2. A centrifugal fan 4 was used to pump the gas mixture through the discharge chamber 2 (resonator 3), and the mixture was cooled in a water heat exchanger 5. Part of the gas flow was tapped after the discharge chamber to the regenerator 6 containing the catalyst and heating element. Self-maintained discharge was kept alive by an electron beam from a gun 1. The fan pumps the gas mixture with volumetric flow rate to 9 m^3/sec. The temperature of the gas mixture in the resonator reached 400°C, the volume of the gas dynamic circuit was 3 m^3, and the discharge zone, 20 liters.

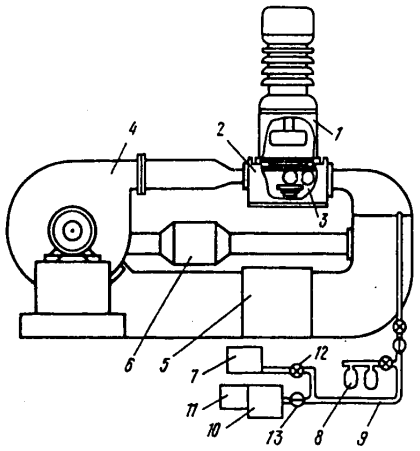

Figure 2. Diagram of an electron beam preionized laser with gas analysis system

The variation in composition of the gas mixture was analyzed by two methods: first, the gas mixture was pumped by means of a vacuum pump 7 through the glass ampules 8 and then analyzed on a mass spectrometer with high resolution; secondly, the continuous gas composition monitoring system was built, the diagram of which is also presented in Figure 2. The gas mixture was continuously removed from the circuit by the pump 7 through the gas line 9, and the mixture was pumped out of the gas line by a diffusion pump 10 and fed to the measuring head of the mass spectrometer 11.

5. Experiments were performed with self-maintained discharge current densities to 20 mamps/cm^2 (which corresponded to an electron concentration to $6 \cdot 10^{10}$ cm^{-3}), for ratios of the electric current density to the gas mixture density up to $1.7 \cdot 10^{-16}$ watts-cm^2 and electron current densities of the gun up to 6 μamps/cm^2. A gas mixture with a total pressure of 50 mm Hg contained 2-4% carbon dioxide, 64% nitrogen, 32% helium and no more than 0.1% oxygen.

The power of the laser with the regenerator switched off dropped by several times with time. The discharge current decreased, the probability of conversion of volumetric self-maintained discharge to arc discharge increased, and the maximum power contributions decreased. All of these phenomena can be explained by changes in composition of the gas mixture. Figure 3, a shows how the discharge current varies as a function of the operating time of the device for the same value of the potential gradient of the discharge electric field E. With time and especially during arc formations, the maximum self-maintained discharge power decreases, which is illustrated by Figure 3,b where curve 5 corresponds to the initial electric power as a function of voltage, and curve 6, the same function after 5 minutes of operation with two arc formations.

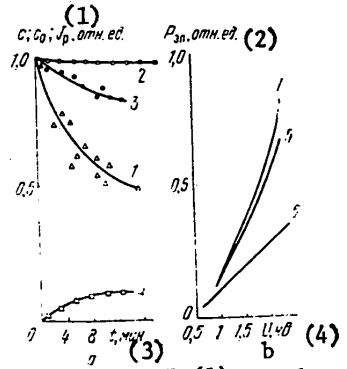

Figure 3. Discharge current J_p(1), carbon dioxide concentration c in the gas mixture in a laser with regenerator (2) and without regenerator (3), oxygen concentration c_0 in a laser without regenerator (4) as a function of operating time (a) and self-maintained discharge power P_{el} in the initial $CO_2:N_2:He:Xe$ = = 1:30:16:0.5 as a function of voltage (b, see the text).

Key:
A. J_p, relative units
B. P_{el}, relative units
C. t, minutes
D. U, kv

The mass spectrometric analysis of the gas mixture from the ampules demonstrated a decrease in CO_2 concentration by approximately 20% of the initial concentration and also the appearance of CO and excess O_2. The O_2 and CO formed were sometimes not in a stoichiometric ratio. This obviously is explained by the processes on the inside surfaces of the GDC elements and release of vapor and gas from them during heating. For example, the presence of water vapor in the amount of 0.1% can have a significant influence on the gas mixture composition as a result of the reaction [13]

$$CO+OH \rightarrow CO_2+H. \qquad (20)$$

If the GDC elements were degassed as a result of prolonged operation of the laser, then the products of decomposition of the CO_2 molecules formed would be in a stoichiometric ratio.

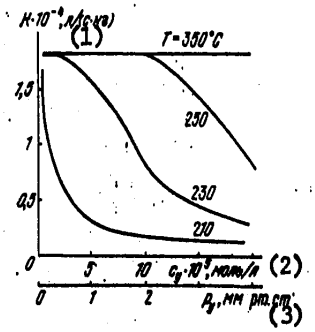

Figure 4. Activity of the catalyst K as a function of concentration c_y and pressure p_y of carbon monoxide

Key:
1. liters/(sec-kg)
2. moles/liter
3. mm Hg

Continuous monitoring of the gas composition demonstrated that after 15-20 minutes of operation 15% of the CO_2 decomposes, 8% of the excess O_2 forms, and then the gas composition stabilizes (see Figure 3, a). A comparison of the curves in Figure 3, a shows that a decrease in conductivity correlates with changes in the gas mixture composition. Considering the sensitivity of the mass spectrometer, it is possible to state that the nitrogen oxide concentration in the given case did not exceed 0.1%.

6. From what has been stated it is clear that for stable operation of a closed-cycle laser it is necessary to regenerate CO_2 from CO and O_2. The regeneration of the gas mixture is best realized by a catalyst on the surface of the active medium; here the materials of the GDC elements and the regeneration systems must not disturb the stoichiometric ratio of the decomposition products. A "by-pass" system for connecting the regenerator to the GDC parallel to the cooler in the discharge chamber, that is, the elements making the basic contribution to the total resistance of the GDC, was realized in the laser. This made it possible to insure calculated value of $\alpha = 0.1$ without using additional pumping devices.

Measurement of the velocity and temperature profile of the gas flow after the regenerator using Pitot tubes and thermocouples demonstrated that the mass flow rate of the gas through the regenerator with connected heating element reaches 10% of the total flow rate to the GDC.

If we set $\tau=60$ seconds, which corresponds to the time of decreasing conductivity of self-maintained discharge by 5%, then for $\tau_k=0.4$ second and $\alpha=0.1$, the required degree of recovery $x=0.067$. By formula (15) it is then possible to determine the steady-state concentration of the carbon dioxide. If decomposition of the CO_2 takes place as a result of reaction (1), then for a value of the rate constant of this reaction $K=10^{-12}$ cm^3/sec under our discharge conditions a CO_2 concentration on the level of 98% of the initial value must be established.

7. Initially a study was made of the possibility of using industrial catalysts ShPK-2 and ShPK-0.5 to recover the gas mixture in the CO_2-laser. These catalysts are γ aluminum oxide granules on which platinum or palladium has been deposited. In spite of the fact that these catalysts are characterized by quite high catalytic activity, they have a number of significant disadvantages: in particular, they absorb carbon dioxide from the gas mixture and have high heat capacity. The latter leads to the necessity for prolonged heating of them when reaching operating conditions. In addition, on loss of seal of the GDC these catalysts absorb water vapor and atmospheric air intensely, which creates an inconvenience in maintaining the laser. During operation the granulated catalyst in the regenerator becomes packed as a result of vibrations, which leads to variation of the linear flow rates through a cross section of the catalyst layer and requires additional filling of the regenerator with catalyst.

Therefore a catalyst free of the noted deficiencies was specially developed and manufactured. It is a metal base on which palladium is applied. The catalyst has quite high activity, it does not form dust on vibration, it does not absorb carbon dioxide and water vapor, it has low gas dynamic resistance and other advantages. The characteristics of the catalytic activity for the metal-based catalysts are presented in Figure 4. The activity K does not depend on the CO pressure, which indicates the first order of the reaction with respect to carbon monoxide (for 0 order with reaction with respect to carbon monoxide (for 0 order with respect to oxygen) in the corresponding pressure range.

Mass spectrometric analysis demonstrated that operation of the laser with a regenerator containing a metal catalyst at a temperature of 300°C and pumping of the gas mixture which amounts to 10% of the total flow rate in the circulating loop leads to decomposition of 2% of the carbon dioxide (see Figure 3, a). The catalyst temperature was estimated by the temperature of the gas passing through the regenerator.

Thus, the measured value of the steady-state CO_2 concentration in the gas mixture agrees with the calculated value.

As the experiments demonstrated (see Figure 3, a), the decomposition of carbon dioxide in the GDC is described by the linear dependence on time only in the initial section. Then even without the regenerator, the decomposition rate slows sharply. This indicates the presence of the processes of recovering CO_2 from CO and O_2 which can take place either in the discharge or on the surfaces (for example, the heat exchanger having branched surface, coated with copper oxides).

The application of a catalytic regenerator in a CO_2-laser with circulation of the working mixture made it possible to obtain stable operation of the laser for several hours. Figure 3, b illustrates the stability of the volt-watt characteristic of independent discharge when using a catalytic regenerator (curve 7, t=15 minutes). As is known, the oxygen content in the initial components of the gas mixture has a negative effect on the characteristics of a CO_2-laser [12]. In the presence of a regenerator and on addition of CO to the gas mixture, there is no necessity for using high-purity gases.

8. Thus, the "by-pass" gas mixture regeneration system with catalytic regenerator is optimal for use in lasers of the selected type. The regenerator catalyst must have high catalytic activity at temperatures of 100-300°C and large volumetric flow rates of the gas flow; stability of the catalytic activity; low gas dynamic resistance and heat capacity; absence of gas and vapor absorption.

As a result of using a catalytic regenerator in an electron beam preionized closed-cycle CO_2-laser it was possible to stabilize the gas mixture composition in the laser; the degree of decomposition of the carbon dioxide was decreased by almost an order in this case. This permits maintenance of the discharge and generation characteristics of the laser on the required level for a long period of time and avoidance of replacement of the gas mixture in the laser.

In conclusion, the authors express their sincere appreciation to G. G. Dolgov-Savel'yev for useful discussion of the obtained results and also O. F. Saprykina and Ye. G. Isayeva for the manufacture of a new type of catalyst.

BIBLIOGRAPHY

1. Lock, E. V. PROC. SPIE, No 2, 1976, p 86.

2. Kosarev, F. K.; Kosareva, N. P.; Lunev, Ye. I. AVTOMASHICHESKAYA SVARKA [Automatic Welding], No 9, 1976, p 72.

3. Basov, N. G.; Belenov, E. M.; Danilychev, V. A.; Kerimov, O. M.; Kovsh, I. B.; Suchkov, A. F. PIS'MA V ZHETF [Letters to the Journal of Experimental and Theoretical Physics], No 14, 1971, p 421.

4. Hoag, E.; Pease, H.; Staal, J. J. ZAR. APPL. OPTICS, No 13, 1974, p 1959.

5. Basov, N. G.; Babayev, I. K.; Danidychev, V. A.; Mikhaylov, M. D.; Orlov, V.K.; Savel'yev, V. V.; Son, V. G.; Cheburkin, I. V. KVANTOVAYA ELEKTRONIKA [Quantum Electronics], No 6, 1979, p 772.

6. Eckbreth, A. C.; Blazuk, P. R. "A.I.A.A. 5th Fluid and Plasma Dynamics Conference," Boston, June (1972); A.I.A.A. Paper, No 72-723.

7. Clotov, Ye. P.; Danilychev, V. A.; Zvorykin, V. D.; Leonov, Yu. S.; Soroka, A. M.; Cheburkin, N. V. KVANTOVAYA ELEKTRONIKA, No 7, 1980, p 630.

8. Nighan, W. L.; Wigand, W. J. PHYS. REV., No A10, 1974, p 922.

9. Sheilds, H.; Smith, A. L. S.; Noris, B. J. PHYS. D., No 9, 1976, p 1587.

10. Napartovich, A. P.; Starostin, A. N. FIZIKA PLAZMY [Plasma Physics], No 2, 1976, p 843.

11. Belomestnov, P. I.; Ivanchenkov, A. I.; Soloukhin, R. I.; Yakobi, D. A. ZHURN. PRIKL. MEKH. I MEKHN. FIZ. [Journal of Applied Mechanis and Technical Physics], No 1, 1974, p 4.

12. Lancashire, R. B. PROC. SPIE, No 86, 1976, p 11.

13. Ochkin, V. I.; Shubin, N. A. KHIMIYA VYSOKIKH ENERGIY [High-Energy Chemistry], No 6, 1972, p 26.

10845
CSO: 1862/75

UDC 535.417.2

CHARACTERISTIC FEATURES OF FORMING RADIATION PATTERN OF LASER EMISSION IN RESONATORS WITH RETROREFLECTING MIRRORS

Moscow KVANTOVAYA ELEKTRONIKA in Russian Vol 8, No 11(113), Nov 81 (manuscript received 12 Feb 81) pp 2397-2407

[Article by Z. Ye. Bagdasarov, Ya. Z. Virnik, S. P. Vorotilin, V. B. Gerasimov, V. M. Zaika, M. V. Zakharov, V. M. Kazanskiy, Yu. A. Kalinin, V. K. Orlov, A. K. Piskunov, A. Ya. Sagalovich, A. F. Suchkov, N. D. Ustinov, Physics Institute imeni P. N. Lebedev of the USSR Academy of Sciences, Moscow]

[Text] A study is made of the characteristic features of shaping the radiation pattern of laser emission in resonators with retroreflecting mirrors. The characteristics of exchange lasing and methods of suppressing it are investigated. The dynamic and static optical inhomogeneities of a medium and optical channel are compensated with five to ten-fold reduction of beam divergence. Intracavity beam steering and the formation of complex radiation patterns of given configuration have been implemented, and radiation homing on a mirror target with angular dimensions of 30 μrad has been realized.

In recent years significant attention has been given to the study of a new physical phenomenon -- wave front reversal (WFR) of optical radiation (see, for example, [1]).

The use of WFR is connected with solving such problems as reduction of laser beam divergence, transmission of optical radiation through nonuniform media, optical focusing of radiation on a target in laser fusion devices. Along with WFR by the methods of nonlinear optics [1], it appears useful in practice [4, 5] to create devices that use classical optical elements such as corner reflectors, triple prisms, rectangular prisms and Dove prisms, lenses and mirrors to solve analogous problems. This arises from the fact that devices based on the enumerated optical elements are less critical with respect to radiation wavelength, width of the radiation spectrum, polarization and power.

In 1970 A. F. Suchkov proposed the study of a mosaic of corner reflectors (triple prisms) and a raster of telescopes with unit power to reduce laser beam divergence for the first time. Then the first experiments were run by V. M. Kazanskiy. However, a systematic approach to this type of system was

started in 1977 after the creation of the first multielement triple-prism mosaic mirrors called, by analogy with [2], retroreflecting mirrors (RM).

The first experimental results pertaining to compensation of optical inhomogeneities occurring during pumping of a neodymium glass rod in a two-pass amplifier were published in [3]. In references [4, 5] which appeared somewhat later, the possibility of transmitting an image through an optically inhomogeneous medium [4] and compensation of optical inhomogeneities in a laser cavity [5] by plastic retroreflecting "gratings" with reflector sizes of 150 microns [4] and 2.5 mm [5] was demonstrated experimentally. Let us note that in contrast to the authors of [4, 5] we have not used a grating with comparatively small "spacing," but RM, that is, a set of many (from 7 to 500) quite large (from 5 to 35 mm) triple prisms inasmuch as we have stated the goal of obtaining a beam with small divergence. The precision of the angle at the apex of the prisms was no less than 1-2"; for the large prisms it was even higher.

The RM used in this experiment are sets of identical total internally reflecting (TIR) triple prisms assembled into a single module without glueing using a special frame.

1. Characteristic Features of Compensation of Dynamic and Static Optical Inhomogeneities of the Active Medium in a Resonator with RM

As is known, the beam divergence of lasers with open resonators, as a rule, is determined by the magnitude of the spatial inhomogeneity of the real part of the dielectric constant of the active medium. If within the limits of the lasing region the real part of the dielectric constant varies with respect to the transverse coordinate by $|\delta\varepsilon'|$, then the angle of divergence of the emission in a flat cavity [6]

$$\theta \approx 2\sqrt{|\delta\varepsilon'|}. \qquad (1)$$

Usually θ is much greater than the diffraction limit. Accordingly, a significant amount of attention has been given to finding static and dynamic methods of compensation of optical inhomogeneities. In this section we shall consider the method of partial compensation of quite smooth nonsteady optical inhomogeneities based on using RM.

In cases where $\delta\varepsilon'(x)$ has a regular nature and does not depend on time, static compensation of the optical inhomogeneities is possible. Actually, if, for example, $\delta\varepsilon'(x)$ is equivalent to a negative lens ($\delta\varepsilon'(x) \sim \alpha x^2$), the laser beam divergence can be estimated by formula (1) quite precisely. However, it is known that in this case the lasing wave front has a shape close to spherical [7]. The sphericalness of the wave front in such a slightly unstable resonator can easily be compensated by a positive lens located outside the resonator so that after this compensation the beam divergence can become close to diffraction. In the majority of cases, however, optical inhomogeneities are not subject to monitoring and vary during the lasing pulse time. Static compensation of wave front deformations turns out to have little effect.

The problem of dynamic compensation arises in connection with which the WFR phenomenon is of great interest.

Let us consider a laser in which the exit mirror is flat and the blind mirror is reversing. A plane wave from the exit mirror, passing through an optically inhomogeneous active medium, is deformed. On reflection from the reversing mirror the wave front retains the spatial shape of the incident wave, but the direction of propagation changes to the opposite.

On the return path through the active medium the wave front deformations will, consequently, be compensated. Thus, the phenomenon of WFR theoretically permits the creation of lasers with beam divergence determined by the light diffraction in the laser aperture and not the optical quality of the active medium. In a number of cases for dynamic compensation of wave front deformations and improvement of the beam divergence, RM can be used. Using RM, it is possible sharply to improve the radiation pattern if the inhomogeneities of the real part of the dielectric constant are comparatively large with respect to absolute magnitude and vary quite smoothly in the direction X transverse to the optical axis of the laser.

Let us note first of all that formula (1) includes the variation of $\delta\varepsilon'$ in the entire lasing region. Therefore if we somehow break down the lasing region into a number of subregions between which there is no radiation exchange and within the limits of which the optical inhomogeneities vary monotonically, the divergence of each such small oscillator diminishes.

Actually, with a decrease in the transverse dimensions of the lasing region Δx for smooth variation of $\delta\varepsilon'(x)$ the absolute variation of $|\delta\varepsilon'(x)|$ also diminishes within the limits of each small lasing region; therefore the overall divergence of the laser beam diminishes. For more specific definition let us consider the case where the inhomogeneity $\delta\varepsilon'(x)$ varies by an exponential law

$$\delta\varepsilon'(x)\sim\varepsilon'_0 \exp(-\alpha x) \tag{2}$$

with a broad active region $\Delta x \sim 1/\alpha$. The situation close to (2) can be realized, for example, in a laser with optical pumping when the pumping emission damps by an exponential law on being propagated into the active medium [8].

Estimating the radiation divergence θ_1 for a laser with lasing region $0 \leq \Delta x \leq 1/\alpha$ by formula (1), we obtain

$$\theta_1 \approx 2\sqrt{|\varepsilon'_0|}. \tag{3}$$

Now let us break down the lasing region into n small regions δx so that

$$\delta x = \Delta x/n \approx 1/\alpha n.$$

The inhomogeneity $\delta\varepsilon'(x)$ in a small laser with number $m(0\leq m<n)$ with accuracy to terms of second order of smallness

$$\delta\varepsilon'_m(x)=\varepsilon_0\exp[-(m+1/2)\delta x][1-\alpha x+(\alpha x)^2/2], \tag{4}$$

and the mean divergence

$$\theta_2\leqslant 2\sqrt{|\varepsilon_0|\alpha\delta x}. \tag{5}$$

The linear part of the inhomogeneity $\delta\varepsilon'_m(x)$ can be compensated if we use a corner reflector which is a set of three mutually perpendicular mirrors instead of the blind mirror in a small laser. After triple reflection the light beam changes direction of propagation to the reverse. A glass pyramid with right angles at the apexes (a triple prism) can be used as the corner reflector. In order to avoid unnecessary losses the base of the prism must be made in the form of one of the centrally symmetric figures: a hexagon, square, rectangle.

A small laser, the resonator of which is formed by a blind mirror made as a corner reflector will be insensitive to inhomogeneities $\delta\varepsilon'$ of the wedge type. Dropping the linear term in (4), for the divergence of such a laser θ_3 from (1) and (4) we obtain

$$\theta_3\leqslant 2\sqrt{|\varepsilon_0|(\alpha x)^2/2}=\theta_1\alpha\delta x/(2\sqrt{2}). \tag{6}$$

Of course, formula (6) is valid if $\theta_3>\theta_d$, where θ_d is the diffraction divergence determined by the corner reflector aperture. Considering the diffraction divergence, the total divergence of the emission of a large laser in the first approximation

$$\theta_0\approx\theta_3+\lambda/\delta x. \tag{7}$$

It is easy to see that if appropriate measures are not taken, exchange lasing between any two corner reflectors occurs in the proposed resonator. Exchange lasing will proceed through a section of the exit mirror, projecting these reflectors on each other. Exchange lasing will exit at angles of

$$\theta'_n=\pm n\delta x/2L, \tag{8}$$

where L is the resonator length.

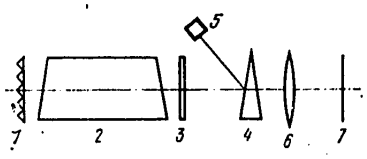

Figure 1. Diagram of the experimental setup for studying exchange lasing

In order to suppress exchange lasing small lasers can be separated by partitions that scatter the emission. For this purpose we have built a sectional active neodymium glass element consisting of 19 thin rods with frosted lateral surface transparent to pumping emission. Rods 30 cm long and 1 cm in diameter were used.

The resonator was formed by a flat semitransparent mirror R=50% and 19-element RM with 70 cm spacing between the mirrors. The sectioning of the active element made it possible to prevent exchange lasing. However, this type of sectioning of the active medium is provided in far from all types of laser active media. Therefore we have given significant attention to investigating the characteristic features of the suppression of exchange lasing by using angle selection of the emission.

1.1. Exchange Lasing Conditions. The experimental study of the peculiarities of the formation of the radiation pattern in resonators with RM was carried out on a tube-pumped iodine laser. A cylindrical quartz cell 80 cm long and 3.7 cm in diameter had openings fixed at the Brewster angle. Four IFP-20000 tubes with aluminum foil reflector were used to pump the working medium $n=C_3F_7I$. The capacitance of the capacitor bank was 4 millifarads. Here, the pumping pulse duration (measured with respect to a level of 10% of the maximum current) was 800 microseconds. Depending on the operating mode of the laser, the energy in the lasing pulse varied from 2 to 9 joules.

The exchange lasing conditions were observed on a device, the optical diagram of which is shown in Figure 1. The resonator was formed by the RM 1 and a semi-transparent flat mirror 3 with reflection coefficient R=20%. Using an optical wedge 4 part of the emission was tapped to the calorimeter 5 to measure the energy in the pulse and to the lens 6 with focal length F=2 meters, in the focal plane of which a screen 7 or photographic film was installed to record the angular distribution of the emission. Adjustment of the resonator was as simple as possible and consisted in setting the semi-transparent mirror normal to the axis of the laser cell by eye.

The pressure of the working medium in the cell 2 was varied from 12 to 80 mm Hg and the resonator length L, from 100 to 250 cm during the experiment. Figure 2 shows the evolution of the angular distribution of the output emission during exchange lasing with an increase in the pressure of the working mix for a resonator length of 1 meter. (In the experiments to study the characteristics of exchange lasing a seven-element RM made of triple prisms with base in the form of a regular hexagon 10 mm high was used for greater descriptiveness of the obtained angular distribution pattern of the emission.)

For small pressures of the working medium of 12-20 mm Hg, which corresponded to small optical inhomogeneities, the characteristic pattern of exchange lasing was observed (Figure 2a [not reproduced]) with 19 channels (as follows from the corresponding theoretical analysis) and with maximum intensity in the main lasing channel directed normally to a semi-transparent mirror.

As the pressure of the working medium increased from 20 to 80 mm Hg (Figure 2,b-d [not reproduced]) and with a corresponding increase in inhomogeneities of the medium, the characteristic spot size in different lasing channels grows, and the brightness of the spots on the screen decreases. Figure 2, c, d [not reproduced] shows the angular distributions of the emission corresponding to an ordinary flat cavity of the same length (1 meter) as the resonator with RM with reflection coefficients of the mirrors R_1=98% and R_2=20% and the same pressure of the working medium, at the top for comparison.

As a result of significant inhomogeneities of the working medium, for a flat resonator the spot (see Figure 2, d [not reproduced]) has the form of a ring which indicates absence of axial emission. At the same time in a resonator with RM the maximum radiation intensity falls on the axis, which indicates compensation of the optical inhomogeneities occurring even under exchange lasing conditions. In a resonator with RM under exchange lasing conditions, in addition to a decrease in the beam divergence, a 25-30% increase in pulse energy was observed by comparison with a flat cavity with the same base.

Let us note that no special measures (such as selecting the working mix, use of high-quality optical system, high-precision adjustment and prevention of misalignment of the flat cavity during the operating process) were taken to achieve small divergence in the laser with flat cavity. The nature of the inhomogeneities of the working medium of the laser was also not specially investigated. Therefore we shall not compare the obtained results with the results of other authors dealing with beam divergence of an iodine laser with flat cavity. In order to determine the angular scale (see Figure 2 [not reproduced]), it is possible to use the fact that the angular spacing between the central spot and the nearest spot corresponding to the inclined lasing channel is 5 mrad.

Figure 3 [not reproduced] shows the evolution of the angular distribution of output emission during exchange lasing with an increase in resonator length. For comparatively short resonator lengths (1 meter, Figure 3, a [not reproduced]) the main part of the radiation is included in the axial lasing channel: the angular spacing between adjacent channels which, just as above, can serve as the angular scale, is d/2L, where d is the height of the base of the triple prism of the RM, L is the resonator length. As the resonator length increases, the angular spacing between adjacent channels θ_k decreases in accordance with the formula θ_k=d/2L, and the intensity distribution by channels becomes more uniform (L=2 m, Figure 3, d [not reproduced]). Obviously, the latter fact arises from a decrease in losses to vignetting for tilted lasing channels with an increase in the resonator length.

Let us note that with an increase in the length of a resonator with RM from 1 to 2 m (in contrast to a flat cavity), no decrease in pulse energy was observed, which also indicates partial compensation of the optical inhomogeneities in a resonator with RM under exchange lasing conditions.

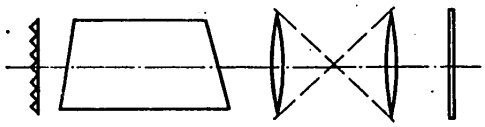

Figure 4. Suppression of exchange lasing by a telescope

For a number of applications, energy concentration in one axial lasing channel is of interest. As applied to a resonator with RM, this implies the necessity for suppressing exchange lasing. For this purpose we introduced a Keplerian telescope into the resonator (see Figure 4). It is known (see, for example [7]), that putting a Keplerian telescope with magnification M=1 in the resonator leads to a decrease in equivalent length of the resonator L_e to

$$L_{\underset{(1)}{э}} = |L_{\underset{(2)}{р}} - 2L_т|, \qquad (9)$$

Key: 1. e=equivalent; 2. resonator

where L_p is the actual resonator length equal to the distance between the flat mirror and the RM; $2L_T$ is twice the telescope length. Selecting the telescope length such that L_e is appreciably less than the cell length with active medium L_k, it is possible to suppress the lasing of the off-axis channels. Actually, on satisfaction of the condition $d/L_e > D/L_k$, where D is the cell diameter, the lasing of the tilted channels will be impossible as a result of incidence of the emission on the side walls of the cell.

Figure 5 [not reproduced] shows the behavior of exchange lasing with a decrease in L_e from 2 meters (Figure 5, a) to 0 (Figure 5, c, [not reproduced]). As L_e decreases, the number of lasing channels decreases and the spacing between them increases (Figure 5, b [not reproduced]); for a defined value of L_e one axial channel remains (see Figure 5, c [not reproduced]). However, decreasing the equivalent length of the resonator, eliminating the exchange lasing, simultaneously increases the beam divergence in the axial channel (see Figure 5, c). (The angular scale of Figure 5 is easily determined from the ratio $d/2L_e$ (where d=1 cm), which is equal to the spacing between the central and adjacent spots.)

We have also investigated another possibility of suppression of exchange lasing as a result of introducing an angle selector into the resonator.

1.2. Resonator with RM and Angle Selector. In the diagram in Figure 4 an iris with apertures such that the axis of angle selector is normal to the semi-transparent mirror was placed in the focal plane of the telescope. Below, the RM with base height of the triple prisms of 0.5 cm was used in all the described experiments.

The angle selector formed a light beam with divergence equal to the pass band of the selector $\theta_c = d_c/F_c$ from spontaneous noise, where d_c is the iris aperture diameter; F_c is the focal length of the telescope lens. The greater part of the emission was coupled out through a semi-transparent mirror, R=20%, and the smaller part returned to the active medium. Here it was amplified in two passes

with reflection from the RM, which permitted exact "fitting" to the hole in the selector iris even in the presence of significant optical inhomogeneities of the active medium. Selecting the pass band of the angle selector $\theta_c < d/2L_e$, we were able to suppress the exchange lasing without energy losses in the pulse. Here the divergence of the stimulated emission is almost equal to θ_c. With a decrease in θ_c, the divergence of the stimulated emission decreased correspondingly, and the output power did not decrease.

It was possible to decrease θ_c in the system shown in Figure 4 with a lens telescope with brightened optical system only to a defined limit θ_c^{min} for which competing lasing occurred as a result of reflection from the surfaces of a telescope lens installed between the cell and the iris. Here the lasing was multichannel, which was observed by the nature of the burn on the angle selector iris. Thus, for example, with a pressure of the working medium of 20 mm Hg $\theta_c^{min} \sim 2$ mrad. The measurements were performed by the 0.5 intensity level.

Discovering that introduction of a lens angle selector into the resonator with RM increases the probability of occurrence of spurious lasing as a result of the blocking optical system of the selector, we replaced the lens telescope in the system shown in Figure 4 by a mirror telescope. In this case spurious lasing did not occur.

In this system limiting values of θ_c^{min} were determined by the following factors. The emission formed by the angle selector with divergence θ_c on amplification in an active medium in two passes with reflection from the RM has divergence at the input to the selector equal to the sum $\theta_c + \theta_{i.comp}$ where $\theta_{i.comp}$ is the divergence caused by inaccuracy of compensation of the wave front distortions which includes imprecision in making the angles of the RM elements, the diffraction divergence, inaccuracy of compensation of the optical inhomogeneities of the active medium and elements of the optical channel. Therefore the decrease in θ_c was not felt in the output power of the iodine laser (according to the system in Figure 4) if $\theta_c > \theta_{i.comp}$.

We were able to weaken this condition by using the system shown in Figure 6 (compare [6]). In this system a semi-transparent mirror was made in the form of a meniscus, one of the spherical surfaces of which had a mirror coating R=20%. The radii of curvature of the meniscus surfaces were selected so that for the emission passing through the meniscus it will be equivalent to a plane-parallel plate with a high degree of accuracy. The angle selector was formed by a blind spherical mirror with focal length F=100 cm, a diaphragm with aperture and the spherical mirror surface of the meniscus with F=100 cm. We increased the size of the iris aperture with an increase in the pressure of the working medium; its minimum value was 0.02 cm at a pressure to 30 mm Hg.

The output emission was coupled out not through the angle selector, but through the meniscus. Therefore θ_c^{min} could be made appreciably smaller than $\theta_{i.comp}$, and the large losses occurring in this case in the angle selector were compensated by the high gain of the iodine laser. For pressures up to 30 mm Hg, $\theta_c^{min} \sim 0.2$ mrad. It is easy to see that the sytem in Figure 6 is equivalent in some sense to the system made up of a two-pass amplifier plus a master oscillator where the role of the master oscillator is played by the angle selector. In the

system in Figure 6 we were able to obtain emission with divergence determined only by inaccuracy of dynamic compensation of the optical inhomogeneities and nonidealness of the RM.

Figure 7 shows the behavior of the focal points (F=200 cm) characterizing the divergence, for laser emission of the system in Figure 6 (b) and emission of a laser with flat cavity (L=100 cm, a) with an increase in pressure of the working medium from 12 to 80 mm Hg. (The output powers were identical for fixed pressures.)

The brightness of the emission when using RM in the resonator is appreciably higher than in the case of a flat cavity. With an increase in pressure, the size of the spot increases (although it is appreciably less than for a flat cavity), which indicates partial compensation of the optical inhomogeneities using the RM. As the angular scale of Figure 7 [not reproduced] it is possible to use the core of the angular distribution depicted in the first picture in Figure 7,b [not reproduced] having angular values 0.5 mrad and corresponding to a pressure of 12 mm Hg. The beam divergence was measured with respect to the 0.5 intensity level: for a pressure of 12 mm Hg this value was 0.5 mrad for a resonator with RM, and for a flat cavity, 2.5 mrad; with a pressure of 80 mm Hg these values were 2 and 20 mrad, respectively (the last pictures in Figure 7).

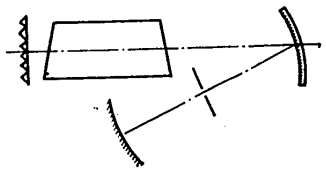

Figure 6. Diagram of an iodine laser with mirror angle selector

Use of the RM in the system shown in Figure 6 made it possible to decrease the beam divergence of the investigated laser by 5 to 10 times as compared to the flat cavity. In addition to the bright core, there is a halo present in the angular distribution of the laser (according to the diagram in Figure 6) obviously caused by diffraction on the RM elements and scattering on the inhomogeneities of the working medium occurring during lasing of the iodine laser and, as is known, having a significant value when working with a material without buffer additives (see, for example [9]).

Let us note that in the system depicted in Figure 6 using the RM exact aiming of the beam at the hole in the angle selector with angular dimensions of 0.2 mrad was realized. Here the edge of the hole of a steel iris was melted.

2. Intraresonator Beam Steering and Forming a Radiation Pattern of Given Configuration

The possibility opened up by the WFR device for intraresonator shaping of emission with given form of the radiation pattern appears to be highly interesting for a number of applications.

Here use is made of the fact that a resonator with WFR mirror in practice loses selectivity and, placing an angular spectrum shaper in it, it is possible to stimulate emission with a shape of the angular spectrum (or radiation pattern) given by the shaper. As applied to the WFR device based on a stimulated Mandelstam-Brillouin scattering mirror, intraresonator shaping of the radiation pattern was demonstrated for the first time by S.A. Lesnik, M.G. Reznikov, M.S. Soskin and A.I. Khizhnyak (see, for example, [1]).

In this section we present results from investigating the intraresonator shaping of the radiation pattern in a resonator with RM.

The diagram of the experimental setup is presented in Figure 8. Here an angular spectrum shaper formed by a meniscus with semi-transparent mirror coating (R=20% and F=100 cm) and a system of reflectors placed in the focal plane of the spherical mirror surface of the meniscus was used as a second mirror in the resonator. The pressure of the working medium was 20 mm Hg.

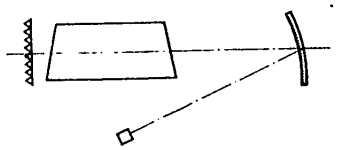

Figure 8. Diagram of a laser with intraresonator radiation pattern shaping

The operating principle of the system consists in the following. Spontaneous noise emission with divergence $\theta_{noise} \sim D/L$ (where D is the cell diameter, L is the distance between the meniscus and the RM equal to 100 cm) is focused by the meniscus, and a light spot $d_{noise} \sim F\theta_{noise}$ in diameter is formed in its focal plane, where F is the focal length of the meniscus. If a system of spatially separated reflectors is placed in the focal plane of the meniscus within the limits of the light spot, then the fluxes, the propagation of which and divergence are determined by the location of the corresponding reflector and its size, is reflected back into the active medium. Thus, for example, a reflector with transverse dimensions d_i placed at a point in the focal plane of the meniscus with coordinates x_i, y_i, shapes the reflected beam entering the medium at an angle $\{x_i/F; y_i/F\}$ with divergence d_i/F. After amplification in the medium (generally speaking, optically inhomogeneous) and reflection from the RM, the system of fluxes is coupled out through a semi-transparent meniscus having a direction of propagation and divergence given by the shaper.

Placing one reflector in the focal plane and shifting it within the limits of the luminescent spot, it is possible to realize precise control of the light beam. Placing a system of reflectors in the focal plane, it is possible to realize lasing with given configuration of the radiation pattern.

Figure 9 [not reproduced] shows a photograph of focal points illustrating the possibility of beam steering and guidance of it to the given angular point by shifting the reflector in the focal plane of the meniscus. The reflector used in

the system had transverse dimensions of d_i=0.2 cm; as the angular scale it is possible to take the angular size of the core of the spots presented in Figure 9 equal to ~2 mrad. For θ_{noise}~40 mrad, accurate beam steering was observed with compensation of the optical inhomogeneities of the medium without noticeably decreasing the pulse power within the limits of the angle of 10 mrad.

Figure 10 [not reproduced] shows photographs of focal points corresponding to stimulated emission with complex patterns of given configuration obtained when placing two, three, four, five and six identical reflectors, respectively, with d_i=0.2 cm in the focal plane.

Let us note that the resonator formed by RM and the angle selector (meniscus plus reflector in the focal plane of the meniscus) is not critical with respect to the accuracy of the setting of the reflector within the limits of the focal point of the luminescence, which greatly simplifies the process of aligning the resonator. To demonstrate this we place the reflector on a disc turning at high speed. If the reflector did not go outside the boundaries of the luminescent spot during rotation, the stimulated emission was not interrupted, and the pulse power was equal to the power in the pulse for a system with stationary reflector.

As the angular spectrum shaper we also used a mirror target of small angular dimension which performed the functions of a second resonator mirror.

In the experiment RM were used with base height of the triple prism of 0.5 cm and working medium with a pressure of 20 mm Hg. In order to increase the Q-factor of the resonator we installed a mirror telescope with magnification M=10 after the laser cell. In this case lasing was realized by a beam converging on the target (from the aperture of the large telescope mirror). The target was exposed to the natural luminescent noise of the active medium of the iodine laser, and if the target was within the limits of the luminescent spot, lasing was stable. We were able to realize lasing in a converging beam on a target with angular dimensions of 30 μrad (determined by the ratio of the target diameter to the distance from the telescope to the target) and reflection coefficient of the emission in the laser aperture (determined by the large telescope mirror) of about 1%. Here the energy in the pulse from the cell output was the same as for a flat cavity 100 cm long with reflection coefficient of the semi-transparent mirror R=20% (2.5 joules). The energy at the target was 0.5 joule.

Conclusions

The results obtained demonstrated that resonators with RM have to a defined degree new properties that distinguish them from traditional optical resonators. They are characterized by weak selectivity with respect to the field structure in the resonator, which, along with compensation of optical inhomogeneities of the active medium, permits shaping of the radiation pattern within comparatively broad limits.

A study was made of the exchange lasing conditions, the optical inhomogeneities of the active medium of the iodine laser were compensated, intraresonator stimulated beam steering, shaping of complex radiation patterns, and irradiation of a target with angular dimensions of 30 μrad by a converging beam were all realized.

In conclusion the authors express their sincere appreciation to Ye. M. Kostikov, S. K. Krivov, L. A. Simonov, M. Yu. Turskiy and M. V. Palamarchuk who made a large contribution to the development of RM, and O. Yu. Nosach for useful discussion of the results of the experiment and constructive critical remarks.

PHOTO CAPTIONS

Figure 2. Evolution of the exchange lasing pattern with an increase in pressure of the working mix.

Figure 3. Evolution of exchange lasing pattern with an increase in resonator length.

Figure 5. Evolution of the multichannel lasing pattern with a decrease in L_e.

Figure 7. Evolution of focal points with an increase in pressure of the working mixture for a flat cavity (a) and a cavity with RM (b).

Figure 9. Intraresonator beam steering.

Figure 10. Shaping a radiation pattern of given configuration.

BIBLIOGRAPHY

1. OBRASHCHENIYE VOLNOVOGO FRONTA OPTICHESKOGO IZLUCHENIYA V NELINEYNYKH SREDAKH [Optical Emission Wave Front Reversal in Nonlinear Media], Gor'kiy, IPF AN SSSR, 1979.

2. USA Patent No 3712706, kl. 350-103.

3. Orlov, V. K.; Virnik, Ya. Z.; Vorotilin, S. P.; Gerasimov, V. B.; Kalinin, Yu. A.; Sagalovich, A. Ya. KVANTOVAYA ELEKTRONIKA [Quantum Electronics], No 5, 1978, p 1389.

4. Barrett, H. H.; Jacobs, S. F. OPTICS LETTS, No 4, 1979, p 190.

5. Mathieu, P.; Belanger, P. A. APPL. OPTICS, No 19, 1980- p 2262.

6. Kirillov, G. G.; Kormer, S. B.; Kochemasov, G. G.; Kulikov, S. M.; Murugov, V. M.; Nikolayev, V. D.; Sukharev, S. A.; Urlin, V. D. KVANTOVAYA ELEKTRONIKA, No 2, 1975, p 666.

7. Anan'yev, Yu. A. OPTICHESKIYE REZONATORY I PROBLEMA RASKHODIMOSTI LAZERNOGO IZLUCHENIYA [Optical Resonators and the Problem of Laser Beam Divergence], Moscow, Nauka, 1979.

8. Borovich, B. L.; Zuyev, V. S.; Katulin, V. A.; Nosach, V. Yu.; Nosach, O. Yu.; Startsev, A. V.; Stoylov, Yu. Yu. KVANTOVAYA ELEKTRONIKA, No 2, 1975, p 1282.

9. Golubev, L. Ye.; Zuyev, V. S.; Katulin, V. A.; Nosach, V. Yu.; Nosach, O. Yu. KVANTOVAYA ELEKTRONIKA, No 6(18), 1973, p 23.

10845
CSO: 1862/75

UDC 621.371:538.566:551.511.6

DETERMINING TURBULENCE PARAMETERS BY LASER BEAM PROBING OF THE ATMOSPHERE

Novosibirsk RASPROSTRANENIYE LAZERNOGO PUCHKA V TURBULENTNOM ATMOSFERE in Russian 1981 (signed to press 18 Feb 81) pp 201-224

[Chapter 8 from book "Laser Beam Propagation in Turbulent Atmosphere", by Valeriy Leonidovich Mironov, Institute of Optics of the Atmosphere, Siberian Department, USSR Academy of Sciences, Izdatel'stvo "Nauka", 1750 copies, 248 pages]

[Text] In addition to meteorological methods of determining parameters of turbulent inhomogeneities in the atmosphere, optical methods have also been developed. A. M. Obukhov [Ref. 180] was the first to point out the possibility of getting information on turbulence structure from studies of the way that a randombly inhomogeneous medium acts on electromagnetic waves. These ideas were further developed in Ref. 354, 74. The development of optical methods of measuring the characteristics of micropulsations of the index of refraction has been prompted primarily by the need for predicting statistical characteristics of the field of laser beams. On the other hand, optical techniques have provided new capabilities for studying the physical principles of atmospheric turbulence itself.

One of the major optical parameters of atmospheric turbulence is the structure characteristic C_n^2. This quantity has an effect on practically all statistical characteristics of the field of a laser beam in the atmosphere. Most extensively used have been optical methods of Ref. 83, 51, 11, 48, 99, 182, 7, 8, 203, 204, 361 and 251 for determining C_n^2 on the basis of distortions of spatial coherence. A method convenient for practical applications [Ref. 11, 48, 99, 182, 340] uses measurement of the half-width of the average diffraction pattern in the focal plane of the reception lens. The initial expression for this method that relates C_n^2 to half-width, was derived in the case of reception of a plane wave, whereas actual measurements in most cases have been done with spatially restricted beams. In this connection, the limits of applicability of the working formula of Ref. 10, 11 have remained unsettled. Ref. 33, 36, 262 consider a generalization of this method to the case where the reception lens is illuminated by a laser beam that has arbitrary diffraction parameters. The resultant relations for determining C_n^2 have been experimentally checked [Ref. 262].

Laser methods of determining C_n^2 based on measurements of coherence distortions require placement of radiating and reception telescopes rigidly fixed in space. This represents a serious barrier to use of these methods on oblique paths. Paths situated in mountainous terrain are an exception [Ref. 99, 184, 186]. Measurements

of distortions of spatial coherence of the field of a laser beam scattered by particles of atmospheric aerosol to determine altitude dependences of the structure characteristic $C_n^2(h)$ were first suggested in Ref. 39. This method does not require the use of lifting devices.

The requirement for spatial stabilization of receiver and emitter raised to different altitudes is considerably relaxed if fluctuations of laser beam intensity are used to determine altitude dependences $C_n^2(h)$. For example, Ref. 356 suggested using measurements of fluctuations of intensity of a laser beam reflected from a mirror sphere raised by a weather balloon. However, the initial relation for determining $C_n^2(h)$ in this case was written on the basis of results found for one-trip beam travel. Besides, this paper did not discuss errors of reconstructing $C_n^2(h)$ due to incorrectness of the solution of an integral equation of the first kind. Based on solution of the physical problem of reflection of an optical wave, the author obtained an equation [Ref. 31] for determining altitude profiles $C_n^2(h)$ in this experimental arrangement, and proposed stable algorithms for processing experimental data. Subsequently, a similar method was used [Ref. 102] for measurements of $C_n^2(h)$ under prairie conditions.

The internal turbulence scale was first determined by an optical method in a model turbulent medium in Ref. 72. These measurements were later repeated in the atmosphere [Ref. 330]. The authors of Ref. 317, 229, 78, 341, 183 found the internal scale from measurements of spatial correlation functions [Ref. 317], time spectra [Ref. 229, 78] and relative dispersion [Ref. 341] of fluctuations of the logarithm of intensity of laser beams on short paths. Estimates of the internal scale are also possible [Ref. 11] with respect to the form of the spectrum of the function of spatial coherence of an optical wave field. All methods considered above for measuring l_0 (excepting Ref. 11) have been based on measurements of intensity fluctuations. Ref. 226, 238 suggested finding the internal scale from measurements of dispersions of phase difference in laser beams on two bases of different sizes. Measurements of the structure function of fluctuations of the phase of laser beams have also been found to be usable for reconstructing the spatial spectrum of fluctuations of the index of refraction in an energy interval. In the region of dissipation of kinetic energy the turbulence spectrum has been reconstructed [Ref. 55] from measurements of the time spectrum of fluctustions of the logarithm of amplitude. Subsequently, phase fluctuations measured simultaneously with intensity fluctuations were used [Ref. 57] for determining the spectrum of fluctuations of the index of refraction over a wide range of wave numbers.

The possibility of determining spectra of fluctuations of the index of refraction from measurements of fluctuations of the center of gravity of optical beams was first pointed out in Ref. 165. Subsequently, parameters of a turbulence spectrum model of form (1.1.39) were determined from measurements of time spectra of displacements [Ref. 89].

In this chapter we examine questions of measuring the parameters of atmospheric turbulence by using laser beams.

§8.1. DETERMINING PARAMETER C_n^2 AND INTERNAL SCALE FROM THE DISTRIBUTION OF INTENSITY OF THE IMAGE OF A LASER SOURCE

8.1.1. Determination of C_n^2 on Horizontal Path

First let us consider determination of the parameter C_n^2 in the case of statistically homogeneous paths ($C_n^2(x') = \text{const}$). Formula (4.1.19) derived for these

conditions in the case of known diffraction parameters of the laser beam incident on the lens (Ω and L/F), fixed diameter and focal length of the reception lens, allow us to determine ρ_0, and hence the structure characteristic C_n^2 from the measured half-width of the distribution of energy intensity of the image y_F.

Upon reception of a collimated laser beam (L/F = 0) under conditions of strong turbulence intensity on the path (q>>1) with reception aperture satisfying the condition $\rho_0 << a_t << L/k\rho_0$, the solution of equation (4.1.19) is written in the simple form

$$C_n^2 = \frac{0{,}86\mu\,(y_F/Fl)^{5/3}}{2{,}91k^{1/3}L}. \qquad (1)$$

Parameter μ in equation (1) takes the values $\mu = 1$, $2^{5/3}$ and $3^{5/6}$ for conditions of a planar wave ($\Omega >> q$), narrow collimated beam ($q^{-1} << \Omega << q$) and spherical wave ($\Omega << q^{-1}$) respectively.

We can see from a comparison of formula (1) with the expression derived for C_n^2 in Ref. 11, 99 for plane wave conditions that using a square-law approximation for the coherence function of form (4.1.4) understates the value of C_n^2 by 9.4%. Calculations like those of Ref. 83, 11 in the case of spherical wave incidence on the reception lens, using rigorous expression (4.1.2) as the coherence function, lead to a formula of type (1) with $\mu = 2.94$. Hence, in case of a spherical wave the relative error of determining C_n^2 using relation (4.1.19) reaches 15%. Finally, using the results of numerical calculation of the distribution of average intensity in the focal plane of the reception lens as shown in Fig. 16 for the conditions of a narrow collimated beam ($q^{-1} << \Omega << q$), we can get a formula of type (1) in which the coefficient $\mu = 4.22$. Thus under conditions of reception of a narrow collimated beam, the error of formula (4.1.19) in finding C_n^2 is maximum, and amounts to 24%. The estimates found above for the error of formula (4.1.19) lie within the limits of errors of measurements of parameter C_n^2 according to recordings of the distributions of average intensity of Ref. 10, 11.

The inequality $\Omega >> q$ implies that under conditions of strong turbulence intensity on the path (q>>1), plane wave conditions necessitate satisfaction of the requirement that the size of the radiating aperture must be not only greater than the radius of the first Fresnel zone, but must exceed the diffraction scale $L/k\rho_0$, which for q>>1 is itself much greater than $\sqrt{L/k}$. Extimates show that in the case of extended paths (of the order of tens of kilometers or more) near the ground, the condition $\Omega >> q$ is not met even for the largest apertures in practical use ($a \cong 20$-30 cm). For example at L = 10 km, $k = 10^7$ m^{-1}, $C_n^2 = 10^{-15}$ cm$^{-2/3}$, condition $\Omega >> q$ becomes $a >> 50$ cm. Thus when measuring the structure characteristic C_n^2 in atmosphere with respect to the half-width of the laser source image in the focal plane of the reception lens, we most frequently must deal with intermediate conditions. In doing this, determination of C_n^2 necessitates using general relation (4.1.19). The values of C_n^2 found from the formula corresponding to plane wave conditions are understated by a factor of $2^{5/3}$ as compared with the true value in reception of a narrow collimated beam.

An experiment [Ref. 262] has been done to check approximate formula (4.1.19). A similar experiment had been done previously in Ref. 11 in verifying a relation

of type (1) for a plane wave. Here simultaneously with recordings of the distribution of intensity $\bar{I}(y)$, the values of C_n^2 were determined with respect to the gradients of mean temperature and wind speed using formula (1.1.46), and then the values of C_n^2 found from optical and meteorological measurements were compared. In our case, there was the possibility of determining C_n^2 from parallel optical experiments. To do this, recordings were simultaneously made of the average intensity in the focal planes of two identical reception lenses as the latter were illuminated by laser beams with different diffraction parameters. The two values of y_F obtained in this way were used to determine the values of C_n^2 from calibration curves plotted according to formula (4.1.19). The values found for C_n^2 were then compared with each other.

The measurements were done on a 1.8 km path passing over even terrain under prairie conditions. Dispersion of the rays in the horizontal plane was equal to 1 m. The reception lenses were simultaneously illuminated by the following sources: 1) single-mode wide collimated ($L/F = 0$, $\Omega = 90$) and diverging (angle of divergence equal to 2.5') beams; 2) single-mode focused ($L/F = 1$, $\Omega = 90$) and diverging beams; 3) single-mode wide collimated ($L/F = 0$, $\Omega = 90$) and narrow collimated ($L/F = 0$, $\Omega = 1$) beams. LG-75 lasers ($\lambda = 0.63$ μm) were used as transmitters. A spherical mirror with diameter of 40 cm was used to shape the wide collimated and focused

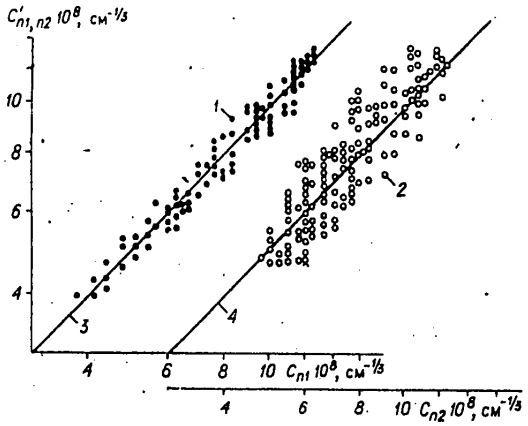

Fig. 61. Comparison of values of C_n found at different diffraction parameters of the laser beam illuminating the reception lens: 1--measurements made with wide collimated (C_{n1}) and divergent (C'_{n1}) beams; 2--measurements with diverging (C_{n2}) and focused (C'_{n2}) beams; 3 and 4--straight lines $C_{n1} = C'_{n1}$ and $C_{n2} = C'_{n2}$

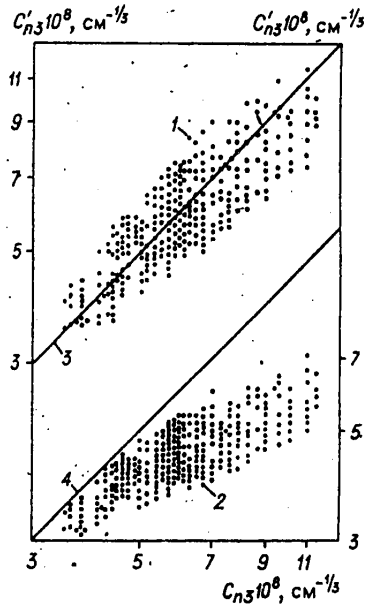

Fig. 62. Values of C_n found with simultaneous measurements in wide (C_{n3}) and narrow (C'_{n3}) collimated beams: 1--processing by formula (4.1.19); 2--processing by formula (1) at $\mu = 1.1$; 3 and 4--straight lines $C_{n3} = C'_{n3}$

beams. The divergent beam was radiation from the laser output. The distributions $\langle I(y) \rangle$ were recorded by scanning with a vertical slit. Reception systems had the following parameters: lens diameter $d = 15$ cm, focal length $F = 1.6$ m, slit width 20 μm, scanning rate $v = 0.113$ mm/min.

The results of the experiment in the form of values of the parameter C_n as found from formula (4.1.19) from simultaneous measurements of y_F with different beams illuminating the reception lens are shown in Fig. 61, 62. It is clear from the figures that the simultaneously determined values of C_n agree satisfactorily with each other. In addition, Fig. 62 shows the values of C_{n3} and C'_{n3} calculated from a formula of type (1) for a plane wave (Ref. 10, 11). The systematic error in determination of C_n that arises in such processing exceeds the scatter of experimental data, and changes as C_n is varied.

Thus as a result of this experiment it has been demonstrated that in determining the structure characteristic of fluctuations of the index of refraction in the atmosphere from measurements of the half-width of the diffraction pattern in the focal plane of the reception lens, it is necessary to account for diffraction parameters of the laser beam that illuminates the lens. The relations derived above for finding C_n^2 applied to a statistically uniform path ($C_n^2(x')$=const), and did not take consideration of the influence of the normal scale of turbulence. Now let us determine the possibility of finding $C_n^2(x')$ and the internal scale for oblique probing of the atmosphere.

8.1.2. Determining Integrated Values of the Structure Characteristic and Internal Scale on Oblique Paths

Let us find the average intensity in the focal plane of a reception lens illuminated by a spherical wave, using formulas (4.1.14), (4.1.22), (2.1.7) and expression (6.4.2) that approximates the structure function of phase fluctuations (6.4.1), corresponding to a spectrum of permittivity fluctuations of type (1.1.22) and (1.1.33) at $\phi_0(\kappa/\kappa_e) \equiv 1$. Let us consider the case where the focal length of the reception lens F_t and its diameter d satisfy relations $kd^2/4L \lesssim 1$, $F_t/L \ll 1$, $D_S(d) \gg 1$. Then the distribution of the average luminous flux passing through a narrow slit (compared with the width of the average diffraction pattern) normalized to the value at the maximum, is written in the form

$$\langle I(\tilde{\varkappa})\rangle/\langle I(0)\rangle = \int_0^1 d\eta \exp\left[-\frac{1}{2}\left(\eta^2 + D_S^{6/5}(\varkappa_э^{-1})\right)^{5/6}\right] \times$$
$$\times \cos(\tilde{\varkappa}\eta) \Big/ \int_0^\infty d\eta \exp\left[-\frac{1}{2}\left(\eta^2 + D_S^{6/5}(\varkappa_э^{-1})\right)^{5/6}\right], \qquad (2)$$

where y is the coordinate of the slit; $D_S(\varkappa_э^{-1}) = 2{,}91 C_{n э}^2 k^2 L \varkappa_э^{-5/3}$;

$$\tilde{\varkappa} = \left(\frac{4}{3}\right)^{3/5} (y/F_t) \sqrt{kL/1{,}22}/\beta_0^{6/5}, \qquad (3)$$
$$\beta_0^2 = 1{,}23\,(8/3)\, C_{n,э}^2 k^{7/6} L^{11/6},$$

and parameters $C_{n,э}^2$ and $\varkappa_э$ are determined from formulas (6.4.3), (6.4.4) in which distance ζL should be reckoned from the reception lens. The quantity $\langle I(y)\rangle/\langle I(0)\rangle$, as a function of the dimensionless coordinate of the slit $\tilde{\varkappa}$, was calculated previously in Ref. 11 at values of the parameter $D_S(\varkappa_э^{-1}) = 0$ and $D_S(\varkappa_э^{-1}) = 1$. It was also suggested there for the case of a homogeneous path ($C_n^2(x') = C_n^2 = \text{const}$, $\varkappa_M(x') = \varkappa_M = \text{const}$) that the values of C_n^2 and $\varkappa_M$ be found by comparing measured functions $\langle I(y)\rangle/\langle I(0)\rangle$ with a family of theoretical curves.

Formula (2) enables us to generalize this technique in the following way for finding equivalent parameters $D_S(\kappa_э^{-1})$ and β_0^2 or $C_{nэ}^2$ and $\kappa_э$.

Experimental data for the distribution of average intensity $\bar{I}(y)$ are normalized to the value at the maximum $\bar{I}(y_m) = \bar{I}_m$, and the quantity y_F is determined that is equal to the half-width of the curve of intensity distribution on level $\bar{I}(y)=\frac{1}{2}$. Then the graph of function $\lg[\bar{I}(y)/\bar{I}(y_m)]$ plotted as a function of argument $\lg[(y-y_m)/y_F]$ is compared with the family of curves $\langle I(\tilde{\kappa})\rangle/\langle I(0)\rangle$ shown in Fig. 63. The parameter $D_S(\kappa_э^{-1})$ is found from the best coincidence of experimental points with one of the curves of this family. The calculated data shown in Fig. 63 enable us to find the value of $\tilde{\kappa}_F$ corresponding to level $\langle I(y)\rangle/\langle I(0)\rangle = \frac{1}{2}$ for each value of $D_S(\kappa_э^{-1})$. The values found in this way are summarized in Table 4.

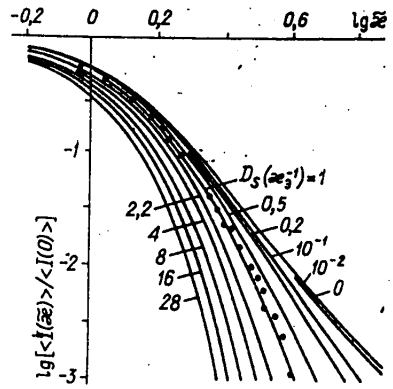

TABLE 4

$D_S(\kappa_э^{-1})$	0	0.5	1	2,2	4	8	12	16
$\tilde{\kappa}_F$	1	0,97	0,96	0,93	0,9	0,88	0,83	0,8

Fig. 63. Distribution of average intensity in focal plane of reception lens; • • • -- experiment

Then using Table 4 and formula (3), we can get the value of the equivalent parameter β_0:

$$\beta_0^{6/5} = \left(\frac{4}{3}\right)^{3/5} \sqrt{\frac{kL}{1{,}22}} \frac{v_F}{\tilde{\kappa}_F} \frac{1}{F_t}. \qquad (4)$$

From the known values of β_0 and $D_S(\kappa_э^{-1})$ we can readily find the equivalent internal scale $l_э$ and the equivalent structure characteristic $C_{n,э}^2$.

The given measurement technique has been used [Ref. 105, 187] for determining values of internal scale $L_э$ on an oblique path 30 km long. The conditions under which the experiment was done are described in §6.4. The reception lens was placed at the lower end of the path and was illuminated by a single-mode collimated laser beam ($\Omega = 0.7$, $\lambda = 0.63$ μm). The parameters of the device for measuring the distribution of average luminous flux transmitted through the slit are described in subsection 8.1.1 of this section. The distribution $\bar{I}(y)$ was recorded by a digital voltmeter over time intervals $\Delta t = 3.5$ s. In order of magnitude, the quantity $\bar{I}(y)$ ranged from 10^3-$3\cdot10^3$ mV at the center to 1 mV at the edges of the distribution curve. Total scanning time averaged 5 minutes. An example of one recording is shown in Fig. 63.

Let us note that the influence of interference caused by scattering on atmospheric aerosol could have led to distortion of the shape of the $\bar{I}(y)$ curve in region

$\bar{I}(y) << \bar{I}_m$. Estimates of the aerosol background were made by formulas [Ref. 97] for the atmospheric haze [Ref. 95] observed under the conditions of the experiment. The amount of the interference was found to be $\bar{I}_m \cdot 10^{-4}$, which is also confirmed by the lack of change in slope of the experimental curve $\bar{I}(y)$ in the region of values $I(y)/I_m \gtrsim 10^{-3}$ (Fig. 63).

The technique outlined above was used to process results of measurements for the purpose of determining parameters β_0^2 and κ^{-1}. Let us note that the narrow collimated beam as a source of illumination of the reception lens, according to results found in subsection 8.1.1 could have led to some understatement of β_0^2 (no more than 15%). At the same time, measurements were made [Ref. 187] of the parameter κ_M^{-1} by the method of Ref. 341 on homogeneous paths near the ground with length $L = 400$ m situated near the reception lens. The results of measurements of κ^{-1} and $\kappa_э^{-1}$ are shown in Fig. 64. The coefficient of mutual correlation between unit values of $\kappa_э^{-1}$ and κ_M^{-1} is 0.9, and the line of regression has the form $\kappa_M^{-1} = 0.83\kappa_M^{-1}$. Inequality $\kappa_M^{-1} < \kappa_э^{-1}$ is in complete agreement with fall-off of the rate of dissipation ε_k with altitude (§1.1). The results of this experiment confirm the feasibility of determining the equivalent internal scale on oblique paths from measurements of average intensity in the focal plane of the reception lens. In the given method of determining the structure characteristic C_n^2, it is necessary to place the optical receiver and laser source at different ends of the path. In measurements on oblique paths such a method becomes difficult to realize because of the need for rigid spatial stabilization of both source and receiver. The next section will present a method of determining C_n^2 that is based on scattering of light by atmospheric aerosol, and is free of the above mentioned disadvantage.

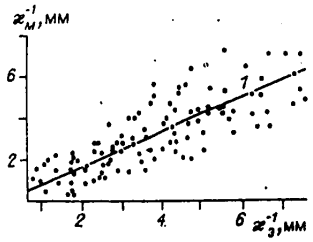

Fig. 64. Comparison of the results of measurements of internal scale by different optical methods: 1--regression line $\kappa_M^{-1} = 0.83\kappa_э^{-1}$

§8.2. LASER METHOD OF DETERMINING PARAMETER C_n^2 BASED ON LIGHT SCATTERING BY ATMOSPHERIC AEROSOL

This technique differs from that described in §8.1 in that the information on parameter C_n^2 is extracted from the average width of the image of an aerosol-filled scattering volume.

As we know [Ref. 95], light scattering by an aggregate of a large number of statistically independent particles takes place incoherently. Setting the radius of coherence of the field of the initial source in formula (4.1.19) equal to zero ($\rho_k = 0$), we get the following expression for the half-width of the image of the scattering volume in the focal plane of the reception lens:

$$y_F^2 = \ln 2 \left(\frac{F_t}{k}\right)^2 \left[\frac{4}{3\rho_0^2} + \frac{k^2 a_v^2}{L^2} + \frac{1}{a_t^2} + \frac{k^2 a_t^2}{L^2}\right], \qquad (1)$$

where $2a_v$ is the transverse dimension of the scattering volume. We will assume that the scattering takes place from the region of focusing of the laser beam

that illuminates the aerosol particles. Then in accordance with expression (4.1.5) the transverse size of the scattering volume is defined as

$$2a_v = 2a_g = \frac{2L'}{ka}\left(1+\frac{4}{3}\frac{a^2}{\rho_0^2}\right)^{1/2}. \qquad (2)$$

Substituting equality (2) in formula (1), we get

$$y_F^2 = \ln 2\left(\frac{F_t}{k}\right)^2\left[\frac{8}{3\rho_0^2}+\frac{1}{a^2}+\frac{1}{a_t^2}+\frac{k^2a_t^2}{L^2}\right]. \qquad (3)$$

Expression (3) enables us to determine the coherence radius of a spherical wave $\rho_{cS} = \sqrt{3}\rho_0$ from the measured half-width of the image y_F. Hence for a statistically uniform path ($C_n^2 = \text{const}$) we can readily find the quantity

$$C_n^2 = (3^{-5/6}1{,}46k^2L\rho_{cS}^{5/3})^{-3/5}.$$

In the case of oblique paths when the structure characteristic varies with altitude, we find by referring to expressions (4.1.22), (2.1.33) that the quantity ρ_{cS} is written as

$$\rho_{cS}(\eta) = \left[1{,}46k^2\int_0^\eta dtC_n^2(t)\left(1-\frac{t}{\eta}\right)^{5/3}\right]^{-3/5}. \qquad (4)$$

In deriving equality (4), it was assumed that the laser beam illuminating the scattering volume propagates vertically upward from below. The upper limit of the integral in (4) is equal to the excess of the scattering volume over the radiating aperture. Equation (4) is a Volterra integral equation of the first kind and enables determination of the profiles of the structure characteristic C_n^2 from values of $\tilde{C}_n^2(\eta) = 1/1{,}46k^2\rho_{cS}^{5/3}(\eta)$ measured for different altitudes.

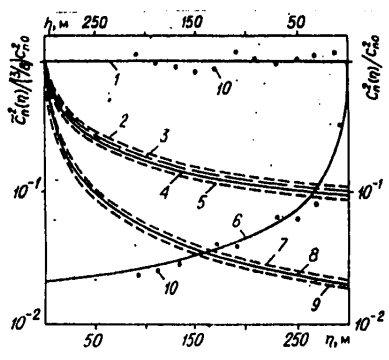

Fig. 65. Reconstruction of the altitude dependences of the structure characteristic $C_n^2(\eta)$: 1 and 6--initial altitude dependences $C_n^2(\eta)$ of form (5) at $\alpha = 0$ and $\alpha = 2/3$ respectively; 2, 3, 4, 5 and 7, 8, 9--altitude dependences of integrated values of $\tilde{C}_n^2(\eta)$ corresponding to formulas (5) at $\alpha = 2/3$ and $\alpha = 4/3$; 2, 7--$\mu = 9/3$; 3--$\mu = 10/3$; 4, 8--$\mu = 11/3$; 5, 9--$\mu = 13/3$; 10--results of reconstruction by algorithm (6.2.4)-(6.2.6)

Fig. 65 shows ratios $\tilde{C}_n^2(\eta)/((C_{n_0}^2 3/8)$, where C_{n0}^2 is the value of the structure characteristic at the lower point of the path, these ratios being calculated for altitude dependences

$$C_n^2(h) = C_n^2(h_0)\left(1+\frac{h}{h_0}\right)^{-\alpha}; \quad \alpha = 0,\ \frac{2}{3},\ \frac{4}{3};\ h_0 = 1{,}5\text{м}, \qquad (5)$$

that correspond to typical conditions of the atmosphere (see §1.2). It can be seen from Fig. 65 that measurement of the quantity $\tilde{C}_n^2(\eta)$ ensures sensitivity sufficient for resolving variations of profiles $C_n^2(\eta)$.

Inversion of integral equation (4) can be accomplished by reducing it to a system of linear algebraic equations and solving this system by the Tikhonov regularization method as was done in §6.2. Examples of dependences $C_n^2(\eta)$ reconstructed in this way in the case of distortion of initial data with relative error of 30% are shown in Fig. 65. An estimate of the errors of reconstruction of functions $C_n^2(\eta)$ due to deviation of the index of refraction in the expression for the spectrum $\Phi_n(x', \varkappa) = 0{,}033\, C_n^2(x')\varkappa^{-\mu}$ from the values $\mu = 11/3$ was made by numerical calculations in which the function $C_n^2(\eta)$ was reconstructed at $\mu = 11/3$ from values of $\tilde{C}_n^2(\eta)$ determined at $\mu \neq 11/3$ (see Fig. 65). The calculations showed that as μ is varied over a range of $\mu = 10/3 - (11.2)/3$ corresponding to the data of Ref. 330, the error of reconstruction does not exceed 8-10%.

Formula (3) was obtained without consideration of aerosol scattering on the path of propagation of the wave from the scattering object to the reception lens. Estimates of the relative contribution of this background to the registered signal in the one-time scattering approximation with the use of the results of Ref. 97 have shown that at $\lambda = 0.63$ μm, particle sizes of 0.05-5 μm, angle of the cone of radiation of the scattering volume equal to $\pi/2$, angle of view of the receiver $\psi = 10^{-4}$, path length $L = 5$ km, and meteorological range of visibility $S_M = 20$ km, this contribution does not exceed 0.1%.

The lidar equation of Ref. 96 is used to estimate the energy characteristics of the ranging signal. Calculations have shown that with a receiver size of $d = 70$ cm, length of scattering volume $l = 10$ m and backscattering coefficient $\alpha_\pi = 3{,}5 \cdot 10^{-6}$ m^{-1} as experimentally determined in Ref. 196, the admissible probing distance with use of a standard LG-38 laser ($\lambda = 0.6328$ μm) is 100 m. If laser power is increased to a few dozen watts, the probing distance can be extended to a kilometer or more. Let us note that the resultant relations for determining C_n^2 can be used with reflection from rough surfaces as well.

In the next section we will consider determination of the altitude dependence of the structure characteristic from measurements of dispersions of weak intensity fluctuations when receiver, source or reflector are situated at different altitudes. In this case, the requirements for spatial stabilization of receiver and source are not so significant if diverging laser beams are used and the receiver systems have a wide field of view.

§8.3. DETERMINATION OF ALTITUDE DEPENDENCES OF PARAMETER C_n^2 FROM FLUCTUATIONS OF THE LASER BEAM FIELD AMPLITUDE

In this method, the altitude dependence of C_n^2 is found by using the expression for dispersion σ_χ^2 of fluctuations of the logarithm of the laser beam field amplitude on an oblique transmission path. For defined diffraction parameters of a diverging laser beam, fluctuations of the logarithm of amplitude can be calculated as shown in §5.1 by the formulas derived for a spherical wave. Passing in formula (5.1.16) to the limiting case of a spherical wave, we write the dispersion $\sigma_\chi^2(\eta) = B_\chi(x(\eta), 0, 0)$ in the form

$$\sigma_\chi^2(\eta) = 0{,}56k^{7/6}\sin^{-11/6}\varphi(\eta)\int_0^\eta dtC_n^2(t)\,Q(\eta, t), \qquad (1)$$

where $Q(\eta, t) = t^{5/6}(1-t/\eta)^{5/6}$; $\eta = H - h_0$ is the difference between the altitudes of the upper and lower points of the oblique path; $\phi(\eta)$is the angle of elevation of the path. If we measure the amplitude fluctuations of the wave reflected from a point reflector, then in accordance with the results of §5.4 the right member of equation (1) must be multiplied by 4. We will treat expression (1) as an integral equation for determining the structure characteristic $C_n^2(h)$ from measured values of function $\sigma_\chi^2(h)$. This equation is valid [Ref. 145] in the region of weak intensity fluctuations $4\sigma_\chi^2 \leq 0.8$ and in the Fraunhofer diffraction zone relative to the internal scale of turbulence ($\lambda\eta/\sin\phi(\eta) >> l_0^2$). In deriving (1), we have also assumed laminar homogeneity of the structure characteristic $C_n^2(h)$ in the atosphere.

If the reception aperture has finite diameter d, the measured values of fluctuations of the logarithm of the received luminous flux $\sigma_p^2(\eta)$ must be recalculated by the formula

$$\sigma_\chi^2(\eta) = \sigma_p^2(\eta)/G\left(d/2\sqrt{\lambda\eta/\sin\varphi(\eta)}\right), \qquad (2)$$

where $G(d/2\sqrt{\lambda\eta/\sin\varphi(\eta)})$ is an averaging function that can be determined from the data of Ref. 126 in the case of direct transillumination, and from the results of §5.4 in the case of ranging transillumination of the atmosphere.

Initial equation (1) is a Volterra integral equation of the first kind. Let us represent this expression in a form that is invariant relative to the horizontal components of the length of the path:

$$\sigma_{\chi n}^2(\eta) = \int_0^\eta dt\zeta(t)\,t^{5/6}(1-t/\eta)^{5/6}. \qquad (3)$$

Here $\sigma_{\chi n}^2(\eta) = \sigma_\chi^2(\eta)\sin^{11/6}\varphi(\eta)/2{,}24k^{7/6}C_{n0}^2$ is the altitude dependence of dispersion normalized to known parameters; $\zeta(\eta) = C_n^2(\eta)/C_{n0}^2$ is the altitude profile of the structure characteristic. Breaking interval $(0, \eta)$ into segments $\eta_j = j\Delta$ (j = 1, 2, ..., n), we reduce integral equation (3) to a system of algebraic equations of the form

$$\sigma_j^2 = \sum_{i=1}^{j}\Phi_{ji}\zeta_i, \qquad (4)$$

where

$$\sigma_j^2 = \sigma_{\chi n}^2(j\Delta), \quad \zeta_i = \zeta((i-1/2)\Delta),$$

$$\Phi_{ji} = (j\Delta)^{11/6}\int_{(i-1)/j}^{i/j} dtt^{5/6}(1-t)^{5/6}.$$

Ref. 31 proved sensitivity of the quantity $\sigma\chi_n^2(\eta)$ to variations of the function $\zeta(\eta)$ that are observed in the atmosphere as sufficient for actual measurements. Here an investigation was also made of manifestation of the incorrectness of equation (3), estimates were made of the errors of reconstruction of function $\zeta(\eta)$ in the case of finite errors of quantity $\sigma_{\chi n}^2(\eta)$, and a demonstration was

given of use of the regularization method proposed in Ref. 232 for solving system of equations (4). In addition, a simpler stable method of solving equation (3) was proposed, based on a distinguishing feature of this equation, namely the fact that dependence on the upper limit of integration appears in the kernel as the ratio t/η. We will consider this method in more detail.

Consider an equation of the form

$$\varphi(x) = \int_0^x dy f(y) Q(y/x), \quad 0 \leqslant y \leqslant x. \tag{5}$$

Taking functions $\phi(x)$ and $f(y)$ as analytic, we approximate them in accordance with the Weierstrass theorem [Ref. 137] by the polynomials

$$\varphi(x) = \sum_{k=1}^{p} \varphi_k x^k, \quad f(y) = \sum_{k=0}^{l} f_k y^k. \tag{6}$$

Substituting expansions (6) in equation (5), we get

$$\sum_{k=1}^{p} \varphi_k x^k = \sum_{k=0}^{l} f_k \lambda_k x^{k+1}, \tag{7}$$

where

$$\lambda_k = \int_0^1 dt Q(t) t^{k+1}. \tag{8}$$

In order for relation (7) to be satisfied for all points of segment [0, x], it is necessary to require equality of coefficients $f_k = \varphi_{k+1}/\lambda_k$, $k = 0, 1, \ldots, p-1$ in accordance with Ref. 70. As a result, the formal solution of equation (5) is written in the form

$$f(x) = \sum_{k=0}^{p-1} \frac{\varphi_{k+1}}{\lambda_k} x^k. \tag{9}$$

Let us estimate the accuracy of reconstructing function f(x) by using equality (9) if in place of the exact function $\phi(x)$ we assign its approximate values $\tilde{\phi}(x)$. Representing function $\tilde{\phi}(x)$ as the polynomial $\tilde{\varphi}(x) = \sum_{k=1}^{p} \tilde{\varphi}_k x^k$, we write the dispersion of random deviations $\Delta\varphi(x) = \varphi(x) - \tilde{\varphi}(x)$ in accordance with Ref. 137 in the form

$$D(\Delta\varphi(x)) = \sum_{i=1}^{p} \sum_{k=1}^{p} \rho_{ik} D^{1/2}(\Delta\varphi_i) D^{1/2}(\Delta\varphi_k) x^{i+k},$$

where ρ_{ik} and $D(\Delta\phi_k)$ are the correlation coefficient and dispersion of random deviations $\Delta\phi_k = \phi_k - \tilde{\phi}_k$. The accuracy of reconstruction of function f(x) by using equality (9) is determined by the quantity

$$D(\Delta f(x)) = \sum_{i=0}^{p-1} \sum_{k=0}^{p-1} |\rho_{ik} D^{1/2}(\Delta\varphi_{i+1}) D^{1/2}(\Delta\varphi_{k+1}) x^{k+i}| / \lambda_k \lambda_i. \tag{10}$$

Since coefficients λ_k in accordance with definition (8) decrease with increasing k, the rms error $D^{1/2}(\Delta f(x))$ expressed by equality (10) increases without limit as the order of the approximating polynomial increases. Herein lies the incorrectness of the solution of integral equation of the first kind (5).

The simplest regularizer [Ref. 231, 233] can be used to get stable solutions From the set of functions $f^{\alpha}(x)=\sum_{k=0}^{p-1}\frac{\varphi_{k+1}}{\lambda_k+\alpha}x^k$, which are the solution of equation

$$\sum_{k=1}^{p}\varphi_k x^k=\sum_{k=0}^{p-1}f_k\lambda_k x^{k+1}+\alpha\sum_{k=0}^{p-1}f_k x^{k+1}, \qquad (11)$$

by varying the regularization parameter α we select the function $f^{0}(x)$ that minimizes functional

$$\varepsilon\left(f^{\alpha}(x)\right)=\int_0^x dx\left[\sum_{k=1}^{p}\varphi_k x^k-\int_0^x dt f^{\alpha}(t)\,Q\,(t/x)\right]^2 \qquad (12)$$

as the solution of integral equation (5). As demonstrated in Ref. 31, algorithm (11), (12) ensures reconstruction of function $\zeta(h)$ with relative accuracy close to that of the initial data for $\sigma^2_{\chi n}(\eta)$. This algorithm was used to reconstruct [Ref. 31] the altitude dependences $C_n^2(h)$ from measurements [Ref. 356] of the dispersion of fluctuations of the logarithm of the amplitude of a laser beam reflected from a mirror sphere which was placed at different altitudes.

The given method of determining $C_n^2(h)$ was put through a trial run [Ref. 182, 102] in measurements of $C_n^2(h)$ under prairie conditions in the vicinity of the town of Tsimlyansk, where extensive statistical material had been obtained previously [Ref. 108] for values of C_n^2 near the ground. The laser source ($\lambda = 0.63$ μm) was raised to a height $h_0 = 1.2$ m at a distance of 260 m from the base of a meteorological tower. The radiation was intensity-modulated on a frequency of f = 10 kHz, split into five beams, and sent at different angles to photocells at heights of h = 4, 7.5, 15, 37.5 and 72.5 m on the tower. Diameter of the input diaphragms was d = 1 mm. Initial diameter and angle of divergence of the beams were 2 mm and 1' respectively.

Fluctuations of the logarithm of field amplitude on the axis of such a beam are equivalent [Ref. 145] to fluctuations of a spherical wave. In accordance with the results of Ref. 126, the averaging action of the reception apertures was negligible. Therefore equation (3) with the substitution $\sigma^2_{\chi}(\eta)=\sigma^2_{\ln I}(\eta)/4$ made in the left member was used to determine altitude dependences $C_n^2(h)$ from measured values of dispersion of the logarithm of intensity $\sigma^2_{\ln I}$. From the form of the kernel of equation (3) we can readily see that perturbations of the turbulent flux at the point of location of the laser emitter and receivers have almost no effect on the measured quantity. The greatest contribution to the value of $\sigma^2_{\chi}(\eta)$ is from layers situated in the middle of the path. The solution of a system of equations of type (4) found with a nonuniform step corresponding to placement of the receivers showed that with a relative error of initial data of 45%, altitude dependences of the type $\zeta(\eta)$ can be reconstructed with accuracy of no worse than 25%. The values of ζ_j determined from solution of system (5) corresponded to heights of 2.6, 4.5, 10, 29 and 57.5 m.

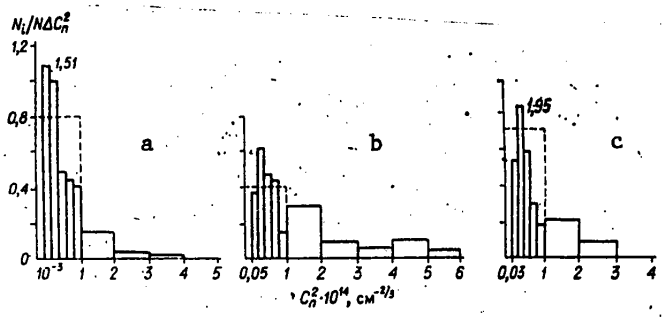

Fig. 66. Histograms of values of C_n^2 obtained in the period from 7:00 to 19:00 hours: a--micropulsation measurements (h = 4 m, N = 240); b, c--optical measurements (N = 220) at h = 2.6 m (b) and h = 29 m (c)

Measurements of $\sigma^2_{lnI}(\eta_j)$, j = 1, 2, 3, 4, 5 were done simultaneously with a five-channel dispersiometer. The frequency passband of each channel was 2.5 kHz. The averaging time was taken as equal to 100 s. The lower limit of measurement of σ^2_{lnI} was 0.003 at an instrument error of 10%. The values of C_t^2 at the point of the receiver of the lower pathwere determined from temperature micropulsations simultaneously with the optical measurements. The experiment was done in August 1974.

Histograms of the probability density function of values of C_n^2 according to data of micropulsations and optical measurements for daytime conditions are shown on Fig. 66. These results agree satisfactorily with a histogram produced by many years of gradient measurements [Ref. 108] of the quantity C_t^2 in the given locale. Curves for sampled average values of C_n^2 as a function of altitude are shown in Fig. 67. Also shown here for comparison are the results of measurements of the

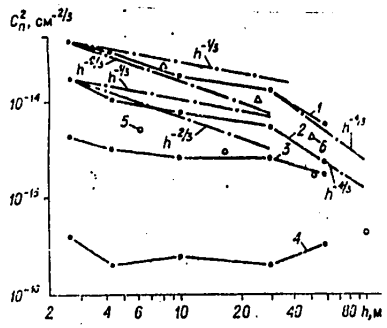

Fig. 67. Altitude dependences $C_n^2(h)$ reconstructed from the results of optical measurements (Tsimlyansk): 1--11-15 h (40 values); 2--7-11 h (35 values); 3--16-19 h (60 values); 4--18 h to 19 h 30 min (6 values); 5--altitude dependence $C_n^2(h)$ obtained in Ref. 292 (Australia) at noontime hours of cloudless summer days; 6--one of the averaged altitude profiles $C_n^2(h)$ obtained in Ref. 98 (Podmoskov'ye) under conditions of developed convection

structure characteristic made by micropulsation thermometers suspended on the cable of a tethered balloon [Ref 292] and fastened to a meteorological tower [Ref. 98]. These data are in satisfactory agreement with our results in absolute magnitude and the behavior of altitude dependence. Fig. 68 compares altitude dependences $C_n^2(h)$ obtained by various methods at different geographic points,

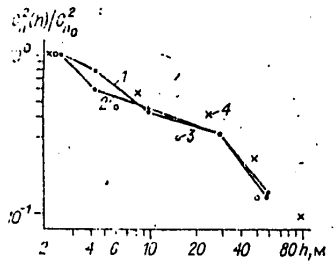

Fig. 68. Comparison of normalized altitude dependences $C_n^2(h)/C_{n_0}^2$: 1, 2--result of optical measurements given as curves 1, 2 on Fig. 67; 3--data of Ref. 292 ($C_{n_0}^2 = 1.2 \cdot 10^{-14}$ $cm^{-2/3}$, $h_0 = 2$ m); 4--results of micropulsation measurements [Ref. 44] (Podmoskov'ye, $C_{n_0}^2 = 4.35 \cdot 10^{-16}$ $cm^{-2/3}$, $h_0 = 2$ m)

but under conditions close to unstable temperature stratification of the atmosphere. All results are normalized to the value of the structure characteristic at the lower measurement point $C_{n_0}^2$. A distinguishing feature of the given empirical dependences $C_n^2(h)$ (which had been previously noted only in Ref. 44) is a "break" at altitude $h = 30$ m, where the quantity C_n^2 begins to decrease in accordance with a power law $C_n^2(h) \sim h^{-4/3}$ typical of conditions of developed convection (see §1.1). In the lower layer ($h \leqslant 30$ m), the quantity C_n^2 decreases with altitude much more slowly. Thus the resultant altitude dependences of the structure characteristic of fluctuations of the index of refraction are confirmed by the results of direct meteorological measurements. In addition to the structure characteristic of refractive index fluctuations, optical methods enable determination of internal turbulence scale. Possibilities for measuring the internal scale by using phase fluctuations of a laser beam field will be considered in the next section.

§8.4. PHASE OPTICAL MEASUREMENTS OF INTERNAL TURBULENCE SCALE

This method is based on measuring the fluctuations of phase difference of optical beams on two bases of different length. The structure functions of phase fluctuations that are necessary for determining the internal scale can be found in the smooth perturbation approximation as was done in §5.1, or by using formula (4.4.2) and expression (4.3.11) for diffraction rays. As a result of calculations, the structure function for the near diffraction zone ($\Omega \gg 1$) of a collimated beam is written in the form

$$D_S(x, \vec{\rho}) = 2{,}91 C_n^2 k^2 L \left[\left(\rho^2 + \varkappa_м^{-2} \right)^{5/6} - \varkappa_м^{-5/3} \right]. \qquad (1)$$

The spectrum of fluctuations of the index of refraction (1.1.22), (1.1.33) was used in deriving formula (1). Distance ρ is measured between the centers of the beams or within the limits of a single beam near its center when $\rho \ll a$. If the

condition $\rho_1 \ll \varkappa_M^{-1}, \rho_2 \gg \varkappa_M^{-1}$ is met for receiver separations ρ_1 and ρ_2, (1) implies a simple relation between internal scale $l_0 = 2.28/\kappa_M$ and the measured ratio $D_S(\rho_2)/D_S(\rho_1) = \rho_2^{5/3}/\rho_1^{5/3}\varkappa_M^{1/3}$. In the general case, graduation curves $D_S(\rho_2)/D_S(\rho_1) = f(\rho_2/\rho_1, \varkappa_M\rho_1)$ should be plotted as a function of argument $\kappa_M\rho_1$ by using formula (1) as the parameter ρ_2/ρ_1 is varied to determine internal scale.

The method was given a trial run on a 95 m path elevated to a height h = 1.4 m over a section of even terrain. Structure functions $D_S(\rho_1)$ and $D_S(\rho_2)$ were determined by a heterodyne phase meter [Ref. 146]. Minimum measurable phase difference was 0.1 rad. Single-mode collimated beams were used with radius $a = 2$ cm. The values of the separations ρ_1 and ρ_2 were varied over a range of 1 mm $\leqslant \rho_1 \leqslant$ 12 mm, $\rho_2 = 67$ and 180 mm.

The minimum and maximum measured values of κ_M^{-1} were 1 and 10 mm. The most probable value of κ_M^{-1} was 4-5 mm. For the purpose of direct verification of the proposed optical method of measurements of internal scale, simultaneous measurements were made of the average values of temperature and wind speed at altitudes of 0.5 and 2 m. These weather data were used to calculate the Kolmogorov turbulence scale η_k. The rate of dissipation of kinetic energy necessary for the calculation was determined in accordance with Ref. 175, 94 from the formula

$$\varepsilon \simeq u_*^2 \frac{dv}{dz} + \frac{g}{T}\frac{H}{C_p\rho}, \qquad (2)$$

where u_* is flowrate, g is acceleration due to gravity, H is vertical heat flux, dv/dz is the gradient of average wind speed, T is average temperature in kelvins, C_p and ρ are the specific heat and density of air respectively. The calculations used the following tabular values: $C_p = 0.24$ cal/g·deg, $\rho = 1.3 \cdot 10^{-3}$ g/cm^3, $\nu = 1.32 \cdot 10^{-1}$ cm^2/s. The values of u_* and H were determined from nomograms [Ref. 94] on data of measurements of the average wind speed and temperature.

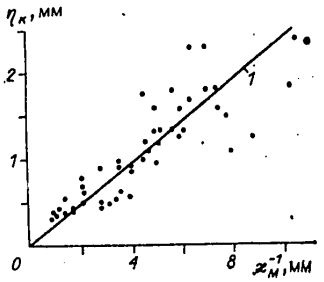

Fig. 69. Correspondence of data of meteorological and optical measurements of internal scale: 1--line of regression $\eta_k = \kappa_M^{-1}/3.5$

Fig. 69 shows the results of simultaneous measurements of the quantities l_0 and η_k. The correlation coefficient calculated from these data was 0.8, and the regression coefficient evaluated by the method of least squares was $\alpha = \kappa_M^{-1}/\eta_k = 3.5 \pm 0.84$. By using formula (1.1.37) we can readily find the relation between the internal scale of model (1.1.33) and the Kolmogorov turbulence scale:

$$l_0 = 8\eta_k. \qquad (8)$$

Thus the conducted experiment proves the applicability of the proposed method of determining the internal scale of turbulence from measurements of dispersion of the phase difference of laser beams to evaluation of the spectrum of fluctuations of the index of refraction in the region of the external scale of turbulence.

§8.5. DETERMINATION OF TURBULENCE SPECTRUM IN GROUND LAYER OF ATMOSPHERE FROM MEASUREMENTS OF PHASE FLUCTUATIONS OF THE FIELD OF OPTICAL BEAMS

If the atmosphere is probed by two parallel laser beams of form (2.1.39) and phase fluctuations are measured in the centers of these beams, then the mutual

correlation function of phase fluctuations can be written in the form

$$B_S(x, \vec{\rho}) = 2\pi k^2 L \int_0^1 d^2\varkappa \Phi_n(\varkappa) \exp(i\vec{\varkappa}\vec{\rho}). \quad (1)$$

Formula (1) has been obtained in the smooth perturbation approximation in the same way as expression (5.1.11), assuming that the condition $\rho >> \sqrt{\lambda L}$ is satisfied and taking the path as statistically uniform. An analogous result follows from using formula (4.4.2) and expression (4.3.11) for diffraction rays.

When the observation points are spaced along one of the components of the vector $\vec{\rho} = \{y, z\}$, e. g. along the y-axis, the correlation function $B_S(x, y)$ assumes the form

$$B_S(x, y) = 2\pi k^2 L \int d\varkappa_2 \int d\varkappa_3 \Phi_n(\varkappa_2, \varkappa_3) \exp(i\varkappa_2 y). \quad (2)$$

We can see from equality (3) that the two-dimensional spectrum of fluctuations of the index of refraction

$$V_n(0, \varkappa_2) = \int d\varkappa_3 \Phi_n(\varkappa_2, \varkappa_3) \quad (3)$$

differs from the one-dimensional spatial spectrum of phase fluctuations $V_S(\kappa_2)$ by a constant quantity $2\pi k^2 L$. Thus the two-dimensional spectrum of fluctuations of the index of refraction (3) can be determined by Fourier transformation from measured values of the correlation function $B_S(x, y)$.

As a first stage in evaluating the applicability of models of spectra $\Phi_n(\kappa)$ of the form (1.1.40), (1.1.38) and (1.1.40), (1.1.39), let us calculate the spatial phase correlation coefficients $b_S(x, y) = B_S(x, y)/B_S(x, 0)$ and compare them with measurements of this quantity. Expressions obtained with the aid of (2) for correlation coefficients corresponding to models (1.1.38) and (1.1.39) take the form

$$b_S(x, y) = \frac{\Gamma(1/6)}{\pi}\left(\frac{\varkappa_0 y}{2}\right)^{5/6} K_{-5/6}(\varkappa_0 y), \quad (4)$$

$$b_S(x, y) = {}_1F_1\left(-\frac{5}{6}, 1; \left(\frac{\varkappa_e y}{2}\right)^2\right) - \frac{1}{\Gamma(11/6)}\left(\frac{\varkappa_e y}{2}\right)^{5/3}. \quad (5)$$

We use the experimental data obtained in Ref. 146 for $b_S(x, y)$. The experiment was done on a horizontal path of length L = 110 m. The height of the path above the even underlying surface was 1.5 m. Emission of an LG-36 helium-neon laser ($\lambda = 0.63$ μm) was split into two identical single-mode collimated beams having output diameter $2a = 2$ cm. The beams were spaced in the horizontal direction with step $\Delta = 5$ cm up to a value of $y_m = 1.1$ m. Fluctuations of the phase difference between the centers of the beams were recorded in the reception plane by a digital optical phase meter. Realizations of duration T = 50 s (sample volume 4000 readings) were used to evaluate the structure function $D_S(y)$, which is the dispersion of the observed process. Measurement results normalized to their value at maximum spacing are shown in Fig. 70. It is clear from this figure that the resultant structure functions are saturated. Hereafter, we will use the expressions

$$\begin{aligned} \hat{b}_s(y) &= 1 - D_s(y)/D_s(y_m), & y \leqslant y_m, \\ \hat{b}_s(y) &= 0, & y < y_m \end{aligned} \quad (6)$$

as an estimate of the correlation coefficient of phase fluctuations.

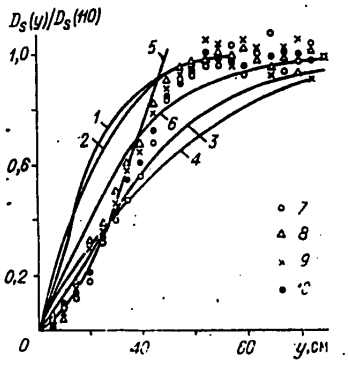

Fig. 70. Normalized phase structure functions: 1, 3--calculation by formula (4) (1--$\kappa_0 = 6.5$ m^{-1}, 3--$\kappa_0 = 3.2$ m^{-1}); 2, 4--calculation by formula (5) (2--$\kappa_e = 26.5$ m^{-1}, 4--$\kappa_e = 11.8$ m^{-1}); 5--function $\alpha y^{5/3}$, where α is selected from best coincidence with experimental data; 6--calculation by formula (4) at $\kappa_0 = 4.3$ m^{-1}; 7-10--experimental values: 7--$D_S(y_m) = 350$; 8--$D_S(y_m) = 470$; 9--$D_S(y_m) = 380$; 10--$D_S(y_m) = 230$

Fig. 70 compares correlation coefficients calculated by formulas (4) and (5) with measured values. Parameters κ_0 and κ_e for the calculated curves were selected to ensure best coincidence of the normalized structure functions with the quantity $1 - b_S(x, y)$ in the saturation region (curves 1, 2) and on the section of power-law increase ($D_S(y) \sim y^{5/3}$) (curves 3, 4). This comparison shows that models (1.1.38), (1.1.39) do not give satisfactory coincidence of calculation with experiment over the whole range of spacing of observation points. Now let us calculate the one-dimensional spatial phase spectrum from the experimental correlation functions, and compare it with the two-dimensional spectrum of fluctuations of the index of refraction (3) that correspond to models (1.1.38), (1.1.39).

According to Ref. 82, we will calculate the Fourier transform of experimental correlation functions (6) by the formulas

$$\bar{v}_S(\varkappa_2) = \frac{\Delta}{\pi}\left[1 + 2\sum_{k=1}^{N-1} b_S(y_k)\, w(y_k)\cos \varkappa_2 y_k\right], \qquad (7)$$

$$w(u) = \begin{cases} 1 - 6(u/M)^2 + 6(|u|/M)^3, & |u| \leqslant M/2; \\ 2(1 - |u|/M)^3, & M/2 < |u| \leqslant M; \\ 0, & |u| > M, \end{cases}$$

where $y_k = k\Delta$, $\bar{v}_S(\varkappa_2) = \bar{V}_S(\varkappa_2)/\sigma_S^2$ is the normalized spectrum; σ_S^2 is the dispersion of phase fluctuations. We make our estimate of spectrum (7) for window width $M = 1.1$ m. Then the confidence interval for $\bar{v}_S(\kappa_2)$ at probability 0.8 is equal to $(0.5\bar{v}_S(\kappa_2),\ 4\bar{v}_S(\kappa_2))$, and the width of the spectral window ($\Delta\kappa_2 = 1.86/M$) is 1.7 m^{-1}.

The finiteness of the width of the spectral window leads to displacement of the spectrum. To evaluate the magnitude of the possible displacement, we calculate the spectrum by formula (7) with step $\Delta = 5$ cm, substituting values of correlation coefficient (4). The spectrum corresponding to correlation coefficient (4) is

$$v_S(\varkappa_2) = \frac{\Gamma(4/3)\,\Gamma(1/2)}{\Gamma(5/6)}\,\varkappa_0^{-1}\left(1 + \frac{\varkappa_2^2}{\varkappa_0^2}\right)^{-4/3}. \qquad (8)$$

We calculate the estimate of the spectrum by formula (7) at $\kappa_0 = 5$ m^{-1}. From the results of the calculation, shown in Fig. 71, we see that possible displacements of the estimate of the spectrum on segment $0.05\ \text{m}^{-1} \leqslant \kappa_2 \leqslant 10\ \text{m}^{-1}$ do not exceed 2% for width of the spectral window $\Delta\kappa = 1.7$ m^{-1}.

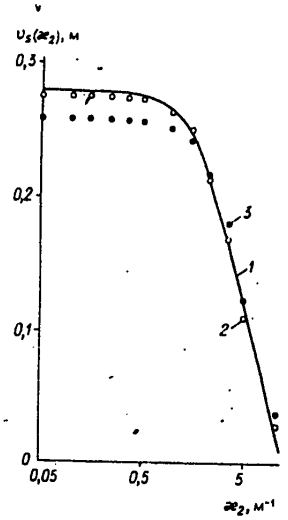

Fig. 71. Influence of spectral window width on estimate of phase spectrum: 1--exact spectrum (8) at $\kappa_0 = 5$ m^{-1}; 2, 3--estimates of the spectrum by formula (7): 2--N-22; 3--N = 15

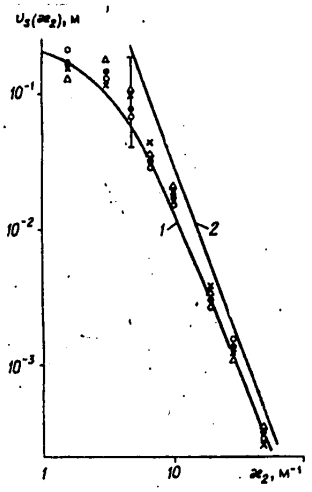

Fig. 72. One-dimensional spatial spectrum of phase fluctuations: 1, 2--model spectrum (8) and power-law asymptote ($\kappa/\kappa_0 \gg 1$) of model spectrum (8) at $\kappa_0 = 4.3$ m^{-1}; symbols for points correspond to Fig. 70

Fig. 72 shows spectra $v_S(\kappa_2)$ calculated by using formulas (6), (7) from the experimental data shown on Fig. 70. The vertical line segment shows the confidence interval. This same figure shows the model spectrum (8). The external scale of the model spectrum ($\kappa_0 = 4.3$ m^{-1}) was chosen from coincidence with experimental values at the point of maximum frequency ($\kappa_2 = 50$ m^{-1}). The normalized structure function corresponding to this spectrum is shown on Fig. 70. As can be seen from a comparison of experimental structure functions and spatial spectra of phase fluctuations with models (1.1.38), (1.1.39), the models cannot describe the spectrum equally well at all space frequencies. The measured spectrum deviates from power-law dependence corresponding to a Kolmogorov-Obukhov 2/3 law at lower space frequencies, and hence for larger spatial scales than given by models (1.1.38), (1.1.39). The external scale determined from relation $L_0 = \kappa_0^{-1} \cdot 2\pi = 1.46$ m coincides with the height of the beam over the underlying surface.

6610
CSO: 1862/71

UDC 621.375.826:681.3

LASER MEASUREMENT SYSTEMS

Moscow LAZERNYYE IZMERITEL'NYYE SISTEMY in Russian 1981 (signed to press 21 Aug 81) pp 2-6, 454-456

[Annotation, preface and table of contents from book "Laser Measurement Systems", by Anatoliy Semenovich Batrakov, Mikhail Mikhaylovich Butusov, Grigoriy Petrovich Grechka, Anatoliy Adamovich Korniyenko, Dmitriy Pavlovich Luk'yanov (editor), Andrey Vladimirovich Mochalov and Yuriy Vladimirovich Filatov, Izdatel'stvo "Radio i svyaz'", 8000 copies, 456 pages]

[Text] The book presents the physical fundamentals and principles of design of laser measurement systems used to do a variety of jobs in lidar, precision registration of linear and angular displacements, velocities and accelerations. Considerable attention is given to the accuracy characteristics of such systems, improving the working efficiency by adapting coherent optical fields to turbulent distortions. Engineering methods are considered for calculating and optimizing the characteristics of laser measurement systems, and unconventional modes of operation are described for promising components of laser equipment.

The book is intended for radio engineers, optics specialists, workers in metrology, and also for graduate students and upperclassmen majoring in electronics, optics and instrument making.

Preface

The unique properties of coherent optical radiation have been responsible for the rapid pace of development and practical application of laser methods and facilities in the most diverse areas of the national economy. The capability of getting high power densities by focusing laser emission into a spot of quite small size has been the basis for technical facilities and development of a new sector--laser technology. Considerable advances have been made in this field. Production has been organized in the Soviet Union and elsewhere for output of industrial equipment for welding, cutting and machining materials, making assembling and aligning components and subassemblies of electronic devices. Therefore it is no wonder that Soviet and non-Soviet publications have reflected fairly complete coverage of an extensive class of problems in laser technology.

Theoretical results of significance as well as important practical advances have been achieved as well in the field of data transmission over coherent optics

communication channels that enable us to send exceptionally large volumes of information on a single optical carrier, have high directionality of emission that increases interference immunity, economy and electromagnetic compatibility of data transmission systems. Many papers have also been published on the theory of optical communications that have dealt with the state of the art and outlook for this field.

In addition, lasers are being successfully used in lidar systems, laser geology and navigation, metrology and geoprospecting, and in scientific experiments. A common feature of such systems is the measurement of certain parameters of objects, the coordinates of bodies in a four-dimensional space-time manifold, characteristics of physical fields that are reflected in the change of informative parameters of coherent optical fields after they have interacted with material objects. In the aggregate, such systems can be called laser measurement systems.

We readily notice that laser measurement systems are fundamentally different from optical data transmission systems that use lasers. In optical communications systems, the source of information precedes the transmitter, and the signal acquires specific information before entering the communication line. On the other hand, in most laser measurement systems the signal radiated by the transmitter does not carry measurement information, but is rather an a priori known periodic or pseudorandom function of time, as occurs for example in lidar, laser spectroscopy and Doppler ranging. Therefore, the fairly well developed methodology of using lasers in communications systems cannot always be directly transferred to laser measurement systems.

Today, considerable progress has been made in the area of practical use of laser measurement systems thanks to advances in fundamental research, technological improvements and the organization of mass production of subassemblies and components of laser systems. At the same time, it should be noted that it is becoming more and more difficult for the specialist to find his way through the constantly increasing stream of publications on laser measurement systems that have not as yet found sufficiently complete and systematized reflection in scientific and technical reference works and monographs. It is only in isolated areas such as laser gyroscopy and applied holography that we see an examination of theoretical questions and problems of practical use of lasers for handling specific measurement jobs. Therefore in this book the authors have made it their goal to gather and generalize the extensive information on the theoretical foundations and principles of designing laser measurement systems that register the parameters of a light wave field varying as a result of interaction with objects of investigation of various kinds (artificial satellites, streams of liquid or gas, acoustic wave forms, gravitational fields and so on).

The considerable diversity of laser measurement systems, their principles of design and methods of analysis have faced the authors with the problem of selecting material and principles for systematizing this material. The investigation of accuracy characteristics occupies a central place in the theory of laser measurement systems. Of important significance for laser measurement systems on the current stage of their development is analysis of potential and real accuracy, determination of factors that limit their ultimate accuracy characteristics under actual operating conditions, and finding effective methods for optimizing these characteristics. In this connection, it has been deemed advisable in this book

to deal primarily with problems of improving the working efficiency of laser measurement systems that can be solved both by optimum selection of their parameters, and by adapting the structure and parameters to characteristics of randomly inhomogeneous media that in many cases separate the measurement part and the object of research.

In choosing material with respect to specific types of laser measurement systems, the authors have striven on the one hand to represent the most widely used systems --lidars, Doppler velocity meters--concentrating attention on problems of choosing their block diagrams and on methods of evaluating accuracy characteristics in which the particulars of coherent optical fields show up most completely, and on the other hand--to demonstrate unconventional measurement methods and facilities that at times have no corresponding analogs in other wave bands. In this connection, the analysis has included laser accelerometers, precision instruments for measuring angular displacements and velocities based on gas ring lasers, holographic interferometers for studying strains and vibrations, and also parametric frequency converters that are of promise for measurement systems.

It is quite natural that not all the enumerated laser measurement systems have today been developed in equal measure. For example, while the area of lidar, optical range finding and laser goniometry has seen development not only of the principles of construction of appropriate instruments but also an element base resulting in production and successful operation of precision range finders and dynamic angle-measuring instruments, at the same time today's laser accelerometers are so far the object of laboratory studies. However, even on this level they have convincingly shown the promise of different versions of laser accelerometers, and the accuracy characteristics already achieved in laser gravimeters are of undoubted interest to a wide range of specialists. Finally, the choice of material has been influenced to some extent by the authors' own scientific interests as well, and some chapters have been written on their research.

The contents of the book could be conditionally divided into three parts. The first part (chapters 1, 2) covers principles of design and possible strategies for using laser measurement systems with consideration of statistical space-time characteristics of perturbing fields of the atmosphere, and methods of adapting an optical signal to turbulent distortions. The second part (chapters 3-9) deals with description of specific types of laser measurement systems and analysis of their accuracy characteristics. The third part (chapters 10, 11) examines problems of improving the element base of laser measurement systems.

Laser measurement systems are undergoing a developmental stage, and have already gained a strong position in some of the most important areas of science and technology. And this process shows a pronounced tendency to develop further. Under these conditions, the authors have not set themselves the task of considering all existing types of measurement systems, and at the same time they realize that in such a rapidly developing field as laser measurement technology it is difficult to single out and present just those aspects that will not be seriously revised in the near future.

The book has been written by a collective of authors. Chapter 1 was written jointly by A. A. Korniyenko and D. P. Luk'yanov, chapter 2 was written by

A. A. Korniyenko, chapter 3--by A. S. Batrakov with inclusion of material furnished by A. I. Bakalyar, chapter 4--by A. S. Batrakov, chapters 5, 7, 10, 11--by D. P. Luk'yanov, chapter 6--by M. M. Butusov, chapter 8 was written by G. P. Grechka, D. P. Luk'yanov and A. V. Mochalov, and chapter 9--by D. P. Luk'yanov, A. V. Mochalov and Yu. V. Filatov.

The authors thank Professor A. G. Sheremet'yev for useful remarks in preparing the draft of the manuscript, and also Professor V. P. Vasil'yev and Doctor of Technical Sciences G. I. Vasilenko for reviewing the book and making critical comments which the authors gratefully took into consideration in revising the manuscript.

All comments and suggestions on the content of the book may be addressed to: Moscow, 101000, Glavpochtamt, a/ya 693.

Contents page

6610
CSO: 1862/62

ABSTRACTS OF ARTICLES IN COLLECTION ON QUANTUM ELECTRONICS

Kiev KVANTOVAYA ELEKTRONIKA: RESPUBLIKANSKIY MEZHVEDOMSTVENNYY SBORNIK in Russian No 20, 1981 (signed to press 19 May 81) pp 111-112

[Abstracts of articles from collection "Quantum Electronics", edited by L. N. Pan'shina, Institute of Semiconductors, UkSSR Academy of Sciences, Izdatel'stvo "Naukova dumka", 1000 copies, 112 pages]

UDC 621.373.8

RING LASER WITH ACTIVE AMPLITUDE GATE

[Abstract of article by Kravchenko, V. I., Milovskiy, N. D. and Popova, L. L.]

[Text] An experimental and theoretical study is done on the characteristics of a traveling-wave ring laser that includes an amplitude gate consisting of split and return mirrors with an additional active substance placed between them. The authors determine the threshold gain, ratio of intensities of opposed waves, and the way that these characteristics depend on the parameters of the active medium and the optical cavity. It is shown that the additional active substance makes little contribution to the overall energy behavior of the laser. However, the presence of an additional amplifying medium in the amplitude gate considerably reduces the time of establishment of single-mode lasing, and is conducive to attainment of maximum coherently emitted power at the highest value of the coefficient of suppression of the counter wave. Figures 8, references 11.

UDC 621.373.8

OPTIMUM WORKING CONDITIONS OF RING LASER WITH AMPLITUDE GATE

[Abstract of article by Milovskiy, N. D. and Popova, L. L.]

[Text] A new technique is developed for calculating the characteristics of lasers with coupled cavities. The method is used for calculating threshold pumping and the ratio of intensities of opposed waves in a ring laser with amplitude gate and a scattering inhomogeneity inside the resonant cavity. Two sets of values of cavity parameters are determined at which the ring laser is characterized either by minimum threshold pumping or by maximum coefficient of suppression of the counter wave. Figures 3, references 10.

UDC 621.378.325

CALCULATING OPTIMUM PARAMETERS OF SODIUM VAPOR PLASMODYNAMIC LASER

[Abstract of article by Bogacheva, S. P., Borisov, I. I., Kubaychuk, V. P. and Reysig, V. A.]

[Text] A numerical study is done on discharge of argon plasma with a small additive (1 mass percent) of sodium from a flat nozzle into a channel of rectangular cross section for the purpose of determining stagnation parameters at which maximum output characteristics of a plasmodynamic laser are attained. The calculations were done over a wide range of initial temperatures (2500-6000 K) and pressures (1-20 atm). It is shown that at a stagnation temperature above a certain value the output radiation power is weakly dependent on pressure. Thanks to the nonmonotonic dependence of electron temperature on pressure, it turned out to be possible to optimize the lasing characteristics of the medium. The paper gives maximum values of inversion, gain and lasing power, and also the stagnation parameters of the plasma stream at which they are attained. Figures 10, references 12.

UDC 621.373.853.08

OPTICALLY PUMPED SUBMILLIMETER PULSE LASERS OF OSCILLATOR-AMPLIFIER TYPE

[Abstract of article by Manita, O. F.]

[Text] The paper describes designs of submillimeter lasers that operate in the pulsed mode with linear transverse pumping. The author gives the results of investigation of the energy and time characteristics of these systems. An examination is made of different lasing conditions as determined by the pressure of the active medium, pumping level, cavity parameters and so on. Optimum conditions are found for maximizing lasing energy. Figures 8, references 10.

UDC 621.378.4

SOME PRINCIPLES OF INTRACAVITY STIMULATED EMISSION OF SECOND OPTICAL HARMONIC

[Abstract of article by Belyy, M. U., Korniyenko, N. Ye., Okhrimenko, B. A., Petrenko, R. A., Strizhevskiy, V. L., Sharapa, A. I. and Yzshchuk, V. P.]

[Text] Based on semiclassical equations for an active medium and truncated equations of nonlinear optics for a nonlinear crystal, an examination is made of intracavity lasing of the second harmonic. A detailed analysis is made of the influence that dissipative and Fresnel losses in a nonlinear crystal have on the efficiency of intracavity lasing of the second harmonic. A scheme of intracavity lasing of the second harmonic with intermediate feedback is proposed for weakening the influence that losses in the nonlinear crystal have on laser emission. In particular, an examination is made of standing-wave and traveling-wave lasers in cases of homogeneous and inhomogeneous broadening of luminescence lines of the active medium with consideration of interference of opposed waves and inertness of the nonradiative transition. Analytical expressions are obtained close to the lasing threshold in all investigated cases. An experimental investigation is made of two schemes of intracavity lasing of the second harmonic and a scheme with intermediate feedback. Results agree well with theory. Figures 8, references 28.

UDC 621.375.82

MATERIALS OF QUANTUM ELECTRONICS BASED ON COMPLEX SEMICONDUCTOR COMPOUNDS. ANHARMONICITY OF LATTICE VIBRATIONS IN CRYSTALS DURING PHASE TRANSITIONS

[Abstract of article by Slivka, V. Yu., Vysochanskiy, Yu. M. and Chepur, D. V.]

[Text] The paper systematizes research data on vibrational spectra of crystals in the vicinity of phase transitions that give information on the nature of phonon-phonon interactions and the part they play in the lattice instability effect. It is noted that different experimental methods must be used to get the most complete representation of the nature of the phase transition. An examination is made of the methods of determining the significance of anharmonic processes and explaining their specific mechanisms. The authors give the results of a study of the lattice dynamics of the new ferroelectric semiconductor $Sn_2P_2S_6$, which is a model object for determining the role of phonon-phonon interactions, studying external influences on the soft mode, and establishing the relation between this mode and a variety of physical properties of the crystal. Figures 6, table 1, references 84.

UDC 621.375.82

MATERIALS OF QUANTUM ELECTRONICS BASED ON COMPLEX SEMICONDUCTOR COMPOUNDS. PHYSICAL PROPERTIES

[Abstract of article by Slivka, V. Yu., Voroshilov, Yu. V. and Chepur, D. V.]

[Text] Data are systematized on the nonlinear, acousto-optical, electro-optical and optical active crystals that are based on complex chalcogenides and chalcogenhalides. Data are presented on birefringence, region of transparency, angles of phase synchronism, acousto-optical quality, nonlinear susceptibility, specific rotation of the plane of light polarization and other parameters that determine the working efficiency of laser devices. Figures 10, tables 7, references 96.

UDC 621.375.82

PRODUCTION AND PROPERTIES OF COMPLEX SEMICONDUCTOR MATERIALS WITH PROMISE FOR QUANTUM ELECTRONICS AND OPTOELECTRONICS

[Abstract of article by Golovey, M. I., Peresh, Ye. Yu. and Semrad, Ye. Ye.]

[Text] Data are given from results of growing and studying the physicochemical, electrophysical and optical properties of semiconductors $AgGaS_2$, $AgGaSe_2$, $CdGa_2S_4$, $HgGa_2S_4$, $LiInS_2$, $InPS_4$, GaSe, Tl_3PSe_4, Tl_3AsS_4 and Tl_3AsSe_3, as well as their possible areas of application. References 46.

UDC 621.372.826:621.315.61

SYNTHESIZING ASYMMETRIC PLANE INHOMOGENEOUS DIELECTRIC WAVEGUIDES. TECHNIQUE AND METHODS OF CALCULATION

[Abstract of article by Andrushko, L. M.]

[Text] A technique is described for synthesizing asymmetric waveguides in the case of sharply differing parameters of the media surrounding the waveguiding

layer. The paper gives normalized distributions of permittivity in the cross section of inhomogeneous waveguides with cutoff frequencies of the zeroth and first modes shifted in comparison to homogeneous waveguides. The new types of waveguides have larger transverse dimensions in single-mode operation. An investigation is made of the way that the cutoff frequency is influenced by the finite value of the parameter a characterizing asymmetry of parameters of external media. Figures 4, references 3.

UDC 621.373.8:621.376.2

USING RESONANT PROPERTIES OF A DISCHARGE IN SYSTEMS FOR STABILIZING EMISSION POWER

[Abstract of article by Baran, V. M. and Kononchuk, G. L.]

[Text] The paper describes two systems of stabilization of the variable component of power of stimulated emission from gas-discharge lasers. The variable power component is obtained by modulation of the discharge current of the tube; negative feedback with respect to radiation and the resonant properties of the discharge are used for stabilization. In the first system, the modulation frequency is automatically tuned to a value corresponding to the given level of the variable power component, and in the second system the resonant frequency of the discharge is controlled. The working frequency in either case is chosen on the left slope of the resonance characteristic curve. Figures 3, references 2.

6610
CSO: 1862/65

MAGNETOHYDRODYNAMICS

SCIENCE SESSION ON THERMOPHYSICAL AND ELECTROPHYSICAL PROBLEMS OF MHD ENERGY CONVERSION METHOD

Moscow TEPLOFIZIKA VYSOKIKH TEMPERATUR in Russian Vol 19, No 5, Sep-Oct 81 pp 1115-1116

[Text] In accordance with a Decree of the General Assembly of the USSR Academy of Sciences dated 14 March 1981 on further development of fundamental research to ensure acceleration of scientific and technical progress and to improve efficiency of social production, a Science Session was held in Moscow, 18-19 May 1981, by science councils of the USSR Academy of Sciences on complex problems of "Methods of Direct Conversion of Thermal to Electrical Energy", "Thermophysics" and "Scientific Principles of Electrophysics and Electric Power."

Participating in the work were members of the USSR Academy of Sciences: academicians B. P. Zhukov, V. A. Kirillin, V. I. Popkov, A. Ye. Sheyndlin, associate members of the USSR Academy of Sciences L. M. Biberman, K. S. Demirchyan, V. M. Iyevlev, B. S. Petukhov, I. S. Khlopkin, Academician of the UkSSR Academy of Sciences I. T. Shvets, eminent scientists of our nation.

In attendance were more than 250 specialists from research, planning and operational organizations of Moscow, Leningrad, Kiev, Vilnius, Khar'kov, Krasnodarsk, Sverdlovsk and elsewhere engaged in research and development aimed at realization of MHD facilities of various types and purposes.

During the two days of work of the session, three meetings were held at which 20 reports were heard and a working discussional group was organized.

The main program of the session was devoted to solving thermophysical and electrophysical problems involved in developing the first industrial unit of the MGDES-500 MHD electric plant; development of pulsed MHD generators for geophysical purposes; research in the field of coal-fired MHD electric plants; investigation of processes in MHD generators using nonideal and nonequilibrium plasma.

The reports presented at the session show the significant scientific and practical advances that have been made by different organizations in solving the formulated problems. These advances include in particular:

--development of methods of calculating flows in high-power MHD generators;
--creation of a technique for calculating radiative and convective heat exchange in industrial MHD electric plants;

--development of effective methods for heat protection of the walls of MHD generators;
--development of MHD generator substitution circuits;
--creation of pulsed MHD facilities and carrying out experiments on electromagnetic depth probing.

At the same time, it was pointed out at the session that the approximate methods now being used for calculations of MHD processes do not account for certain real effects that are important for planning and development of MHD power units; work has been inadequate on electrical engineering aspects involving the development of conversion systems for MHD electric plants; there has been a lag in development and realization of superconductive magnet systems for MHD generators; not enough attention is being given to joint research on the problem of making a solid-fuel MHD electric plant; further work is needed on problems of using nonequilibrium and nonideal plasma as a working fluid for the MHD generator.

The session placed particular emphasis on the need for increasing reliability (service life) of MHD generators used for power industry requirements.

Four major areas of development in research on magnetihydrodynamics were distinguished at the session that require particular attention and concentration of efforts in the immediate future:

--creation of the first industrial MHD power unit in the world with capacity of 500 MW [MGDES-500] at Ryazan State Regional Electric Plant; solution of a complex of thermophysical and electrophysical problems associated with development of equipment for the MGDES-500 plant;
--development of research on a broad front aimed at creation of promising coal-fired MHD electric plants; joint research by different organizations on this topic to solve the problem as rapidly as possible;
--creation and national economic use of pulsed MHD facilities for predicting earthquakes and for mineral prospecting;
--studying processes in MHD generators on nonideal and nonequilibrium plasma, including a T-layer MHD generator; development of new and promising arrangements using MHD devices.

Work of the session showed that all major areas of MHD research have yielded some important results that are of great significance for the solution of standing problems.

It was strongly urged at the session that all organizations and science councils of the USSR Academy of Sciences taking part in the work give consideration to the recommendations, critical comments and suggestions offered in papers, questions and discussions.

Academician A. Ye. Sheyndlin gave a survey report entitled "The Most Important Thermophysical and Electrophysical Problems Involved in Developing an Industrial MHD Power Facility". The paper was received with considerable interest and followed by a lively discussion. Reports were then heard dealing with more specific thermophysical and electrophysical problems of MHD energy conversion.

6610
CSO: 1862/63

OPTICS AND SPECTROSCOPY

UDC 621.378.325

PROPERTIES OF RESONATORS WITH MIRRORS FORMED BY SET OF INVERTING ELEMENTS

Moscow KVANTOVAYA ELEKTRONIKA in Russian Vol 8, No 11(113), Nov 81 (manuscript received 15 Jan 81) pp 2345-2349

[Article by I. M. Bel'dyugin]

[Text] The problem of finding the field amplitudes of the oscillation modes of a resonator formed by mirrors consisting of a set of inverting elements of the triple prism, corner reflector or other type is analyzed. A discussion is presented of the problem of the influence of optical inhomogeneities of the medium and dephasing of the mirror elements on the behavior of the resonator mode fields.

At the present time devices have been developed which provide partial compensation of phase distortions of emission [1, 2] and which are used to solve the same problems as are solved by the phenomenon of wave front reversal in nonlinear media. These devices are composite reflecting matrices formed by a set of inverting elements. The properties of such matrices that are useful for applications arise from the fact that each element of them has within some limits the property of converting the field of radiation incident on it by the law

$$U_{out}(\mathbf{r}_\perp)=U_{in}(-\mathbf{r}_\perp), \tag{1}$$

where U_{in}, U_{out} are the field amplitudes of the incident and reflected waves, respectively; the origin of the coordinates is considered to be at the center of the element, and the Z-axis coincides with its axis.

Let us demonstrate that optical elements which are component elements of the matrices such as reflectors of the "cat's eye" type, corner reflectors, triple prisms and also elements of cut replicas realize conversion (1). Actually, each of the enumerated elements is a retroreflector element, that is, it has the property of reflecting beams incident on it strictly in the opposite direction. The transfer matrix of such an element is

$$T=\begin{vmatrix} -1 & B \\ 0 & -1 \end{vmatrix}, \tag{2}$$

where B is a parameter which has the dimensionality of length and depends on the position of the reference plane. For fields interacting with a real retroreflector element which are of interest for applications, using (2), it is possible to write

$$U_{\text{out}}(x) = \left(+\frac{i}{\lambda B}\right)^{1/2} \int_{-\tilde{a}}^{\tilde{a}} U_{\text{in}}(y) \exp\left[-\frac{i}{\lambda B}\pi (x+y)^2\right] dy, \qquad (3)$$

where 2ã is the size of the element along the transverse coordinate x; λ is the radiation wavelength. Now if we select the reference plane so that B=0, then from (3) considering the fact that in this case the product of the exponent times the factor in front of the integral is a δ-function, (1) follows directly.

For applications it is of interest to study the properties of the devices containing inverting elements as component elements. This paper is devoted to a study of the properties of resonators with mirrors in the form of matrices consisting of a set of identical inverting elements that generate a periodic structure.

Let us first consider the problem of transformation by such mirrors of plane waves incident on them. Considering that a plane wave of length λ is incident on the matrix at an angle $\theta_i \ll 1$, and using (1), it is easy to find the angular distribution of the reflected wave in the plane of incidence

$$I(\theta) \sim \left\{\frac{\sin\left[\frac{2\pi}{\lambda}\tilde{a}(\theta-\theta_i)\right]}{\frac{2\pi}{\lambda}\tilde{a}(\theta-\theta_i)}\right\}^2 \left\{\frac{\sin\left[\frac{2\pi}{\lambda}\tilde{a}(2N+1)(\theta+\theta_i)\right]}{\sin\left[\frac{2\pi}{\lambda}\tilde{a}(\theta+\theta_i)\right]}\right\}^2, \qquad (4)$$

where 2N+1 is the number of inverting elements in the mirror in the corresponding transverse direction. From (4) it follows that for $N \gg 1$, the angular spectrum of the reflected emission is a series of sharply expressed (δ-shaped) peaks at a distance of $\lambda/2\tilde{a}$ from each other modulated by the first cofactor. The characteristic angular dimension of this cofactor $\lambda/2\tilde{a}$, and its primary peak coincide with the retroreflector direction θ_i. It is also necessary to note that one of the δ-shaped peaks for which the second cofactor in (4) is responsible, coincides with the direction of mirror reflection ($-\theta_i$) of the incident wave.

Let us consider two limiting cases: $\theta_i \ll \lambda/2\tilde{a}$ and $\theta_i \gg \lambda/2\tilde{a}$.

In the first case from the above-described picture of the intensity distribution in the angular spectrum of a reflected wave it follows directly that the matrix reflects the wave incident on it as a plane mirror. This result can be understood, for example, from constructing wave fronts by the Huygens principle. Having the dimensions of the inverting elements approach zero, that is, satisfying the condition $\theta_i \ll \lambda/2\tilde{a}$, it is possible to neglect the characteristic features of wave propagation from individual elements and construct the wave front as on reflection from a smooth plane surface. This result also indicates that the resonator formed by the mirrors in the form of the investigated matrices has a set of modes analogous to the modes of a plane resonator of the same dimensions.

Here, obviously, the number of such modes must not exceed the number of mirror elements, the angular divergence of their radiation must be less than $\lambda/2\tilde{a}$, and they must be unstable with respect to disturbances leading to a change in direction of the emission by an amount greater than $\lambda/2\tilde{a}$.

In the second case from (4), it follows that the matrix reflects the radiation in a retroreflector direction θ_i with indeterminacy with respect to the angle $\sim\lambda/2\tilde{a}$, which coincides with the results of [2]. The problem of resonator modes, the divergence of the radiation of which $\theta\gtrsim\lambda/2\tilde{a}$ requires special investigation in this case.

We shall consider that the resonator of interest to us is formed by a reflecting matrix and an infinite plane mirror. For determinacy we shall consider the matrix apertures and the inverting elements rectangular. Then, inasmuch as the variables with respect to orthogonal directions are separated, it is sufficient to consider only the one-dimensional integral relations. If we consider inhomogeneities of the resonator medium to be slowly varying and concentrated near the reflecting matrix, then, limiting ourselves to the linear term in the expansion of the dispersion of the radiation phase front in the aperture of each element and using (1) in the Huygens-Fresnel approximation for field amplitudes of the oscillation modes at the matrix mirror of the resonator we obtain the integral relation

$$\gamma U(x)=\sqrt{i}\sum_{n=-N_1}^{N_2}\int_{-a}^{a}U(2na-y)\exp\{-i\pi(x-y-2na)^2+i2\varphi_n\}\,dy, \tag{5}$$

where $a=\tilde{a}/(L\lambda)^{1/2}$; L is the resonator length; $\phi_n=k\xi_n$; k is the wave number; ξ_n is the aberration measured at the point x=2 na.

In order to find solutions to equation (5) corresponding to modes with radiation divergence $\theta\gtrsim\lambda/2\tilde{a}$, let us consider the fact that any pair of individually taken inverting elements forms a resonator, the field of which is almost completely localized within the aperture of the elements with the exception of the low-intensity "tails" going beyond the limits of this aperture, incident on adjacent elements and forming a coupling between the fields of these resonators. This permits the use of an idea analogous to the idea of the strong bond method in solid-state physics [3], and it makes it possible to find a field on the entire surface of a reflecting matrix in the form of a linear combination of fields localized on individual inverting elements considering the influence of fields of only adjacent elements on each other.

Considering what has been stated above, let us write the expressions for the resonator mode field amplitudes:

$$U_p^{(\pm)l}(x)=\sum_{m=-N_1}^{N_2-l}C_{m,p}^{(\pm)l}U_p(x-2ma)\exp[i4\pi la(x-2ma)]\pm$$
$$\pm D_{m,p}^{(\pm)l}U_p(x-2ma-2la)\exp[-i4\pi la(x-2ma-2la)], \tag{6a}$$

$$U_p^0(x)=\sum_{m=-N_1}^{N_2}C_{m,p}^0U_p(x-2ma) \tag{6b}$$

for $\ell \neq 0$ and $\ell = 0$, respectively. Here the index $\ell = 0, 1, \ldots, N_1+N_2$ corresponds to fluctuations in an elementary resonator formed by k and $k+\ell$ ($k=-N_1, \ldots, N_2$) elements; the function $U_p(x)$ is a solution of the integral equation

$$\gamma U(x) = \sqrt{i} \int_{-a}^{a} U(-y) \exp[-i\pi(x-y)^2]\, dy, \tag{7}$$

which is the equation for the field amplitudes of a resonator formed by two inverting elements which are located at a distance of 2L opposite to each other. Here the solutions of (7) actually coincide with the well-investigated (see, for example [4]) solutions of the equation for a flat cavity.

Substituting (6a), (6b) in (5), multiplying (5) by $U_p(2ma-x)\exp[-i4\pi\ell a\times(x-2ma)]$ and $U_p(2ma+2\ell a-x)\exp[i4\pi\ell a\,(x-2ma-2\ell a)]$ and integrating both sides of (5) in the interval (-a, a), considering (7) we obtain

$$\begin{aligned}
&\gamma\left[C_{m,p}^{(\pm),l} + B_p\left(\exp\{i8\pi la^2\}\, C_{m-1,p}^{(\pm),l} + \exp\{-i8\pi la^2\}\, C_{m+1,p}^{(\pm),l}\right)\right] = \\
&= \pm\gamma_p \exp\{-i4\pi l^2a^2\}\left\{D_{m,p}^{(\pm),l} \exp\{i2\varphi_{l+m}\} + B_p\left[D_{m-1,p}^{(\pm),l}\times\right.\right. \\
&\times\left(\exp\{i(2\varphi_{l+m-1} + 8\pi la^2)\} + \exp\{i(2\varphi_{l+m} - 8\pi la^2)\}\right) + \\
&\left.\left. + D_{m+1,p}^{(\pm),l}\left(\exp\{i(2\varphi_{l+m+1} - 8\pi la^2)\} + \exp\{i(2\varphi_{l+m} + 8\pi la^2)\}\right)\right]\right\};
\end{aligned} \tag{8a}$$

$$\begin{aligned}
&\gamma\left[D_{m,p}^{(\pm),l} + B_p\left(\exp\{-i8\pi la^2\}\, D_{m-1,p}^{(\pm),l} + \exp\{i8\pi la^2\}\, D_{m+1,p}^{(\pm),l}\right)\right] = \\
&= \pm\gamma_p \exp\{-i4\pi l^2a^2\}\left\{C_{m,p}^{(\pm),l} \exp\{i2\varphi_m\} + \right. \\
&+ B_p\left[C_{m-1,p}^{(\pm),l}\left(\exp\{i(2\varphi_{m-1} - 8\pi la^2)\} + \exp\{i(2\varphi_m + 8\pi la^2)\}\right) + \right. \\
&\left.\left. + C_{m+1,p}^{(\pm),l}\left(\exp\{i(2\varphi_{m+1} + 8\pi la^2)\} + \exp\{i(2\varphi_m - 8\pi la^2)\}\right)\right]\right\}.
\end{aligned} \tag{8b}$$

where $B_p = \int_{-a}^{a} U_p(-x)\, U_p(x+a)\, dx$; γ_p is the eigenvalue corresponding to the solution $U_p(x)$ of equation (7). Equations (8a), (8b) must be solved with the boundary conditions

$$C_{-N_1-1,p}^{(\pm),l} = C_{N_2+1-l,p}^{(\pm),l} = D_{-N_1-1,p}^{(\pm),l} = D_{N_2+1-l,p}^{(\pm),l} = 0. \tag{9}$$

Let us consider two limiting cases. In the first case we shall consider that the optical inhomogeneities of the medium vary little or, more precisely,

$$|\exp\{i2\varphi_m\} - \exp\{i2\varphi_{m+k}\}| \ll |B_p| \tag{10}$$

for all possible values of indexes m and k and for all values of the index m

$$\varphi_m \approx \varphi.$$

Then, considering that $|B_p| \ll 1$, it is possible to set:

$$D_{m,p}^{(\pm),l} = C_{m,p}^{(\pm),l} + e_{m,p}^{(\pm),l}, \quad |e_{m,p}^{(\pm),l}/C_{m,p}^{(\pm),l}| \ll 1 \tag{11}$$

and

$$\gamma = \pm\gamma_p \exp\{-i(4\pi l^2a^2 - 2\varphi)\} + \Delta_p^{(\pm),l}, \quad |\Delta_p^{(\pm),l}/\gamma_p| \ll 1. \tag{12}$$

Considering (9) and (11), (12) from (8) we find

$$\Delta_{p,k}^{(\pm),l} = \pm\gamma_p \exp\{-i(4\pi l^2 a^2 - 2\varphi)\}\cos(8\pi l a^2)\cos\left(\frac{k\pi}{N_2+N_1+2-l}\right)B_p;$$

$$C_{m,p}^{(\pm),l(k)} = A_p^{(\pm),l,(k)}\sin\frac{\pi k(m+N_1+1)}{N_2+N_1+2-l}; \tag{13}$$

$$\varepsilon_{m,p}^{(\pm),l,(k)} = \frac{\Delta_{p,k}^{(\pm),l}C_{m,p}^{(\pm),l,(k)} \mp B_p\gamma_p \exp\{-i(4\pi l^2 a^2 - 2\varphi)\}\times \left[C_{m-1,p}^{(\pm),l,(k)}\exp(-i8\pi l a^2) + C_{m+1,p}^{(\pm),l,(k)}\exp(i8\pi l a^2)\right]}{\pm\gamma\exp\{-i(4\pi l^2 a^2 - 2\varphi)\}},$$

where $k=1, 2, \ldots, N_2+N_1+1-l$; $A_p^{(\pm),l,(k)}$ are arbitrary complex constants.

Thus, in this case the fields on the individual elements of a matrix mirror are related to each other according to expressions (13) as a result of partial overflow of radiation to adjacent elements. The situation and the relations (13) are essentially analogous to the situation and corresponding relations occurring in solid-state physics in the case of powerful valence electron bonds in atoms [3].

In the latter case when the inequality (10) has the opposite value it is possible to neglect the overflow of radiation from element to element:

$$\gamma_{p,m}^{(\pm),l} = \pm\gamma_p \exp\{-i(4\pi l^2 a^2 - \varphi_m - \varphi_{m+l})\},$$
$$C_{m,p}^{(\pm),l}\exp(i\varphi_m) = D_{m,p}^{(\pm),l}\exp(i\varphi_{m+l}) = A_{m,p}^{(\pm),l},$$

where $A_{m,p}^{(\pm),l}$ are arbitrary constants.

Thus, in this case, which corresponds to strongly varying inhomogeneities of the medium or, what amounts to the same thing, powerful dephasing of the matrix elements, the fields on individual pairs of inverting elements of the matrix are formed independently of each other.

The estimate of to what degree the phase distortions of the mirror consisting of a set of inverting elements are compensated, is also of interest for application. Let us consider, for example, a lens D in diameter with a focal length f as a source of optical distortions. On transmission of a well-collimated beam through this lens, the beam acquires angular divergence

$$\theta_n = D/f. \tag{14}$$

If we use a mirror consisting of a set of inverting elements, for example, of the "cat's eye" type to compensate the phase distortions introduced into the beam by the lens, then the resultant divergence of the beam considering the wave properties of the radiation

$$\theta \approx 2d/|f| + \lambda/d, \tag{15}$$

where d is the transverse dimension of the element.

From (15) it follows that the minimum attainable divergence with this method of compensation of the phase distortions

$$\theta_{min}=2\sqrt{2\lambda/|f|} \tag{16}$$

is realized for

$$d_{opt}=\sqrt{\lambda|f|/2.} \tag{17}$$

Let us assume for estimation D=2 cm, f=10^2 cm, λ=1 micron, θ_ℓ=20 milliradians. Then from (16), (17) θ_{min}=2.8 mrad, d_{opt}=0.7 mm.

Let us note that the diffraction limit of the divergence in this case $\theta_D=\lambda/D$=0.05 mrad.

The author expresses his appreciation to S. P. Vorotilin for assistance in individual phase of this work.

BIBLIOGRAPHY

1. Orlov, V. K.; Virnik, Ya. Z.; Vorotilin, S. P.; Gerasimov, V. B.; Kalinin, Yu. A.; Sagalovich, A. Ya. KVANTOVAYA ELEKTRONIKA [Quantum Electronics], No 5, 1978, p 1389.

2. Barrett, H. H.; Jacobs, S. F. OPT. LETTS., No 4, 1979, p 190.

3. Davydov, A. S. KVANTOVAYA MEKHANIKA [Quantum Mechanics], Moscow, Nauka, 1973.

4. Vaynshteyn, L. A. OTKRYTYYE REZONATORY I OTKRYTYYE VOLNOVODY [Open Resonators and Open Waveguides], Moscow, Sov. radio, 1966.

10845
CSO: 1862/75

OPTOELECTRONICS

UDC 621.38

ELECTROLUMINESCENT IMAGE CONVERTER WITH MEMORY

Tbilisi OPTOELEKTRONIKA, KVANTOVAYA ELEKTRONIKA I PRIKLADNAYA OPTIKA in Russian 1980 (signed to press 12 Sep 80) pp 38-43, 142-143

[Article by M. I. Brodzeli, E. L. Kertsman, G. D. Konstantinov and R. A. Polyan, and table of contents from book "Optoelectronics, Quantum Electronics and Applied Optics", edited by Sh. Sh. Gvatua, Institute of Cybernetics, GSSR Academy of Sciences, Izdatel'stvo "Metsniyereba", 1000 copies, 144 pages]

[Text] References 1 and 2 were the first to demonstrate the feasibility of infrared-to-visible image converters based on semiconductors with width of the forbidden band $\Delta E = 1.2$ eV and zinc sulfide electrophosphors (Ep). In contrast to previously known photoconductor-electrophosphor systems, the proposed image converters had memory limited by the time of shielding of the electric field in the semiconductor as a consequence of heat generation. Therefore in the widespread case of image converters based on silicon ($\rho \approx 10^4$ $\Omega \cdot$cm), the storage time at $T = 300$ K was no longer than 10^{-3} s.

It was reported in Ref. 3 that image converters based on p- or n-Si with concentration of ionized dopant $N \approx 10^{12}$-10^{13} cm^{-3} and ZnS(Cu) electrophosphor have much longer memory. A layer of $SiO_2 \sim 10^{-5}$ cm was applied by the plasmochemical deposition method to both sides [4] on Si slices of thickness $L_П \approx 10^{-2}$ cm. The resultant DSD structures after removal of a voltage pulse had strong polarization [5, 6]. A layer of ZnS(Cu) in a binder (VS-530 lacquer) was applied to one side of the DSD to thickness $L_{ЭП} \approx 10^{-3}$ cm. The electrodes were semitransparent layers of silver. The MSDSEpM structures were supplied with voltage $U(t) = U_0 \sin 2\pi ft$ at $U_0 = 10^2$ V, $f = 10^2$-10^6 Hz. The requirements for working conditions and geometry of the image converters take the form

$$W = \left(\frac{E_П U_П(t)}{4\pi q n_{СТ}}\right)^{1/2} \gg L_{эд}; \quad L_П \gg L_{эд}, \qquad (1)$$

where $E_П$, $U_П(t)$, W, $n_{СТ}$ are permittivity, voltage, length of the depleted region and steady-state concentration of ionized dopant for the semiconductor at the given U(t).

The infrared image ($\lambda = 10^{-4}$ cm) with exposure time of 0.1-10 s went to the input of the image converter and was stored on the ZnS(Cu) phosphorescing background as a negative or positive. Storage time with continuous readout was 10^2 s, and increased if readout was done in sine-wave voltage bursts with low duty factor.

In our research, additional experiments were done to explain such long memory of the image converter. To be certain that electronic processes in the ZnS(Cu) had no effect on the current characteristics of the structures as measured by the technique of Ref. 5, 6, the measurements done on the MDSDEpM were repeated on asymmetric specimens of MDSDM. Results were analogous.

1. A constant voltage pulse $U_П \cong 100$-300 V with duration of 1-10 s was applied to the MDSDEpM. After removing $U_П$, voltage $U(t) = U_0 \sin \omega t$ was switched on, and a transient process was observed with duration $t_{пер} \cong 10$-100 s during which there was a strong change in the background luminescence brightness of the electrophosphor $B_Ф(t)$ and current $I(t)$ through the specimen. Upon completion of $t_{пер}$, the quantities $B_Ф$ and I took on steady-state values $B_Ф^{СТ}$ and $I_{СТ}(t)$. Depending on the polarity of $U_П$, the background either was quenched or increased in brightness during time $t_{пер}$. Oscillograms of currents $I_1(0)$ and $I_2(0)$ for these cases taken at time $t = 0$ of activation of $U(t)$ are shown on Fig. 1a, b. Comparison of $I_1(0)$

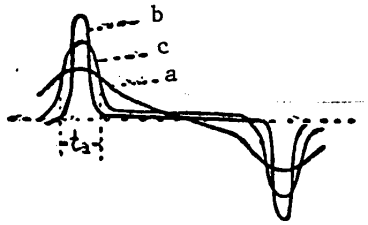

Fig. 1. Oscillograms of current through MDSDEpM structure: a--$I_1(0)$; b--$I_2(0)$; c--$I_{СТ}(t)$ with screening interval $t_э$

($B_Ф << B_Ф^{СТ}$) with the behavior of $I_{СТ}(t)$ (Fig. 1c) shows that when $B_Ф$ is quenched, the time interval of field screening in the semiconductor is longer than the steady value $t_э$, and corresponds to lower capacitive current amplitude. Reverse effects hold for $I_2(0)$ in case $B_Ф >> B_Ф^{СТ}$.

As we know [Ref. 5], under conditions of screening $|U(t)| \leqslant U_э(t_э) = \frac{qL_п n_{ст}}{C}$ current $I = CU_0\omega \cos \omega t$, where $C = \frac{C_{опэ} C_{эд}}{C_{опэ} + C_{эд}}$ is the total capacitance of the dielectrics ($C_Д \cong C_{ЭП}$) and space charge ($C_{опэ}$), which is concentrated at the surface of the semiconductor when $|U(t)| \leqslant U_э$. $C_{опэ}$ is determined by the depth of nonequilibrium depletion W:

$$W = \frac{\varepsilon_п \varepsilon_0}{C_д} \left\{ \left[1 + \frac{C_д^2}{\varepsilon_п \varepsilon_0 q n_{ст}} \cdot |U(t) + V_F| \right]^{1/2} - 1 \right\}, \qquad (2)$$

where ε_0 is the permittivity of vacuum, $C_Д$ is capacitance of the dielectric, q is elementary charge,

$$V_F = \phi_k + Q/C_Д. \qquad (3)$$

The voltage of flat zones (3) depends on the contact potential difference ϕ_k and the sum Q of the charges in the dielectric and on the surface states. Because of the smallness of $C_Д \cong C_{ЭП}$, the contribution of (3) and (2) is most noticeable in the case of the semiconductor-dielectric-electrophosphor interface where in addition there may be an appreciable charge built into the two-layer dielectric.

Under the influence of $U_П$, charge Q may change both in amplitude and in sign, which has an effect on $V_F(U_П)$, W and C. As can be seen from (2)-(3), the relation W(Q) shows up well at small U(t), which occurs under screening conditions. Then $W<<L_П$, $C_{ОПЗ}$ is close to $C_{ЭЛ}$, and we can get an idea of the reduction or increase in C(Q) from comparing $I_1(0)$, $I_2(0)$ respectively with $I_{СТ}(t)$ in interval $t_э$ over time $t_{пер}$.

If the quantities $|U(t)+V_F(U_П)|$ and W have increased after the action of $U_П$, the percentage of U(t) on the electroluminescent layer during time $t_{пер}$ will become less than the steady-state value, which leads to quenching of the background. Reverse polarity of $U_П$ will give the opposite effect.

2. Bursts of sine-wave voltage $\overline{U}(t)$ with duration of 1 s were applied across the MDSDEpM structures. As in the case of $U_П$ (Fig. 2a), after cessation of $\overline{U}(t)$ the

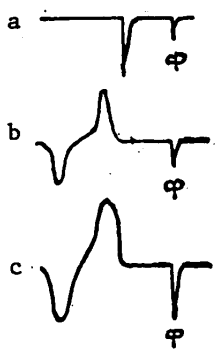

Fig. 2. Photoresponse (Φ) after cessation of $U_П$ (a) and $\overline{U}(t)$ (b--in darkness; c--under illumination)

specimens showed a photoresponse to the probing light pulse, indicating formation of a polarization field. The action of illumination G on the input of the image converter during $\overline{U}(t)$ intensified the photoresponse, i. e. the polarization (Fig. 2c). Consequently, when an alternating voltage is switched on there is a constant component of the electric field present in the specimen that depends on the level of G. This conclusion is confirmed by the corresponding behavior of the second harmonic of current I.

Cessation of pulse G with exposure of 0.1-10 s in mode $U(t)=U_0 \sin \omega t$ caused a transient process ($t_{пер} \cong 10$-100 s), during which quenching or intensification of $B_Φ$ was observed depending on the conductivity of the specimen and the initial sign of Q, which can be attributed to the relation established between G and polarization processes. Image converters that operated at $B_Φ<<B_Φ^{СТ}$ after cessation of G were switched by a pulse $U_И$ of given polarity in time of 1-10 s to the state $B_Φ>>B_Φ^{СТ}$ and vice versa as a consequence of a change in sign of Q.

Comparison of the results given in section 2 with section 1 shows that illumination G influences Q and $V_F(G)$ analogously to $U_П$. Both factors are equivalent in the sense of changes in Q, $|U(t)+V_F(U_П, G)|$ and brightness $B_Φ$.

3. When an infrared image appears at the input of the image converter, W decreases in proportion to the level of photoemission, which produces a corresponding increase in the voltage across the electrophosphor layer. Therefore, the converted image at the output of the image converter is always positive. After cessation of the infrared signal, the processes described in section 3 ensure storage of both a positive and a negative (Fig. 3 [photo not reproduced]). Because of this, a recorded light pattern can be added to or subtracted from a subsequent one.

The sensitivity of the image converter is determined by the coefficient of capacitance coverage with respect to light $K = C_{light}/C_{dark} = W_{dark}/W_{light}$, and allows for some shift due to dependence of W on V_F ($U_П$, G). The maximum value of $K = K_{max} = L_П/L_{эП}$ is determined by the geometry of the structure. The contrast at the output of the image converter can be controlled by regulating the background through variation of $U_П$ and G.

Storage of the image converter is determined by the relaxation time τ_{rel} of the charge induced in the dielectric and the surface states by the action of the field and the light. Therefore, realization of long-term memories with parallel processing of optical data necessitates structures of the semiconductor-dielectric-imaging medium type with maximum τ_{rel}.

The authors thank R. M. Akopyan for useful discussions.

REFERENCES

1. Brodzeli, M. I., Kovtonyuk, N. F., Polyan, R. A., Sikharulidze, D. G., Chavchanidze, V. V., USSR Author's Certificate No 506243 with priority from 13 Jul 73.

2. Brodzeli, M. I., Kovtonyuk, N. F., Polyan, R. A., Sikharulidze, D. G., Chavchanidze, V. V., "Report to Seminar on Display Techniques", Kiev, June 1974. Published in collection "Tekhnika indikatsii" [Display Techniques], Kiev, "Naukova dumka", 1976.

3. Brodzeli, M. I., Kertsman, E. L., Konstantinov, G. D., Polyan, R. A., "VIII Vsesoyuznaya nauchno-tekhnicheskaya konferentsiya po mikroelektronike" [Eighth All-Union Scientific and Technical Conference on Microelectronics], report No 7.53D, Moscow, MIET, 1978.

4. Kovtonyuk, N. F., "Elektronnyye elementy na osnove struktur poluprovodnik-dielektrik" [Electronic Components Based on Semiconductor-Dielectric Structures], Moscow, "Energiya", 1976.

5. Akopyan, R. M., Brodzeli, M. I., Konstantinov, G. D., Polyan, R. A., FIZIKA I TEKHNIKA POLUPROVODNIKOV, Vol 12, No 7, 1978, p 1254.

6. Akopyan, R. M., Brodzeli, M. I., Konstantinov, G. D., Polyan, R. A., FIZIKA I TEKHNIKA POLUPROVODNIKOV, Vol 12, No 7, 1978, p 1424.

Contents page

6610
CSO: 1862/69

PLASMA PHYSICS

PLASMA HEATING IN ACUTE-ANGLED MAGNETIC TRAP WITHOUT USE OF INJECTION

Moscow PIS'MA V ZHURNAL EKSPERIMENTAL'NOY I TEORETICHESKOY FIZIKI in Russian Vol 34, No 11, 5 Dec 81 (manuscript received 6 Oct 81) pp 594-597

[Article by M. S. Ioffe, B. I. Kanayev, V. P. Pastukhov, V. V. Piterskiy and Ye. Ye. Yushmanov]

[Text] A specific high-vacuum discharge enabling ohmic heating of plasma was produced in an acute-angled annular trap with electrostatic blocking of the apertures.

A magnetoelectrostatic trap (MET) is an acute-angled magnetic system in which leakage through the peak is blocked by electrostatic barriers set up by using narrow (order of Debye radius) apertures with grounded walls and negative blocking electrodes ("reflectors") behind them. The most convenient method for heating plasma in an MET is by electron beam injection from the region of the reflector [1]; another usable method is SHF heating [2]. The typical magnitude of electron and ion temperatures obtained in the experiments amounts to 50-100 eV at a density of $\approx 10^{11}$-10^{12} cm^{-3} [3].

A new mechanism for introducing energy into plasma, a mechanism without analogy amongst other methods used for heating in an MET or other type of trap was demonstrated on the ATOLL apparatus. A diagram of the arrangement is shown in Figure 1 and some details of the magnetic aperture are shown in Figure 2. The electron gun 4 is a heated emitter which replaces a small part of one of the reflectors. The supplemental electrodes 3 (Figure 2) serve for blocking secondary emission from the reflectors and the gun's emission. Under "ordinary" conditions, hydrogen plasma is produced and sustained by the gun's electron stream and, largely, by the stream of secondary emission electrons knocked out of the reflectors by the ions striking them and then sucked into the trap under the effect of the reflectors' potential which is usually about 2 kV. The plasma in the trap takes on a negative potential of about 1 kV. Feeding to the supplemental electrodes a negative potential greater than that on the reflectors stops the injection of electrons and leads to collapse of the plasma. However, with a sufficiently intense magnetic field (over 15 kGs in the small apertures) it proves possible for there to exist a state when a plasma with ordinary parameters ($n \approx 10^{12} cm^{-3}$, $T_e \approx 30$ eV, $T_i \approx 50$-100 eV, $P \approx 10^{-6}$ tor) is self sustaining in the trap without any supply of electrons from outside. This

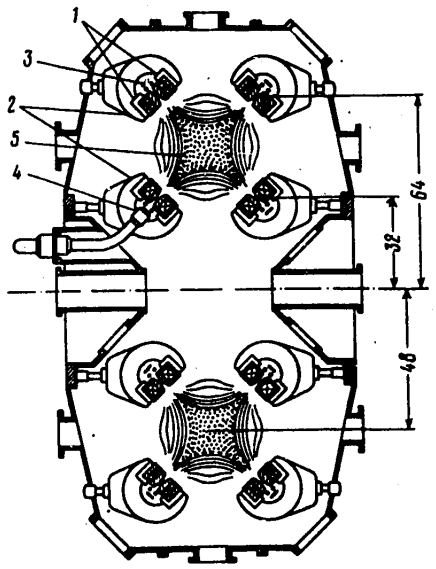

Figure 1. Diagram of the ATOLL Trap: 1-magnetic field coils; 2-clamps; 3-reflectors; 4-electron gun; 5-plasma. Dimensions are in centimeters.

state represents an unusual high-vacuum discharge (between reflectors and ground) with a current of 10 A or more, in which electrode processes do not participate and the source of plasma heating is the currents flowing within the plasma between regions of different potential. The plasma's material balance holds due to ionization of neutral hydrogen.

What mechanisms lead to the establishment of this state? The specific nature of them is governed by the geometry of the MET. The escape of electrons from the trap down the magnetic field is blocked by the electrostatic barriers between the apertures and reflectors, but a rather intensive transfer of electrons takes place across the magnetic field to the walls of the apertures (we will put aside the nature of this transfer). These losses have to be balanced by similar losses of ions. The latter can not escape to the walls as the electrons do since, relative to them, they are in a deep potential well, but then do escape freely down the magnetic field to the reflectors. The intensity of these ion losses runs below the losses of electrons due to the magnitude of the plasma potential. If the potential were zero the ions would escape freely through the entire breadth of the magnetic aperture and that escape would exceed the escape of electrons. In order to lower it, the plasma gets the above-mentioned negative potential, with the result that there remains for the ions' escape only a narrow corridor in the center of the aperture (Figure 2); in other parts of the aperture their escape is blocked by the electrostatic barrier created by the field of the aperture's grounded walls.

That is the source of the development of the plasma's negative potential. Direct observations have shown that, in the crosswise direction, its absolute magnitude

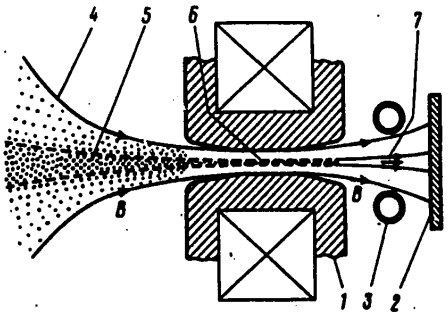

Figure 2. Diagram of the Magnetic Aperture: 1-coil body which forms the aperture; 2-reflector; 3-supplemental electrode; 4-force line restricting the trap's volume; 5-cnetral region of plasma with the greatest negative potential; 6-escape corridor for ions; 7-stream of escaping ions.

decreases noticeably toward the periphery yet within the trap's confines, and that there exists within the plasma a substantial electric field of 50 V/cm. This field then is the principal factor in the "self heating" process: the outward-diffusing electrons, subjected to the difference of potentials, take on energy, part of which is passed on by way of reverse thermal conductivity into the central regions of the trap, covering the losses to ionization, radiation and the like, i.e., providing sustainment of the plasma. The ions get their energy because of this same electric field whose acceleration effect surpasses the roll-up effect of the relatively weak magnetic field (about 300 Gs at the edge of the plasma). As a result, an ion born on the periphery "slides down" to the bottom of the potential well, i.e., to the center of the plasma formation, and goes on to execute periodic cycloid-type motion. Coulomb collisions play no part in the process since the times τ_{ii} and τ_{ie} far exceed the lifetimes of the ions in the trap.

Such are the mechanisms operating in the ATOLL in conditions of plasma self-sustainment. With some conditionality one can define the described heating as "transverse ohmic", thereby implying that the heating is done by currents flowing in the transverse electric fields. One of the conditions for the existence of self-sustainment is, as was noted, a rather strong magnetic field. Its role here is evidently conected with the fact that as B increases, the intensity of transverse transfer of electrons decreases and, hence, the escape of ions must also decrease, which involves the plasma's increasing its negative potential. This increase of potential, in turn, intensifies ohmic heating, making self-sustainment possible. Another condition is the purity of the hydrogen: with admixtures of about 5% (e.g., N_2), the described discharge begins to go out. This is evidently caused by the circumstance that the admixtures, first, increase radiation losses and, second, lower the negative potential of the plasma since the heavier ions leave the trap at a lower speed and the corridor in the aperture must then be wider.

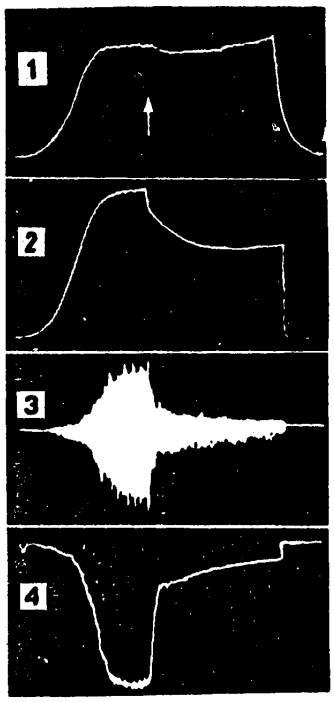

Figure 3. Conditions With Injection and Without Injection at B > 15 kGs. Time base 8 msec. Arrow shows moment of injection blocking: 1-radiointerferometer signal; 2-stream of ions to reflectors; 3-noise signal from probe; 4-electron stream to an electrode beyond the plasma edge.

The virtue of injectionless heating is its obvious technical simplicity which might even be termed "ideal" since the heating requires nothing more than that combination of electric and magnetic fields which makes up the very trap. Another advantage lies in physical character and consists in the fact that with such heating, the electron bunches that usually give rise to instabilities in the plasma are not in evidence. Thus, one can expect better confinement in this instance, which is qualitatively confirmed by the ATOLL experiments. It can be seen in Figure 3 that while the density of the plasma in the trap is practically unchanging during transition to the injectionless mode, ion losses decrease. It can also be seen that the noise level and intensity of electron transfer across the magnetic field are reduced.

BIBLIOGRAPHY

1. Azovskiy, Yu. S., Karpukhin, V. I., Lavrent'yev, O. A. et al., FIZIKA PLAZMY, Vol 6, 1980, p 256.
2. Zalesskiy, Yu. G., Komarov, A. D., Lavrent'yev, O. A. et al., Ibid., Vol 5, 1979, p 954.
3. Gormerano, C., NUCL. FUS., Vol 19, 1979, p 1094.

5454
CSO: 1862/81

STRESS, STRAIN AND DEFORMATION

UDC 539.2.219

PRECURSORS OF MECHANICAL DESTRUCTION OF LARGE SPECIMENS

Moscow DOKLADY AKADEMII NAUK SSSR in Russian Vol 260, No 3, 1981 (manuscript received 2 Apr 81) pp 616-619

[Article by A. A. Semerchan, G. A. Sobolev, B. G. Salov, V. N. Badanov, V. A. Budnikov, A. V. Kol'tsov, V. F. Los', R. M. Nasimov, A. V. Ponomarev, I. R. Stakhovskiy and V. A. Terent'yev, Institute of Physics of the Earth imeni O. Yu. Shmidt, USSR Academy of Sciences, Moscow]

[Text] The construction of high dams, nuclear electric plants and other large structures in recent years, frequently situated in territories subject to earthquakes, has brought to the fore the question of predicting damage to large-scale objects under the zction of prolonged mechanical stresses. This problem is closely associated with prediction of the destruction of a rock massif by earthquakes, rockslides and so on [Ref. 1].

The model of avalanche-unstable crack formation developed in the Soviet Union states that the process of preparation for fracture of an inhomogeneous medium is qualitatively repeated on different scale levels [Ref. 2]. The patterns of this process can be studied therefore on models of materials in different stressed states. However, in the case of a small-sized specimen we cannot avoid the influence of the boundaries and the loading device, and no detailed investigation can be made of the spatiotemporal patterns of the different physical fields that reflect the internal state of the material under strain. Transfer of these results to full-scale conditions necessitates a quantitative study of the scale factor as well.

The unique 50,000 metric ton press at the Institute of High-Pressure Physics, USSR Academy of Sciences, has given us the capability of studying the destruction process on large specimens. Some results in this direction have been obtained on concrete [Ref. 3].

This paper is the first to make a detailed investigation of the process of preparation for fracture by simultaneous registration of six mechanical, acoustic and electric parameters. A significant feature of the experiment was the use of many pickups placed in different sections of the specimen, enabling determination of the spatial structure of the investigated fields, and the change in this structure as the instant of fracture approaches.

The experiments utilized two granite specimens with measurements of 50 x 50 x 70 and 70 x 70 x 70 cm that had been previously studied petrographically and also by irradiation with respect to area by elastic waves, and by mapping the electric potential of the surface.

Each specimen underwent several uniaxial loading cycles with an increase in the maximum load on each succeeding cycle. On the initial stage of a cycle, the load was applied at a rate of $(2-8)\cdot10^7$ Pa per hour, and then increased more slowly at a rate of $4\cdot10^6$ Pa per hour. The experiment was terminated upon appearance of macrocracks commensurate in length with the dimensions of the specimen.

The strain field was studied by strain gages cemented on two faces of the specimen. There were 84-104 sensors on each face, measuring displacements of the surface in the direction of application of the load u_y, in the perpendicular direction u_x, and at an angle of 45° to these directions. Thus, all components of the two-dimensional strain tensor were studied for elements of area measuring 5 x 5 and 3 x 3 cm covering the entire surface of the faces. Measurement accuracy was $6\cdot10^{-5}$. In contrast to results found on small specimens, where deformation is an effective characteristic of the entire specimen, it was found in the given case that the surface is divided up into elements with different behavior. Side-by-side with elements undergoing mainly compression are neighboring expanding sections on individual stages of loading. The differences that show up on early loading stages are firmly retained and amplified as the instant of fracture approaches. Fig. 1 (curves 1, 2) shows the change in the quantity $\partial u_x/\partial x + \partial u_y/\partial y$ that characterizes the reduction or increase in area of two neighboring elements as the load is increased. It can be seen that the rates of change in area for the elements are appreciably different. Macrocracks had a tendency to arise at boundaries between zones of compression and expansion.

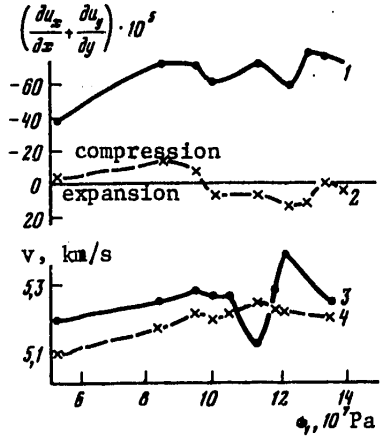

Fig. 1. Change in area of adjacent elements of the surface of a specimen (1, 2) and the velocities of longitudinal elastic waves over neighboring paths (3, 4) as a function of the mechanical stress applied to the specimen

In the course of the experiment, the specimen was periodically exposed to elastic waves on frequency of 70 kHz. The location of the transmitting and receiving sensors enabled determination of zones of reduced or elevated velocities of elastic waves in the body of the specimen within 0.4%, as well as tracking the evolution of these zones with the approach of fracture. It was found that such zones measuring several centimeters arise and disappear as strain increases. Regions with elevated velocities may form around a zone with reduced velocities and vice versa. This effect is apprently due to a fall-off in stresses within such a "soft" zone, while at the same time the stresses increase in adjacent sections. Fig. 1 (curves 3, 4) shows an example of origination of anomaly of velocities on two neighboring paths.

Ultrasonic emission from cracks arising in the specimen was registered in an experiment with the participation of U. S. specialists H. Spetzler and C. Sonderheld, using the Nicol-2090 apparatus. Simultaneous recording of these signals at eight points enabled determination of crack location. Most of the registered signals had a frequency in the range of 50-150 kHz, corresponding to an emitting crack length of the order of 1 cm. Development of such crack systems was confirmed by visual inspection of the specimen after the experiment.

Investigation of the space-time distribution of ultrasonic emission showed that localized actively emitting regions of enhanced crack formation arise that are separated by "silent" zones. Migration of the active regions through the volume of the specimen is observed; an increase in activity in one region leads to a simultaneous reduction of activity in other regions. On the last loading stage, ultrasonic emission from all regions fades, and then increases abrputly just before macrocracks appear.

Electric resistance of the specimen was measured with accuracy of 5% by a four-electrode method on direct current with switching of polarity. One supply electorde was placed on each of the four lateral faces of the specimen, and the 20 reception electrodes were distributed over the surface of two faces. It was found in the experiment that when an active region of acoustic emission appeared at a distance commensurate with the spacing of the reception electrodes (10 cm), it was also registered by the change in resistance. A typical characteristic was anisotropic anomaly of electric resistance such that upon an increase in one direction, a drop was observed in the perpendicular direction. Fig. 2 shows an

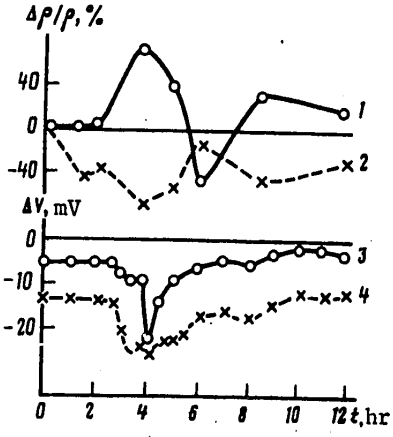

Fig. 2. Change of electric resistance (1, 2) and electric surface potential (3, 4) of specimen in the region of development of microcrack formation

example of an anomaly calculated from the readings of two mutually perpendicular pairs of electrodes (curves 1, 2). The source of the anomaly in this case was located in the depth of the specimen 15 cm from the reception electrodes, and coincided with the zone of intense crack formation revealed by ultrasonic emission. The anisotropy of anomalies of electric resistance is apparently associated with the presence of preferential orientation of the cracks that arise in the specimen.

Use of unpolarized silver chloride electrodes enabled observation of variations of the electric surface potential of the specimen with accuracy to 1 mV. The initial state of the specimen is characterized by a smoothly changing field with deviations of the potential on the surface of about 5 mV. The regions of crack formation distinguished by ultrasonic emission and by electric resistance are also revealed by an increase in density of isolines of potential with maximum values up to 30 mV. The lifetime of electric potential anomalies is determined by the intensity of the strain process (crack formation) and electric relaxation phenomena, and is of the order of tens of minutes to hours for granite specimens of the given dimensions.

Fig. 2 (curves 3, 4) shows an example of the change in potential difference ΔV between the far (zero) electrode and two others installed 15-20 cm from the same zone of crack formation that was revealed by changes of electric resistance ρ. The nature of the variations of electric potential is apparently associated with the ion transport mechanism.

Generation of rf electromagnetic radiation that may arise during crack formation [Ref. 4] was monitored by a frame tuned to 157 or 775 kHz. At sensitivity of the reception equipment of 1.8 mV/m on the low frequency and 0.24 mV/m on the high frequency, no correlation was observed between the recorded electric pulses and acoustic emission of cracks.

These experiments done on large specimens brought us to the following conclusions. Regions of active strain and microstresses with mechanical, electrical and acoustic properties that differ sharply from the ambient medium appear in the material long before macrofracture. Comprehensive observation of the evolution of these regions by measuring the strain field, elastic wave velocities, acoustic emission, electrical resistance and electric potential enables us to keep track of the state of the specimen, and to determine the place and time of development of macrocracks.

REFERENCES

1. Sadovskiy, M. A., VESTNIK AKADEMII NAUK SSSR, No 11, 1971.

2. Myachkin, V. I. et al., IZVESTIYA AKADEMII NAUK SSSR: FIZIKA ZEMLI, No 10, 1974.

Semerchan, A. A. et al., DOKLADY AKADEMII NAUK SSSR, Vol 251, No 2, 1980.

4. Deryagin, B. V., Krotova, N. A., Smigla, V. G., "Adgeziya tverdykh tel" [Adhesion of Solids], Moscow, 1973.

6610
CSO: 1862/92

THEORETICAL PHYSICS

UDC 533.9

ABSOLUTE AND CONVECTIVE INSTABILITY IN PLASMA AND SOLIDS

Moscow ABSOLYUTNAYA I KONVEKTIVNAYA NEUSTOYCHIVOST' V PLAZME I TVERDYKH TELAKH in Russian 1981 (signed to press 15 May 81) pp 2-6

[Annotation, preface and table of contents from book "Absolute and Convective Instability in Plasma and Solids", by Adol'f Mikhaylovich Fedorchenko and Nikolay Yakovlevich Kotsarenko, Izdatel'stvo "Nauka", 3000 copies, 176 pages]

[Text] The problem of instability is closely related to the most important problems of modern physics: the problem of stabilizing processes in fusion devices, as well as the problem of developing up-to-date methods for generating and amplifying electromagnetic and acoustic waves.

This book is the *first monograph in world literature* on the theory of absolute and convective instability in plasma and solids. Criteria are derived for convective and absolute instability, spatial amplification, and are used as a basis for analyzing specific systems encountered in electrodynamics of microwaves, optics, acoustics, gas plasma and plasma of solids.

The book is intended for a broad class of specialists working in the field of microwave electronics, the theory of wave processes and plasma physics. It will also be useful to graduate students and upperclassmen of the corresponding specialties. Figures 34, table 1, references 67.

Preface

The problem of instability of physical systems described by partial differential equations first came up in the solution of hydrodynamic problems.

The theory of hydrodynamic instability has been dealt with in a number of detalied monographs by both Soviet and non-Soviet authors. However, in the fifties in connection with fusion research the problem of instability was once more on the agenda, but with much broader scope. Research on the theory of plasma instability in turn stimulated research in other areas of physics, and particularly in solid state physics. The same problem was closely associated with the problem of generating, amplifying and converting wave processes over a wide range of frequencies and wave modes. The need has arisen for sound criteria of absolute and convective instability, as well as spatial amplification. It was also necessary to develop practical methods of analyzing the dispersion equation that is the basis of the theory of instability of physical systems with distributed parameters.

At present, such work is basically complete, but all results are scattered through separate journal articles with the exception of a short survey by A. I. Akhiyezer, R. V. Polovin published in 1972 in USPEKHI FIZICHESKIKH NAUK. In the Soviet literature there is no complete and systematic exposition of questions associated with the theory of instability of systems with distributed parameters. Therefore the time has arrived for writing a monograph that would fill this breach, if only in part. The authors hope that this book will serve the purpose.

This book presents from a unified standpoint the theory and methods of studying the nature of instability of physical systems of various types that are described by partial differential equations. These methods are grounded in the theory of wave processes in linear systems since the development of an instability on the initial stage may be described by the concept of snall perturbations of the investigated state. It has turned out that it is sufficient to know only the dispersion equation that relates the wave vector to the frequency of the given wave process in order to establish the threshold of the instability and its nature. This has made it possible to develop a unified approach to investigation of instabilities in different systems regardless of their nature and frequency band.

The first part of the book is devoted to introducing basic concepts and substantiating criteria of instability and spatial amplification. This part also points out the simplest methods of analyzing the dispersion equation, and in particular a rigorous presentation is given of the widely used method of weakly associated waves. Understanding of the first part of the book assumes that the reader is acquainted with certain concepts from the theory of functions of a complex variable. The theorems used in the book from the theory of functions of a complex variable are presented without proof at the end of the book in the form of an Appendix.

The second part of the book contains a detailed examination and analysis of examples of unstable systems from various fields of physics: lasers and masers, acoustic amplifiers and oscillators, Gunn diodes, systems of the TWT and backward-wave TWT type, two-beam amplifiers and so on.

The bibliography on the given topic is enormous, and therefore only those monographs and papers are listed at the end of the book to which citations are made in the text.

Most of the book is an exposition of results that have already been published in the literature, but that have been presented here from a unified standpoint. A considerable portion of the material is based on lectures given by one of the authors at Kiev University starting in 1970.

The authors thank the reviewer of this book, Doctor of Physical and Mathematical Sciences P. Ye. Zil'berman for constructive comments, and also Professor V. L. Bonch-Bruyevich of Moscow University upon whose initiative the book has been written

A. M. Fedorchenko
N. Ya. Kotsarenko

Contents page

6610
CSO: 1862/93

- END -